Masteroppgave

NTNU
Norges teknisk-naturvitenskapelige universitet
Fakultet for ingeniørvitenskap
Institutt for bygg- og miljøteknikk

Gabriele Gaiti

3D CFD Simulation of Morphological Changes in 180° Bend due to Different Spur Dike Shapes

Masteroppgave i Hydropower Development
Veileder: Nils Rüther
Juni 2020

NTNU
Norwegian University of
Science and Technology

Gabriele Gaiti

3D CFD Simulation of Morphological Changes in 180° Bend due to Different Spur Dike Shapes

Masteroppgave i Hydropower Development
Veileder: Nils Rüther
Juni 2020

Norges teknisk-naturvitenskapelige universitet
Fakultet for ingeniørvitenskap
Institutt for bygg- og miljøteknikk

NTNU
Kunnskap for en bedre verden

Contents

List of Figures

List of Tables

Abstract

This study focuses on the analysis of different submerged dikes shapes and successions in a rectangular channel with a 180° bend and 2% bed slope in order to prevent scouring and sediment aggradation. To achieve this goal a computational fluid dynamic (CFD) model is used. The numerical modelling software deployed is SSIIM, developed by Prof. Nils Reidar B. Olsen at NTNU (Norges Teknisk-Naturvitenskapelige Universitet).

Scouring in an unmodified rectangular channel with a 180° bend and 2% bed slope occurs on the outer side of the curve, while we observe a sediment aggradation and deposition in the inner side (see Chapter 2.4). Different shapes of dikes, successions and relative elements positions were studied in order to find reasonable alternatives for effective dikes river training measures. Already known dike's shapes (as I-shape, L-shape, T-shape) (Nayyer et al., 2019) were analyzed, additionally a new shape concept designed by the Author, called Broken L-shape (BL-shape) was examined. A focus was made on BL results in order to understand if the new concept could be a valide alternative to the already known spur dike's shapes. First, the system response to each singular spur dike shape, placed at 90° of the 180° turn is analyzed and compared. Results shows different configurations behaviour towards banks scour protection, sediment aggradation, flow channelization and sediment transport. None of the singular-dike configurations could prevent sufficiently the bank scouring on the outer side of the turn under the defined system conditions. Then a succession of same shape spur dikes were considered. The results shows, under the defined system conditions, that spur dikes successions are more effective than the single-dike configuration in preventing banks scouring, deflecting bed shear stresses from critical areas to the middle of the channel. All the different successions analyzed have provided satisfying bank scour protection function. The successions analysis showed that different shapes, positioned in the same locations, have a different behaviours and bank scour prevention magnitude. Energy dissipation and sediment transport analysis were carried out on system level. Successions results showed a gradual decrease of the outer bank scour protection and bed shear stress deflection from configuration T5, passing through configuration I5 and L5, to configuration BL5 (see Table 10 in Chapter 8). Higher the scour protection function, higher are the drawbacks of the selected succession towards sediment aggradation, flow channelization and sediment continuity. From a river training point of view, the applied measures are commonly designed to distribute the stresses and the bed level patterns as uniformly as possible along the section, downsizing critical areas. The interaction of BL-shape succession with the flow results in a lower bank scour protection but a more evenly distributed bed shear stress and bed level pattern respect the other analyzed shapes, making the aforementioned shape-option an interesting and suitable alternative for river training measure using spur dikes.

1 Introduction

The history of human society is closely linked to the river. The river has been used as a source of water and resource supply, agricultural support, trade instrument, energy generator and much more. The history of flooding is unquestionably intertwined with the history of human river societies. Since ancient times, man has been able to identify the sediments transported by the river as a resource. The Egyptians have exploited this resource for centuries to fertilise areas adjacent to the River Nile. On the other hand, the destructive power of floods is formed by the strength of the water flow and by the strength of the sediments carried by it. This makes sediments and water as much life-giving as they are destructive. This made men soon realize the need to control the rivers and their sediments.
The most common practice of river control is so-called river training. Control strategies can be expensive and sometimes even detrimental to the environment. Scour control on river embankments and constructions plays a major role in the control and management of sediments. In a natural river system the scour is particularly critical in the proximity of river bends, favouring wear on the outer bank and deposition of sediment on the inner side of the curve with consequent sediment aggradation. Scour on river banks and buildings can cause dramatic situations also in the event of flooding. According to Julien (2010) approximately the 85% of the 571000 bridges in the United States are built over waterways. These rivers are continuously changing their boundaries as their beds and embankments due to the flow and flood interaction over the channel. Scour on structures plunged, totally or partially, into the river stream is the most common cause of structure failure during floods. These structure's interaction with the river system can cause severe consequences both upstream and downstream. A dam, for example, influence the system balance by trapping the sediment incoming upstream the construction, resulting in higher erosion and bank degradation on the system downstream. Moreover the deposition and aggradation of the trapped sediments diminish the reservoir storage and increase the flooding risk. Also structures aiming to control the stream and channel dimensions can have a severe impact over the river system. Measures as channel straightening or bed level modification can have impact over the entire fluvial system by changing its flow behaviour and consequently the stream interaction with channel. Therefore, the study of structures to prevent wear and to deflect the flow forces in a favourable way assumes primary importance. The actual most common types of structure for river-training, in order to avoid banks scour, are stream barbs, submerged vanes and spur dikes.

The use of submerged vanes is a less-cost and equally effective alternative technique to conventional river training measures (Odegaard, 2017). The vanes are generally a sequence of linear, submerged, small flow-deflecting structures. They are designed to deflect the flow forces and generate secondary current circulation in order to modify the near bed flow pattern, deflect the flow, change magnitude and direction of shear stresses and sediment transport in the cross section (Odegaard and Wang, 1991). In a river curve the flow centrifugal force acting on the bend is the main cause of scouring. The submerged vanes main concept is that the secondary current, generated by the interaction of the structure with the flux, counteract to the flow centrifugal force acting on the bend. The result from the application of this structures is a change of the river bed levels, aggrading on one and degrading on the other side of the submerged vanes (Odegaard and Wang, 1991).

Stream barbs are rock structures, often directed towards upstream (repulsive), favouring sedimentation around the construction (Jamieson et al., 2007). The main studies on stream barbs

where oriented towards ecological impact and structures or banks prevention from scouring. The solution is a low construction and general maintenance cost option. The studied effect of these structures, generally places in sequence, has shown an improving of the morphological aspect in particular regarding sediment transport and scour prevention. The driving effect produced by their interaction with the flux is the creation of eddies due to their vertical flow separation and overtopping flow conditions (Jamieson et al., 2009).

Spur dike is generally a concrete structure, but different materials and construction techniques have been historically used all over the world. This alternative is a flexible solution due to the different shapes-alternatives that could be investigated and the consequent combinations with inclination, submergence and other physical parameters. Experimental and numerical studies regarding T-shaped spur dike in a 90° channel bend have been already carried out (Vaghefi and Radan (2016), Vaghefi et al. (2017), Vaghefi et al. (2018b), Vaghefi et al. (2019), Vaghefi et al. (2018a), Vaghefi et al. (2015), Vaghefi et al. (2012)). The results shows that a T-shape spur dike can provide effective outer bank scour protection (Vaghefi et al., 2015). All these studies on the T-shape spur dike were not oriented to find the best shape, but to understand the flow-scour behaviour after a T-shape dike interaction in different situations, as different positions, submergence, dimensions, presence of attractive/repulsive before and/or after the structure. A drawback of this river (but also coastal) flow training measure is the local scour around the structure, with consequent possible erosion issues and related structural failures (Yazdi et al., 2010). Other already known structure's layout as I-shape, L-shape, T-shape and their successions, were analyzed by Nayyer et al. (2019). The results from this research stated that, under the set conditions and dike structure dimensions:
"The L-shaped spur dike in the first position has smaller area of high shear stress and turbulent energy than the other geometries near the tip of the spur dike and also has a positive effect on downstream spur dikes, especially on the T-shaped spur dike." (Nayyer et al., 2019) and
"Streamlines indicated that a horizontal vortex formed upstream of the T-shaped spur dike and can create a wide erosion area for this geometry. This area for first spur dike formed in the location of the maximum scour depth on the mobile bed, which causes maximum erosion volume for this geometry. Vortex between consecutive spur dikes formed with weak strength and caused sedimentation in this area." (Nayyer et al., 2019).
Based on previous studies considerations, this dissertation aim to broaden the study of the effects of different submerged dike shapes, in a 180° bend, in order to find different suitable alternatives to the already known spur dike's shapes. Comparable alternatives that could deflect the flow forces, avoid scouring on the outer side of the curve, avoid sediment deposition at inner side and consequent lateral gradient formation, with an eye to sediment's fluvial continuity and flow channelization. Before the advent of the digital computing power, build a physical model was the only way to verify and understand the complexity of the interactions of structures over a modeled channel and flows. Setup a a physical model is still costly, time consuming and sometimes difficult, but nowadays more and more scientists are starting to evaluate their hypothesis by using a numerical model first, then a physical model to confirm (or refute) the results obtained. The fast and continuous development of numerical models has enhanced the research on river-training structure impact over the modeled river system, enabling a deeper understanding of hydraulic dynamics. The improvement of numerical modelling techniques has led to to more accurate results, often verified by paired physical model, resulting in an increased use of numerical simulations as well as a wider choice of softwares.

1.1 Hypothesis and Main Parameters

This study uses the CFD (Computational Fluid Dynamic) software SSIIM, developed by Nils R.B. Olsen at the Department of Hydraulic and Environmental Engineering at the Norwegian University of Science and Technology (NTNU). The validity of SSIIM 3D numerical modelling of systems has been proved (Rüther et al. (2009), Minor et al. (2007)), thus the goodness of the results presented is confirmed. The Author suggests however a further study oriented to validate the results obtained from numerical modelling simulation through a physical model, in order to understand possible unexpected behaviour of the model as it is set up.
The main hypothesis of this study are multiple:

1. Verify the use of different configurations of spur dikes as effective measures of scour prevention on the outer side of a channel with a $180°$ bend and 2% bedslope .

2. Compare the different dike-shape alternatives in order to understand their different behaviour, virtues and drawbacks, according to the shape.

3. Verify the suitability of a new dike shape designed by the Author, called BL-shape, from a river-training measure perspective.

This study is based on the fact that the goodness of spur dike interaction on the river system as an effective river-training measure in order to avoid scouring in critical areas is already, theoretically and historically, confirmed by numerous studies and a wide use all over the world. This study aims to compare different shapes of spur dikes, in singular and in succession configurations, in order to verify their ability to avoid, or diminish, scouring at the outer side of a channel with a $180°$ bend, bedslope of 2% and guarantee the sediment continuity towards downstream. Previous researches stated the goodness of successions respect a single dike impact on the channel (Nayyer et al., 2019). In particular the results obtained by Vaghefi et al. (2015) and Nayyer et al. (2019) have highlighted the system response towards T and L shape combined successions. The parameters that must be understood in order to prove the goodness of the selected river-training measure are, generally but not only, the bed shear stress pattern and the bed lateral gradient occurring at the structure cross section and in critical areas.

1.1.1 Lateral Gradient

The lateral gradient is the inclination of the bed level, along the cross section, from the deepest point, corresponding to the area of maximum scour, to the embankment. In Figure 1.1.1(b) is clearly showed the lateral gradient occurring along an undisturbed channel bend and along the straight part of the channel, where the gradient is theoretically null. In this situation the lateral gradient is considered as the inclination of the bed, from the deepest point, at the outer side of the bend, to the inner embankment, respect the horizontal reference. From a river training perspective, the lateral gradient should be minimized in such a way to obtain a hydraulic system ideally as close as possible to the uniform and undisturbed one, identified in the straight channel without any riverbed lateral gradient (top image in Figure1.1.1(b)). In an undisturbed channel with $180°$ bend, the zone of maximum erosion corresponds to the external side of the turn, while in the inner side the level of the riverbed rises from the initial condition due to the deposition of sediments (see bottom image in Figure 1.1.1(b)) aiding in the formation of a lateral gradient. The scour and deposition pattern, that determines the lateral gradient, can be seen in more detail through the bed shear stress pattern, thus showing their close correlation. Also, flow channelization due to structure interaction with the river section is often link with steep lateral gradient.

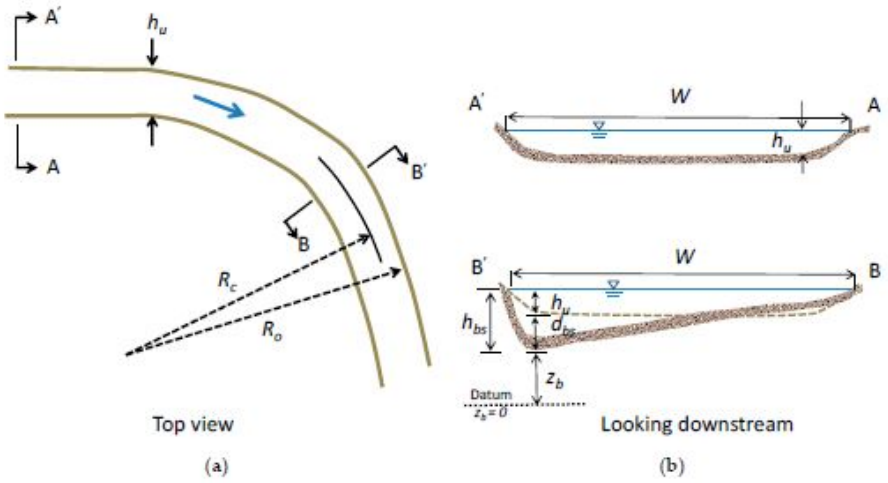

Figure 1.1.1: Definition sketch showing bend scour. (**a**) top view; (**b**) cross-section looking downstream. (Guo et al., 2017)

1.1.2 Bed Shear Stress Pattern

The bed shear stress pattern is the spatial distribution of the bed shear stress over the channel system. The shear stress is the index parameter of the mechanism that generate scour or promotes the deposition of sediments. From river training point of view, the bed shear stress pattern should be as uniform as possible, trying to avoid critical areas with high stresses, resulting in bed scour, channel deepening and consequent flow regime modification. When spur dikes are used, the undisturbed bed shear stress pattern is modified by the structures interaction and, generally, the area of maximum scour will not correspond anymore to the outer side of the curve, but will be shifted to the area at the dike's toe, changing the related lateral gradient for the specific configuration. High bed shear stress scour generated from the dike interaction with the system, generally, results in high lateral gradient. For further details see Chapter 2.4.

The previous studies as Vaghefi et al. (2015) and Nayyer et al. (2019) have shown some limitations of the analyzed shapes (I, L, T) towards these main parameters as lateral gradient and bed shear stress pattern. In fact, the studied shapes and successions, also if providing a good scour protection on the outer bank, have shown the presence of a lateral gradient that could be improved, in order to provide as result a hydraulic condition closer to the theoretical uniform and undisturbed condition of the straight channel. Towards this point of view the Author, based on the consideration from Nayyer et al. (2019) (see Introduction) about L-shaped spur dike smaller area of high shear stress and turbulent energy and its positive effect on downstream spur dikes, has developed and simulated a new shape-type called Broken-L, consisting in the classic L-shape dike with an opening in part of the structure perpendicular to the flow. This structure has been thought in order to distribute the stresses more evenly along the cross section in order to obtain a smaller bed level lateral gradient as possible, providing a suitable alternative to the already known dike shapes from a river-training perspective. In this study has therefore been chosen to analyze and compare the already known shape as I, L, T and the new BL shapes (see Figure 4.8.1), both as singular structure and as successions, in order to understand and compare performances towards scour protection and sediment continuity of the system, verifying the suitability of the new BL-shape as a new river training measure.

1.2 Limitations

Underlying the above considerations, the simulation reported in this research, while being technically correct (Rüther et al., 2009), however, has limitations due to the technical difficulties inherent aspects that cannot be treated in all their complexity in this only thesis, as:

1. Results from numerical simulation are not supported by a paired physical model.
2. The system, as it is set up in the simulations, is not representative of a real channel. This study aims to understand the behaviour of the dike structures in a controlled environment, in order to compare to the actual available dike-shape solutions.
3. No dynamic sediment inflow considered.
4. Steady flow simulations.
5. Dikes structure used have perfectly vertical impermeable walls, no fluid-dynamic slope of walls were considered.
6. Structure's wear and related issues and maintenance are not considered.
7. No ecological aspects were considered.

2 Background Theory

2.1 Water Properties

In this study we consider the water as an incompressible, Newtonian fluid. The freshwater mass density, although the awareness of its slight variation as the temperature changes, is considered as 1000 kg/m^3. Therefore, the related specific weight γ is considered equal to 9810 N/m^3.

$$\gamma = \rho g \tag{2.1}$$

The fluid deformation on the flow boundary cause a shear stress τ_{zx} (see Figure 2.1.1) (as vector of the stress force parallel to the material surface) as function of the fluid dynamic viscosity μ and the deformation rate:

$$\tau_{zx} = \frac{F}{A} = \mu \frac{dv_x}{dz} = \rho \upsilon \frac{dv_x}{dz} \tag{2.2}$$

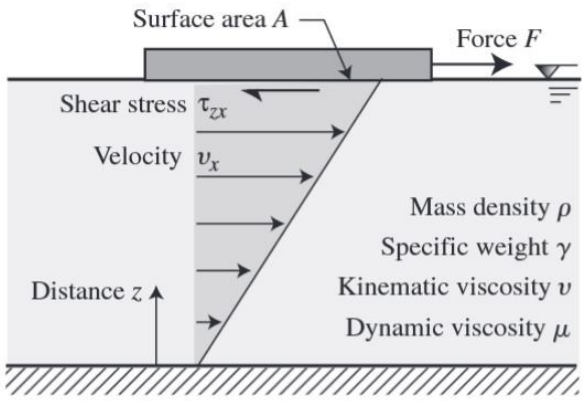

Figure 2.1.1: Newtonian fluid properties (Julien, 2010).

where the dynamic viscosity μ is:

$$\mu = \rho \upsilon \tag{2.3}$$

where υ is the kinematic viscosity of the fluid, defined as 1*10^{-6} m^2/s, at 20°.

2.2 Sediment Properties

Each singular sediment particle have a mass density ρ_s defined as:

$$\rho_s = \frac{\gamma_s}{\gamma}\rho = G\rho = M_s V_s \tag{2.4}$$

where M_s is the mass of the sediment, V_s is the volume, G is called specific gravity and γ_s is the specific weight of the particle defined as:

$$\gamma_s = \rho_s g = G\gamma \tag{2.5}$$

Usually a non-homogeneous set of sediments in terms of diameters, type, material and properties is present in the system. Therefore a common way to measure the quantity of sediments that satisfy a specific diameter limit is called particle size distribution, showing the weight percentage of material finer then a given sediment size. For example d_{50} represent the median grain size, so the size among the batch, for which the 50% of the material is finer.

2.3 Incipient Motion

There are many factors that influence the equilibrium of a non-cohesive particle plunged in a fluid. Destabilizing forces, acting on the grain due to the flow interactions, are counterbalanced by stabilizing forces. The weight of the particle pushes the equilibrium towards stability, while buoyancy, lifting and dragging forces pushes towards incipient motion. Moreover a randomness factor should be applied on the balance to account for the specific grain placement and turbulence forces, that could both stabilize as well as destabilize the particle equilibrium. When the bed shear stress (Formula 2.2) exceed the so-called critical shear stress for the bed sediment's grain, the particle will start its incipient motion accordingly to the energy vectors acting on it. The balance acting on a grain particle is shown in Figure 2.3.1, where F_B, F_G, F_L and F_D are the buoyancy, gravity, lift and drag forces respectively. φ_0 is the angle of repose (or friction angle) and β is the bed-slope angle.

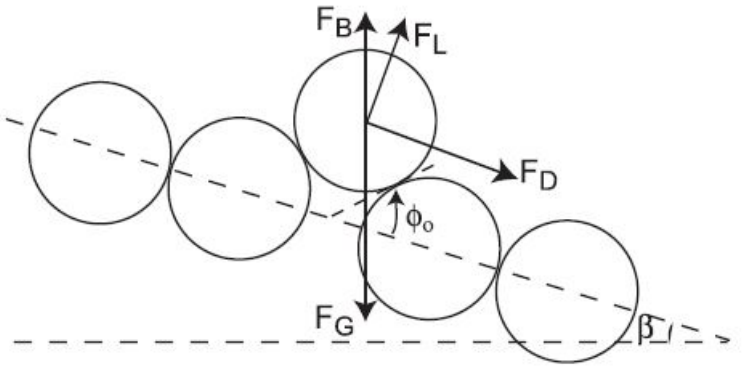

Figure 2.3.1: Force balance on a grain (Wiberg and Smith, 1987).

Assuming bed-slope angle β=0, the vector F_D become horizontal and its value is determined by:

$$F_{\mathrm{D}} \cong \tau_0 {d_{\mathrm{s}}}^2 = \rho {u_*}^2 {d_{\mathrm{s}}}^2 \tag{2.6}$$

Then the balance between the vertical forces results in a total vertical stabilizing force F_V:

$$F_{\mathrm{V}} = F_{\mathrm{G}} - F_{\mathrm{L}} - F_{\mathrm{B}} \tag{2.7}$$

$$F_{\mathrm{V}} \sim (\rho_{\mathrm{S}} - \rho) g d_{\mathrm{S}} \tag{2.8}$$

The ratio between destabilizing/stabilizing forces defines the dimensionless shear stress, called Shields parameter (Shields, 1936):

$$\tau_* = \frac{\tau_0}{(\rho_{\mathrm{S}} - \rho) g d_{\mathrm{s}}} = \frac{\rho_{\mathrm{m}} {u_*}^2}{(\rho_{\mathrm{S}} - \rho) g d_{\mathrm{s}}} \tag{2.9}$$

Where τ_0 is the shear stress at bed level and u_* is the shear velocity:

$$u_* \equiv \sqrt{\tau_0/\rho} \tag{2.10}$$

When the shear velocity is critical (u_{*C}), using the Formula 2.2, the so-called Critical Shield Number is obtained. Therefore a particle which is subjected to a shear stress (Formula 2.9) higher then its Critical Shields stress (Formula 2.9) will start its incipient motion. Based on the Shields work, Yalin and Karahan (1987) has improved the original Shied diagram, showing that the Shields stress at incipient motion τ_{*c} varies with the particle Reynolds number Re_*, for values <100 while its roughly constant to 0.047 for higher values. This means that different critical values of τ_* will occur by changing hydraulic regime (see Figure (2.3.2).

$$Re_* = \frac{u_* d_S}{\upsilon} \tag{2.11}$$

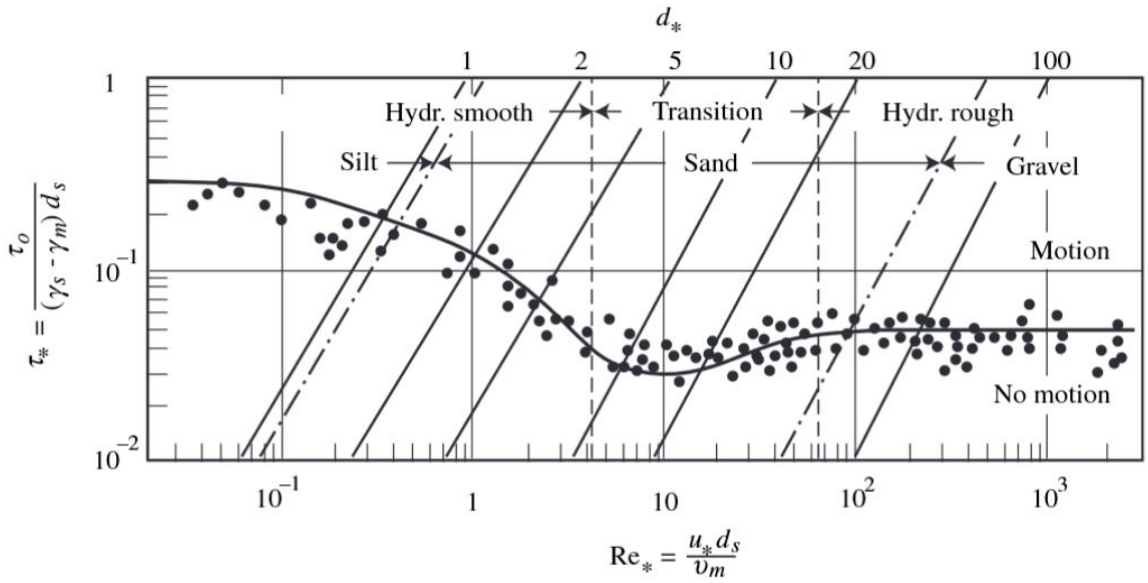

Figure 2.3.2: Shields Diagram (Yalin and Karahan, 1987).

The shear stress induced by the streamflow over a sediment particle is not constant over the system. It depends on the deformation rate, determined principally by velocity and submergence in the flow. Therefore local conditions determined by the interactions from the structures plunged, totally or partially, in the streamflow, can change the shear stress pattern from the undisturbed configuration by changing the physical parameters that characterize the system. Change in the cross section lead to a modification of the velocity pattern and submergence, which lead to a change in the related shear stress that could possibly result in scouring on the boundaries surfaces. Moreover the material characteristic of the sediments and the structures (and their related roughness coefficient) may increase or decrease the shear stress applied on their surfaces.

2.4 Scouring and Sediment Aggradation

Scouring on structures plunged in a moving fluid is related to the interaction of the flow strength with the surfaces and the strength of material which the submerged volumes are made of. When particles are present in the fluid, their impact interaction with the structure's surface can promote, or avoid, erosion and its prediction is of great economic importance (Chanson, 2004). Erosion is on the whole closely related to the amount of energy introduced into the system by the flow. The interaction force between the fluid, the particles and the submerged surfaces is called shear stress (see Chapter 2.1) and it is dependent on flow energy, surfaces roughness, hydrostatic and hydrodynamic conditions. Shear stress has an essential function in the transfer of energy from the flow to the submerged surfaces and sediments. It is indeed the cause of the differentiation of the riverbed levels by inducing different stresses on sediments surfaces, according to local fluid and sediment dynamics and eventual structures interactions. When the shear stress exceed the so-called critical shear stress (or Critical Shields Number, see Formula 2.9) for the bed sediment's grain, the particle will start its incipient motion accordingly to the energy vectors acting on it. The parameters that influence the shear stress are multiple and can differ accordingly to different bed structure and configuration, river morphology, hydrodynamic conditions, and sediments characteristics.

Table 1: Shear stress influencing parameters.

Sediments		**Flow and Morphology**		**Flow and Gravity**	
d	Grain diameter	β	Bed slope	ρ	Fluid density
σ	Grain-size distribution	h	Water depth	ν	Kinematic viscosity
SF	Grain shape	v	Velocity	g	Gravity
ρ_s	Sediment density		Turbulence		
φ	Angle of repose		Bed structure		

Scour can be related to the sediment transport capacity and to the flow condition of the system. Different bed configuration can therefore lead to different responses.
From a sediment point of view, the particle size distribution can influence the erosion pattern. Assuming same particles material, finer grains will need a lower bed shear stress in order to start their incipient motion (as in Chapter 2.3) due to their smaller volume and related lower weight, decreasing the influence of the stabilizing forces on the particle equilibrium. A common phenomenon, after the initial motion of the finer particles, is the shielding from the flow done by bigger particles on the smaller ones. This process is considered as another one of the random factors influencing the sediment particle balance. This phenomenon is called bed armouring (Van Rijn, 1993). This results in more shear stress needed, respect the critical bed shear stress for the chosen particle, in order to achieve its incipient motion. Then the possibility of the existence, between the particles, of cohesive forces when their diameter is smaller then 62 μm (Julien, 2010) should be taken into account. Cohesiveness between grains also increase the bed shear stress needed to start the particle incipient motion. Moreover, a change in the channel dimensions will impact on the related flow conditions. Steeper slopes results in a lower bed shear stress needed in order to start incipient motion of particles. On the extreme situation consisting in bed slope steeper then the repose angle of the particles, the sediments will start their motion, even in absence of fluid, resulting in an unstable bed (Chanson, 2004). A change of bed slope or channel width or height will also result in a change of the related flow pattern. A decrease of the bed slope will decrease the flow velocity, decreasing the bed shear stress and the related sediment transport and scour magnitude. This situation is common in the downstream

reach of the river system, where the sediment inflow is usually larger then the sediment transport capacity, resulting, generally, in wide meandering river. The widening itself of the river section result in a decrease of the flow velocity with same consequences as stated above.
Structures have an impact on the river system by modifying its physical properties and dimensions, as well as their flow interaction. Several numerical studies has been conducted on scour behaviour around cross-river structures in river bend, as piers (Dodaro et al. (2014), Yen et al. (2001), Nagata et al. (2005), Roulund et al. (2005)) and spur dikes (Zang et al. (2005), Zang et al. (2009)). These studies have shown that, for the same river-training configuration placed on the outer bank of the bend, an increase in flow energy entering the system leads to an increased scouring.
Several empirical bend scour equations have been developed for a undisturbed channel bend (Melville and Coleman, 2000). Many parameters are involved influencing the scour pattern and magnitude as in Table 1. A schematic representation of how flow forces change the morphology of the river bed along a curve is shown in Figure 1.1.1. The bed level differences between sections upstream the turn and along the bend are remarkable. The flow forces modify the bend morphology digging on the external side of the curve and raising the internal side. The scour pattern generated by the shear stress interaction with the bed sediments generate the lateral gradient as index of disturbance from the undisturbed straight-channel condition (as mentioned in Chapter 6). This inclination of the river bed from situation (**a**) to (**b**) in the Figure 1.1.1, shows the disturbance of the flow over the sediments pattern due to the river bend. This interaction, as also observed by Odegaard and Wang (1991), lead to a different sediment pattern along the bend section. Higher flow forces acts on the outer side of the bend, favouring a higher velocity and consequent higher shear stress. On the outer side, this results in scouring and deposition of only the heaviest fraction of the sediments, while the finer particles are moved downstream or, through secondary current circulation, deposited in the inner side of the bend. Because of this process a differentiation of the sediment particles along a bend section is built. Thus, the relationship between bend scour and sediment aggradation is clear for undisturbed channel bend, but it could not be in system with submerged structure interactions. The related lateral gradient is an observed channel response due to the flow interaction that, generally, river-training measure try to avoid or, at least, diminish in magnitude.

2.5 Sediment continuity

Sediment continuity is an important concept for river engineer. The hydrological component, sedimentology and river morphology are the basis in order to understand the behaviour of the entire river environment (Maddock, 1999). In natural basins, sediments are introduced into the river system from weathering and erosion of soils, organic material and minerals and other in-stream sources. The river reach behave differently along its path due to its morphological, hydrological and sedimentological characteristics. In particular in upstream the river reach, the flow is more turbulent due to higher bed steepness gradient. This cause a prevalent erosion and weathering mechanism that start to introduce sediments into the river system. In lowland areas, the transported sediments settles along the river bed and banks. This change in the deposition rate happens in a long area from the river source to its estuary. Sediment continuity concept aims to guarantee a proper transit of the sediments towards downstream the river reach, despite the possible presence of river-behaviour perturbations. In case of submerged structures, the interaction between the submerged surfaces with the sediments and the flux could change the undisturbed shear stress pattern and consequently change the deposition pattern of the sediment downstream and, possibly, upstream the structures. The interaction could modify the deposi-

tion or erosion behaviour in the area affected by its disturbance, influencing the overall channel response. The possible variation of the bed level, the flow behaviour, the sediment yield and sediment quality have an impact also on the environmental quality of the river. In particular, the presence of contaminants like heavy metals, pesticides and other organic pollutants has biological impacts the local aquatic environment system. Also the change in river morphology, caused by change in sediment yield, should be studied locally in order to understand the potential beneficial or detrimental effect on the aquatic environment (Maddock, 1999). Regarding the simulations done in this study appear reasonable to consider the best outcome, from a sediment continuum point of view, the balance between sediments incoming and sediment exiting the system. This consideration is because of the shortness of the system consider, indeed in a real river system the change in deposition ratio appears over long distances or due to particular conditions (like headworks or lakes) that in this study are not considered.

Table 2: Variables summary.

Variables	Symbols	SI Units
Geometric variables (L)		
Length	L, x	m
Area	A	m^2
Volume	V	m^3
Diameter	d_s, d_{50}	
Kinematic variables (L, T)		
Velocity	v, u, u_*	m/s
Acceleration	a, g	m/s^2
Kinematic viscosity	υ	m^2/s
Discharge	Q	m^3/s
Dynamic variables (M, L, T)		
Mass	m	kg
Force	$F=ma$, mg	$N = kg*m/s^2$
Pressure	$p= F/A$	$Pa = N/m^2$
Shear stress	τ, τ_0, τ_c	$Pa = N/m^2$
Energy	E	J = N*m
Mass density	ρ,ρ_s	kg/m^3
Specific weight	γ, $\gamma_s= \phi_s*g$	N/m^3
Dynamic viscosity	$\mu=\rho*\upsilon$	Pa*s = kg/(m*s)
Dimensionless variables (-)		
Slope	S_0,S_f	
Specific gravity	$G =\gamma_s / \gamma$	
Reynolds number	$Re = v*h / \upsilon$	
Grain shear Reynolds number	$Re_* = u_* d_s / \upsilon$	
Froude number	$Fr= v / \sqrt{gh}$	
Shields parameter	$\tau_* = \tau / (\gamma_s-\gamma)d_s$	

3 SSIIM Numerical Model

The numerical model used in this study is SSIIM, abbreviation of "Simulation of Sediments movements In water Intakes with Multiblock option". This software, developed at Norwegian University of Science and Technology (NTNU) by Nils Reidar B. Olsen, solves the three-dimensional Reynolds-averaged Navier-Stokes equations in order to compute the flow (Olsen, 2018). SSIIM model has three computational steps:

1. Pre-processing:
   Consist in the generation of grid and input data. Could be done by using tools or grid generator included in the software.

2. Computation processing:
   Consist in the resolution of the system dynamics as set in the pre-processing step. The software can calculate flow and sediments interactions.

3. Post-processing:
   Consist in the visualization of the results. Could be done in-software or is possible to generate graphs for other visualization software as ParaView and Tecplot

Two versions of SSIIM are available:

1. SSIIM 1:
   Use structured grid, resulting in a faster solving and less memory allocation.

2. SSIIM 2:
   Use unstructured grid, resulting in the ability to model complex geometry ad wetting-drying conditions. This version is provided with more sediments transport algorithm respect the version 1.

All the simulations made in this study are made by using SSIIM 1 version.

3.1 Flow Calculations

For a turbulent, non-compressible and constant density flow, the velocity vectors can be obtained by the following equation (Olsen and Stokseth, 1995):

$$\frac{\partial U_{\mathrm{i}}}{\partial t} + U_{\mathrm{j}} \frac{\partial U_{\mathrm{i}}}{\partial x_{\mathrm{j}}} = \frac{1}{\rho \partial x_{\mathrm{j}}} \left(-P\delta_{\mathrm{ij}} - \rho \overline{u_{\mathrm{i}} u_{\mathrm{j}}} \right) \tag{3.1}$$

$$\frac{\partial U_{\mathrm{i}}}{\partial x_{\mathrm{i}}} = 0 \tag{3.2}$$

Where:

1. $\boldsymbol{U_i}$ and $\boldsymbol{U_j}$ represents Reynolds-averaged flow velocities in the two directions.

2. $\boldsymbol{i}$ and $\boldsymbol{j}$ are the directions respectively towards the flux and orthogonally to the flux.

3. $\boldsymbol{t}$ represent time.
4. $\boldsymbol{x_i}$ and $\boldsymbol{x_j}$ represent position vectors.
5. ρ represent the density of the fluid.
6. $\boldsymbol{P}$ represent the dynamic pressure.
7. $\delta_{\boldsymbol{ij}}$ is the Kronecker delta, which is 1 if i=j, and 0 if i not = j.
8. $\rho\overline{\boldsymbol{u_i}\ \boldsymbol{u_j}}$ represents the turbulence term as Reynolds stresses.

A Power-law scheme is used to reduce diffusive flux and SIMPLE method is the default method for pressure corrections (Olsen, 2018). The numerical methods are further described by Patankar (1980), Melaaen (1992), Olsen (1991).

There are two ways to calculate the turbulence shear stress, one by using a k-εmodel, and one by using a simpler turbulence model.

3.1.1 k-εmodel for turbulence shear stress

The Reynolds stresses are solved by using a *k*-ε model on 3D, structured, non orthogonal grid (Minor et al., 2007).

$$\frac{\partial k}{\partial t} + U_{\mathrm{j}}\frac{\partial k}{\partial x_{\mathrm{j}}} = \nu_{\mathrm{T}}\left(\frac{\partial U_{\mathrm{i}}}{\partial x_{\mathrm{j}}} + \frac{\partial U_{\mathrm{j}}}{\partial x_{\mathrm{i}}}\right) + \frac{\partial}{\partial x_{\mathrm{j}}}\left[\left(\nu + \frac{\nu_{\mathrm{T}}}{\sigma_{\mathrm{k}}}\right)\frac{\partial k}{\partial x_{\mathrm{j}}}\right] - \epsilon \tag{3.3}$$

$$\frac{\partial \epsilon}{\partial t} + U_{\mathrm{j}}\frac{\partial \epsilon}{\partial x_{\mathrm{j}}} = \frac{\partial}{\partial x_{\mathrm{j}}}\left[\left(\nu + \frac{\nu_{\mathrm{T}}}{\sigma_{\varepsilon}}\right)\frac{\partial \epsilon}{\partial x_{\mathrm{j}}}\right] + c_{\varepsilon 1}\frac{\epsilon}{k}R_{\mathrm{ij}}\frac{\partial U_{\mathrm{j}}}{\partial x_{\mathrm{i}}} - c_{\varepsilon 2}\frac{\epsilon^2}{k} \tag{3.4}$$

Where:

1. ν represent the kinematic viscosity.
2. ε represent the turbulence dissipation.
3. $\nu_{\boldsymbol{T}}$ represent the eddy viscosity.
4. $\boldsymbol{k}$ represent the kinetic energy.

The kinetik energy k is given from the formula:

$$k = \frac{\overline{u_{\mathrm{iu_j}}}}{2} \tag{3.5}$$

The eddy viscosity ν_T is given from the formula:

$$n_T = c_\mu \frac{k^2}{e} \tag{3.6}$$

The five closure coefficients are empirical constants (Launder and Spalding, 1974):

- $\boldsymbol{c_\mu}$ = 0.09
- $\boldsymbol{c_{\varepsilon 1}}$ = 1.44
- $\boldsymbol{c_{\varepsilon 2}}$ = 1.92
- $\sigma_{\boldsymbol{k}}$ = 1.0
- σ_ε = 1.3

3.1.2 Simpler model for turbulence shear stress

The introduction of eddy-viscosity concept is made together with the Boussinesq approximation to model the Reynolds stress term, as stated in the manual (Olsen, 2018):

$$-\overline{u_i u_j} = \nu_T \left(\frac{\partial U_i}{\partial x_j} + \frac{\partial U_j}{\partial x_i} \right) \tag{3.7}$$

3.1.3 Wall-law

In the simulation walls-law is used. The empirical formula utilized for rough walls is (Schlichting, 1979):

$$\frac{U(z)}{U_*} = \frac{1}{\kappa} \ln \frac{30y}{k_S} \tag{3.8}$$

Where:

1. $\boldsymbol{U_*}$ represent shear velocity.
2. $\varkappa$ represent a constant equal to 0.4 .
3. $\boldsymbol{y}$ represent the distance to the wall.
4. $\boldsymbol{k_S}$ represent the roughness.

3.2 Sediments Computation

The bed movements are made by a continuous sediment movements and re-settling. This mechanism will cause the water to lose energy, in particular as kinetic energy, then loose velocity. This can be considered as an added roughness (Einstein and Chien, 1955). Experiments (Einstein and Chien (1955)) showed that a relationship can be addressed between a modified velocity distribution and sediment concentration, by modifying the $\varkappa$ parameter that is constant in the wall-law (formula 3.8):

$$\kappa = \kappa_0 \frac{1}{(1 + 2.5c)} \tag{3.9}$$

Regarding the sediments, SSIIM calculates the transport by size fraction (Olsen, 2018). The sediment transport is divided in suspended load and bed load.

3.2.1 Suspended Load

The suspended load is modeled by convection-diffusion equation for sediment concentration:

$$\frac{\partial c}{\partial t} + U_{\mathrm{j}} \frac{\partial c}{\partial x_{\mathrm{j}}} + w \frac{\partial c}{\partial z} = \frac{\partial}{\partial x_{\mathrm{j}}} \left(\Gamma \frac{\partial c}{\partial x_{\mathrm{j}}} \right) + S \tag{3.10}$$

Where:

1. ***c*** represent the sediment concentration or, in SSIIM, the volume fraction.
2. ***w*** represent fall velocity of the sediment particle.
3. Γ represent the diffusion coefficient from k-εmodel.
4. ***S*** is the term representing the erosion pick-up rate, using by default the Van Rijn formula for suspended sediments (1984).

$$\Gamma = \frac{\nu_{\mathrm{T}}}{S_{\mathrm{c}}} \tag{3.11}$$

Where S_c is the Schmidt number set to 1.0 to default. For the concentration of suspended sediments near the bed SSIIM uses the Van Rijn formula (1984):

$$c_{\mathrm{bed}} = 0.015 \frac{D^{0.3}}{a} \frac{\left(\dfrac{\tau - \tau_{\mathrm{c}}}{\tau_{\mathrm{c}}} \right)^{1.5}}{\left[\dfrac{(\rho_{\mathrm{s}} - \rho_{\mathrm{w}}) g}{\rho_{\mathrm{w}} \nu^2} \right]^{0.1}} \tag{3.12}$$

Where:

1. ***D*** represent the sediment particle diameter.
2. ***a*** represent the reference level, set equal to roughness height.
3. τ represent the bed shear stress.
4. τ_c represent the critical shear stress.
5. ρ_s represent the sediment density.
6. ρ_w represent the fluid density.
7. ***g*** represent gravity.
8. ν represent the fluid's kinematic viscosity.

3.2.2 Bed Load

Bedload is calculated using Van Rijn's bedload transport formula (1984):

$$q_{\mathrm{b}} = 0.053 {D_{50}}^{1.5} \left[(S_{\mathrm{s}} - 1) g \right]^{0.5} * \left(\frac{T^{2.1}}{{D_*}^{0.3}} \right) \tag{3.13}$$

Where:

1. $\boldsymbol{q_b}$ represent the volumetric transport.
2. $\boldsymbol{D_{50}}$ represent the median particle size by weight.
3. $\boldsymbol{S_s}$ represent the specific sediment gravity.
4. $\boldsymbol{D_*}$ represent the scaled particle parameter.
5. ***T*** represent the transport stage parameter.

Regarding the bed height, that is calculated by Van Rijn equation (1987). The effective roughness is modeled from Van Rijn formula (1987):

$$k_{\mathrm{S}} = 3 d_{90} + 1.1 \Delta \left(1 - e^{\frac{-25\Delta}{\tau_{\mathrm{c}}}} \right) \tag{3.14}$$

For further equations and explanations the Author suggest to look at *"Computational fluid dynamics in hydraulic and sedimentation engineering"* from N.R.B. Olsen (1999) and *"SSIIM User's Manual"* from N.R.B. Olsen (2018).

4 Singular Dike Configuration and Comparison

This study is focused on the effect of different spur dikes shapes, in a channel with 180°curve, in order to avoid scouring and sediment aggradation, with a particular attention to sediments continuity and flow channelization. Although the best effect of successions has already been proven with respect to singular shapes (Nayyer et al., 2019), in this study it was decided to analyse also the individual cases in order to understand the different behaviours of singular configurations and thus have a better and deeper understanding of the system's response towards successions interactions. The position of the different tested dikes, in singular configuration, was chosen at 90° along the curve because of geometrical reasons. In fact, 90° along the 180° curve appear to be the best position, for a singular structure, in order to mitigate the effect along the curve.

4.1 Channel Dimensions

The channel configuration used is the same for all the simulations, in order to have comparable results, and consists in a channel with two straight parts and a 180° curve, a constant slope of 2% and dimensions as follow in table 3 and sketch 4.1.1:

Table 3: Channel Dimensions.

Channel constant slope	2%	
Starting reference level	+0.712	*masl*
Ending reference level	0.000	*masl*
Length of straight parts of the channel	11.48	*m*
Channel width	1	*m*
Curve internal diameter	7.5	*m*
Curve external radius	4.5	*m*

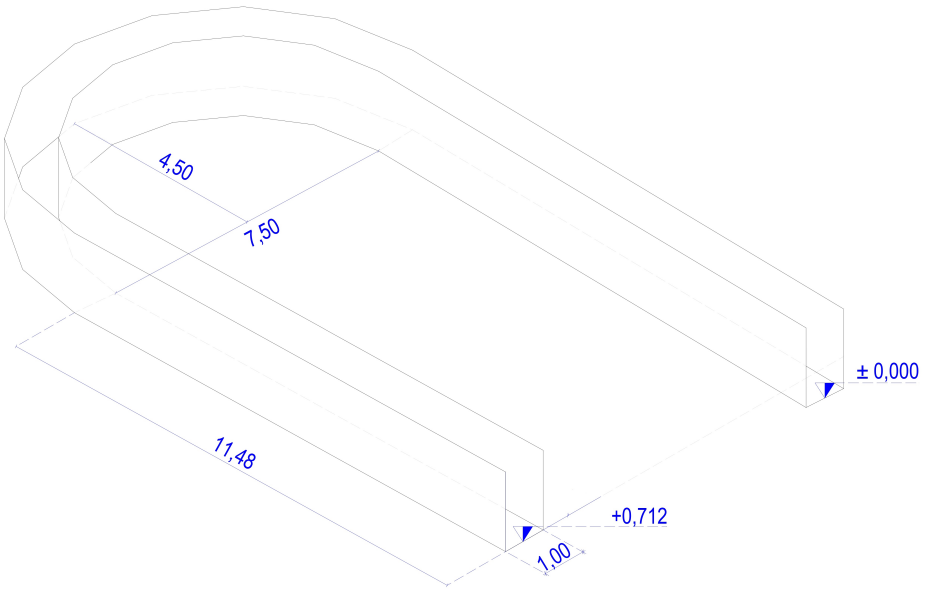

Figure 4.1.1: Channel dimensions.

4.2 Simulations Parameters

Set up a hydraulic numerical model in SSIIM is complex and needs deeper understanding of several themes as hydraulics, sediment transport, sediment characteristics and computing, because of the interconnection of these sets of parameters into the software. The same set has been used for all the simulations, both singular and successions configurations, in order to have comparable results. Thus, the only parameters that change from configuration to configuration are the spatial dimensions of the spur dikes structures. Here follows the list of parameters used and, in parentheses, the related command from the main set up *control* file.

- 0.007 Roughness for walls and bed (F16).
- 10.0 time step in sec and 100 as inner iterations (F33).
- 1500 n°of iteration for flow procedure and 5 as minimum iteration between water surface updating (K1).
- 0.053 m^3/s incoming flow (W1).
- Resulting simulation time from commands F33 and K1 of 4h and 10 min.
- Sediments Properties (G1, S and I and N commands):
  - 7 sediment sizes (see Table 4).
  - No sediment inflow.
  - Sediments are uniformly distributed in all the cells, at the start.

Table 4: Sediments characteristics.

Sediment n°	**Sediment size [m]**	**Fall Velocity [m/s]**	**Fraction**
1	0.0066	0.36	5%
2	0.0041	0.28	5%
3	0.0028	0.23	10%
4	0.0017	0.18	20%
5	0.0010	0.13	20%
6	0.0006	0.09	20%
7	0.0003	0.05	20%

- Free surface (F36).
- Transient sediment computation algorithm (F37).
- Bed load calculation from Van Rijn formula (F84).
- Law of walls (K2).
- Grid properties (G1, G3, G6):
  - 255 cross sections.
  - 21 grid lines on streamwise direction.
  - 6 grid lines in vertical direction.
  - Vertical grid distribution each 20% of water depth.
  - Free surface option.

4.3 Undisturbed Channel

For undisturbed channel the Author means the channel as set up from the previous section, without any structure in it. This is meant to show the natural behaviour on the flow under the stated conditions and is the basic condition from which to extrapolate the effects of the various configurations. The flux is flowing from the left channel towards the right. The results are extrapolated in a Paraview file in order to better understand and visualize the results. This is For a detailed analysis of the *control* file used, see Appendix A Figure I.

4.3.1 Results

The simulation results are in accordance with the theory described before and the effects actually measured in real channels. The flow interact with more strength on the outer side of the curve where the stream deflection is made. The simulation has highlighted a bed level deepening in the outer side of the bend due to the centrifugal force of the flux because of the channel flow-deflection.

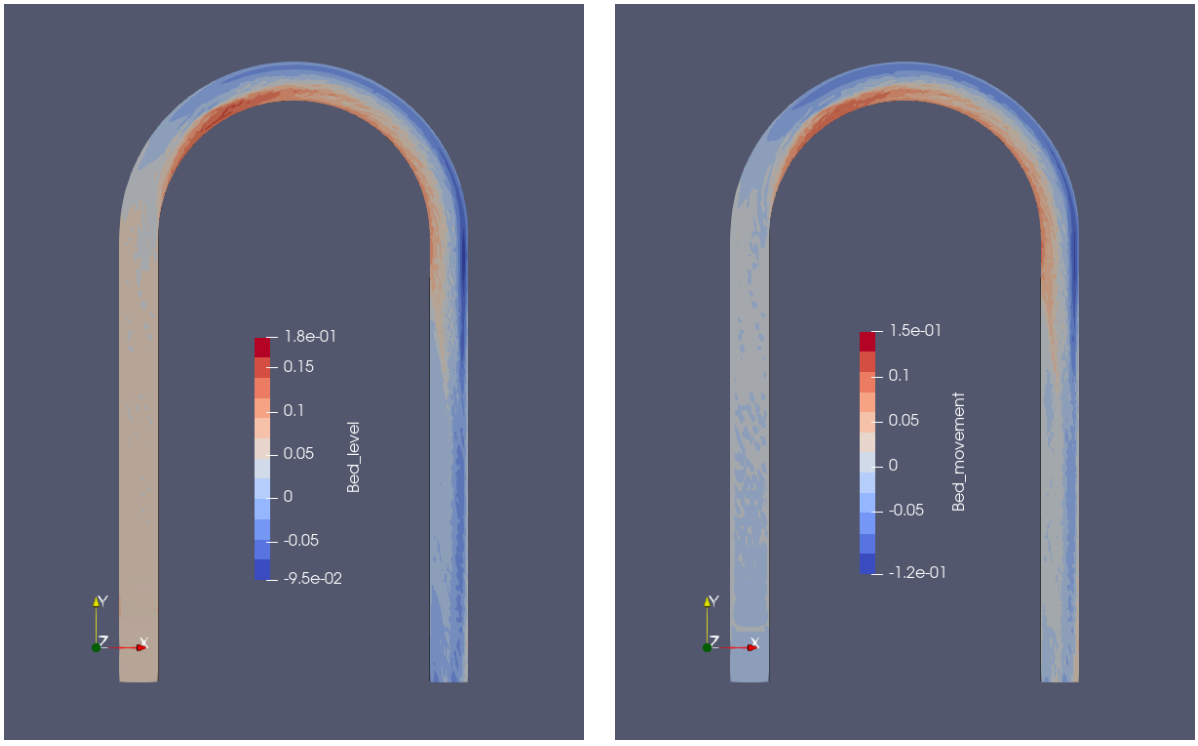

(a) *Bed Level* (b) *Bed Movement*

Figure 4.3.1: Undisturbed Channel Bed Results.

The deepest level is at the end of the curve, on the outer side and is about -0.095 m respect the starting level. The secondary current formed by the flux deflection due to the 180°curve causes a sediment deposition towards the inner side of the curve. This mechanism enhance the sediment aggradation and the related creation of a lateral gradient. The sediment deposition pattern is extrapolated from Figure 4.3.3 (b) showing the deposition of the finest fraction on the inner side of the curve and the bigger fraction on the outer side as result of sediment aggradation and lateral gradient formation. This morphological parameter is not constant and unique all over the bend, neither in the system. Therefore in order to understand the magnitude of the resulting gradient, the average of lateral gradients extrapolated from 5 positions along the curve (precisely at 60°, 90°, 120°, 150°and 180°along the curve) has been made.

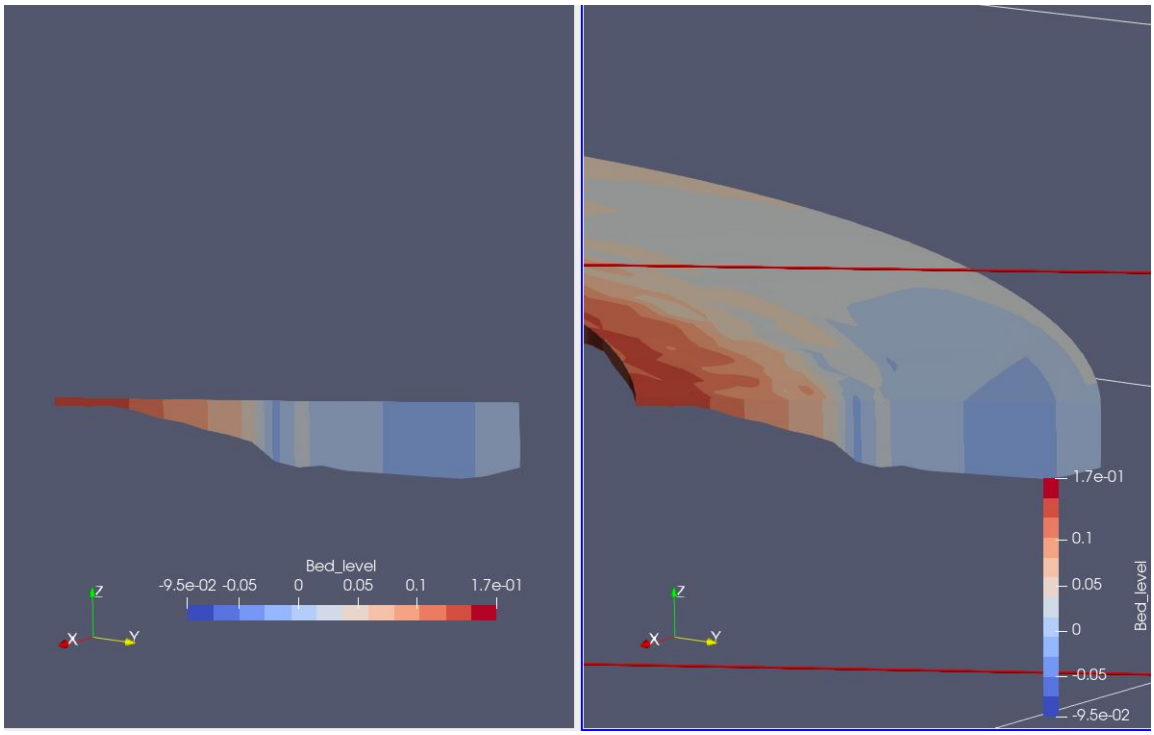

Figure 4.3.2: Channel cross section at 60°.

Each lateral gradient has been extrapolated from the system cross-section at the specific angle of reference along the curve, meaning 0° as reference angle for the first curve-cross-section, from upstream, and 180° for the last. From Figure 4.3.2 is clear that the bed level is not linear nor constant along the section, therefore the gradient has been extrapolated as the angle between the deepest point of the cross-section and the bed level at the inner side.

Table 5: Undisturbed Channel Lateral Gradient along the curve.

Undisturbed Channel	
Reference Angle [°]	*Lateral Gradient [°]*
60	*10.63*
90	*9.08*
120	*9.27*
150	*9.52*
180	*11.56*
Averaged Lateral Gradient	**10.01°**

The bed movement shows how and where the bed level changed from the initial condition. The result follows the bed level output and is strictly related to it. The bed shear stress result shows how the stress behave on the bed of an undisturbed channel. The result clearly shows high stresses on the outer side of the bend, while the inner side is barely affected. This pattern results in a deepening of the channel on the outer side due to the high shear stress, that is able to start the incipient motion of a bigger size of particles and their transport towards downstream, leading to a high scouring of the bed level and higher forces acting on the outer bank, as possible

cause of erosion. The low stress acting on the inner side is favouring the sediment deposition of the fraction that is moved by the secondary currents. The secondary current has lower strength then the main current, resulting in a incipient motion of just the smallest fractions of sediments.

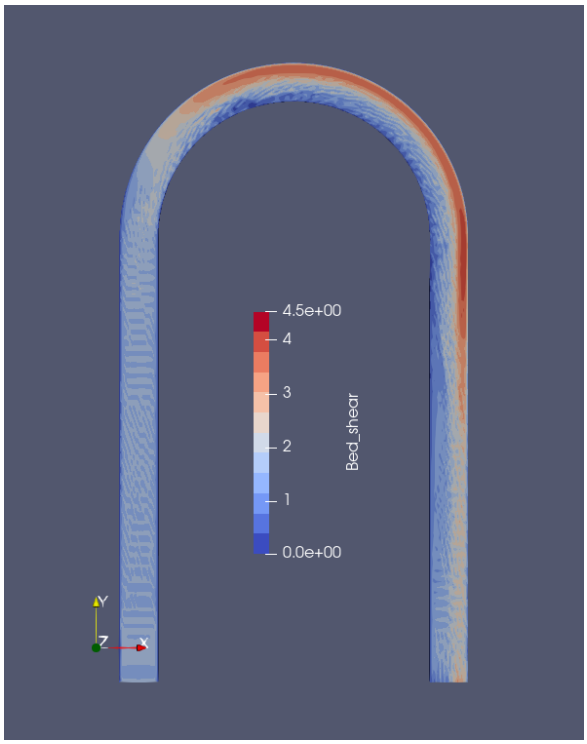

(a) *Bed Shear Stress*

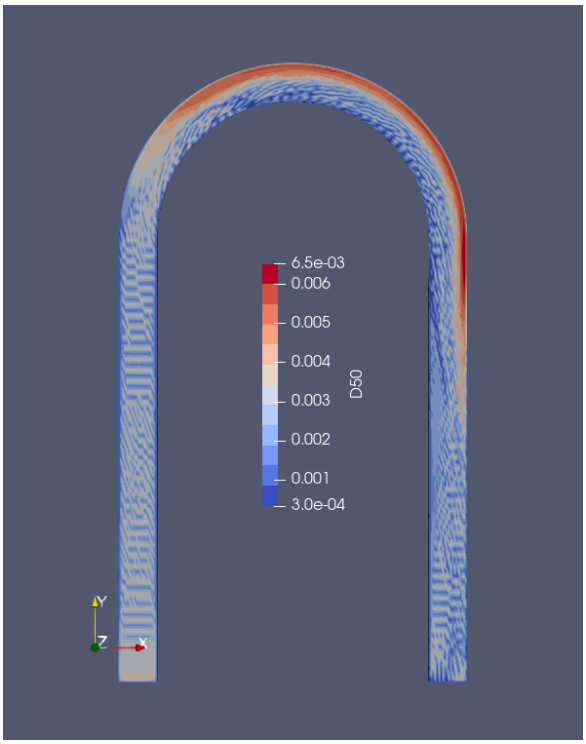

(b) D_{50}

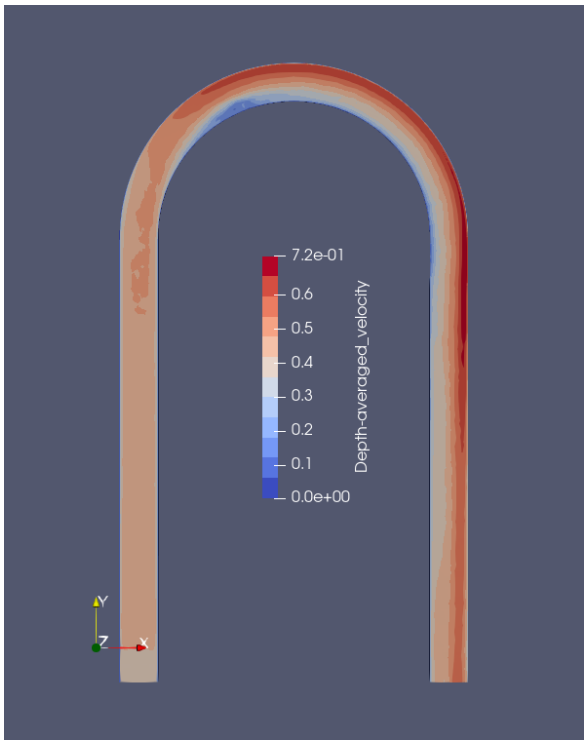

(c) *Depth Averaged Velocity*

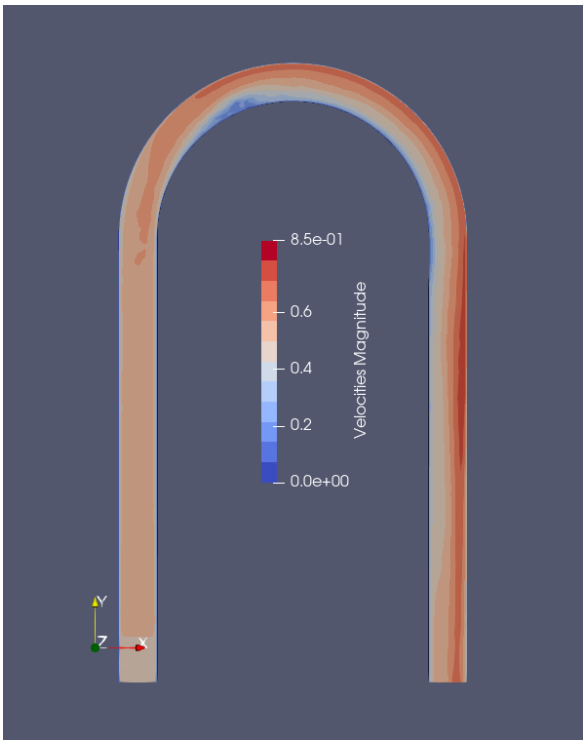

(d) *Velocity Magnitude*

Figure 4.3.3: Undisturbed Channel Results.

These results shows how in a realistic situation the outer side of a river bend is often heavily

affected by flow scouring. Moreover, shows how the river morphology could change as function of the stresses induced by the flow. Sediment deposition is showed at the inner side of the curve, specially in the first half, where the secondary current generated is stronger respect at the end of the curve. This is confirmed by D_{50} result that shows how only the biggest fraction of the sediments are present on the outer side of the channel, where the stresses are higher. This is accordingly to what previously stated, regarding higher shear stress on the outer side of the bend, resulting in a higher sediment-size incipient motion capability of the flow. Its also interesting to see how the bed shear stress pattern results in changes in bed morphology along the straight channels and the consequent formation of dunes.

From an hydraulic point of view, the velocity profile is an important indicator of the shear stress behaviour. The results confirm the relationship between velocity and shear stress. In particular the depth-averaged velocity represent the mean velocity averaged over the cross-sectional depth, while the velocity magnitude is the velocity vector calculated as:

$$VelocityMagnitude = \sqrt{U^2 + V^2 + W^2} \tag{4.1}$$

Where U, V and W are the 3 velocity vectors directed towards x-axes, y-axes and z-axes respectively. These parameters are important in order to understand the hydraulic response of the system, the consequent bed shear stress pattern resulting from the velocity conditions along the channel and the sediment distribution. The higher velocity is situated on the outer side of the channel where occurs higher stresses, then higher scouring, so bed level deepening and bigger sediment fraction sedimentation. The results shows also a low depth-averaged velocity index on the inner side of the first half of the turn corresponding to the higher sedimentation area, lower shear stress and higher bed level.

4.4 Singular I-Shape Configuration

This is the most intuitive spur dike shape. It has been positioned at 90°on the curve, corresponding to the middle. The dimensions of the spur dike used is reported in the picture 4.4.1, the spur dike height is set to the 60% of the water depth. The results are extrapolated in a Paraview file in order to better understand and visualize the results. The results shows how this shape is able to deflect the flow energy but is not managing as good as wanted the stress pattern both upstream and downstream. For a detailed analysis of the *control* file used, see Appendix A Figure II.

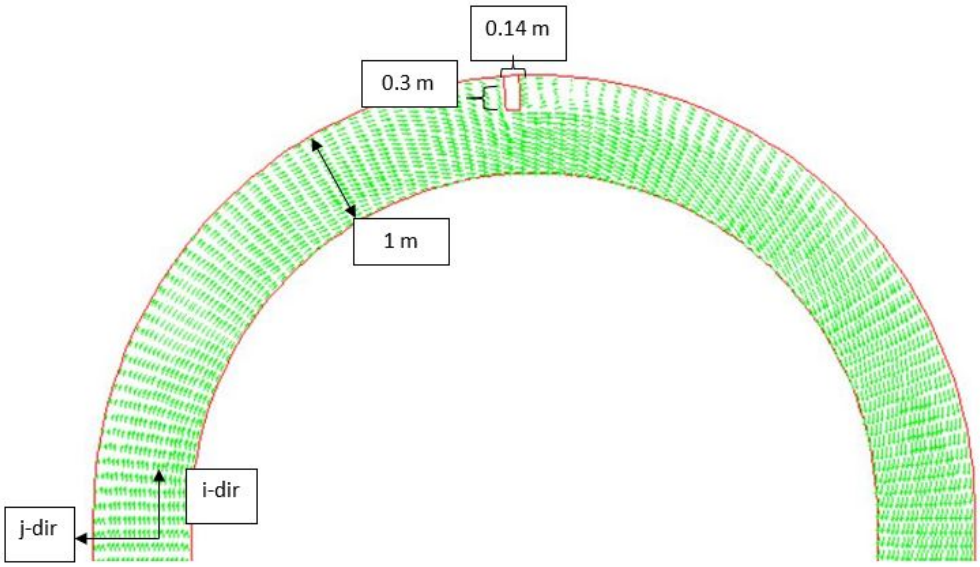

Figure 4.4.1: I shape spur dike (SSIIM view).

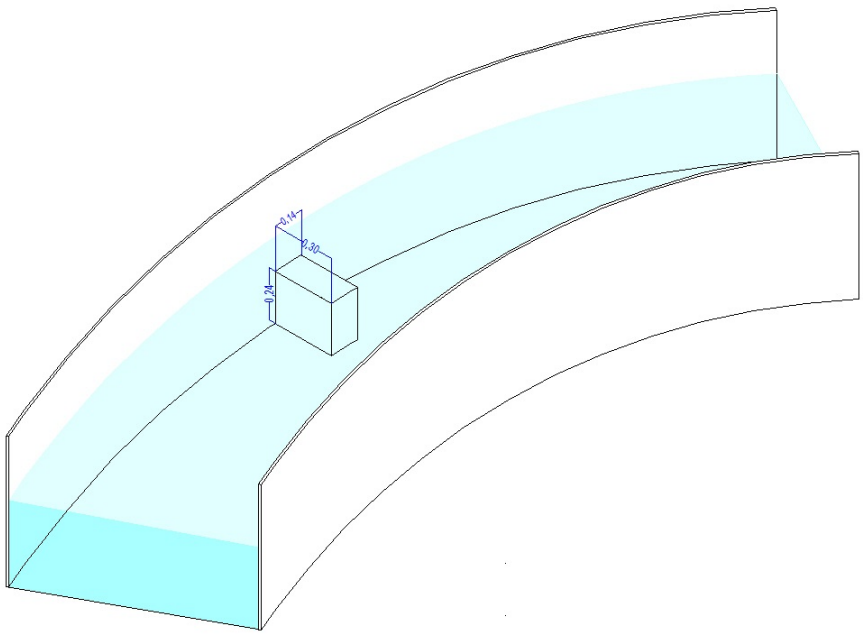

Figure 4.4.2: I shape spur dike (CAD view).

4.5 Singular L-Shape Configuration

The L-shape type of spur dike was chosen to be analyzed due to its shape that can be considered the link between the T-shape, already deeply studied on a 90°bend (Vaghefi and Radan (2016), Vaghefi et al. (2017), Vaghefi et al. (2018b), Vaghefi et al. (2019), Vaghefi et al. (2018a), Vaghefi et al. (2015), Vaghefi et al. (2012)), and the new BL-shape. Moreover the results from Nayyer et al. (2019) about the goodness of this specific shape, specially in successions, has made worth its analysis. The results are extrapolated in a Paraview file. The dimensions of the spur dike used is reported in the picture 4.5.1, the spur dike height is set to the 60% of the water depth. For a detailed analysis of the *control* file used, see Appendix A Figure III.

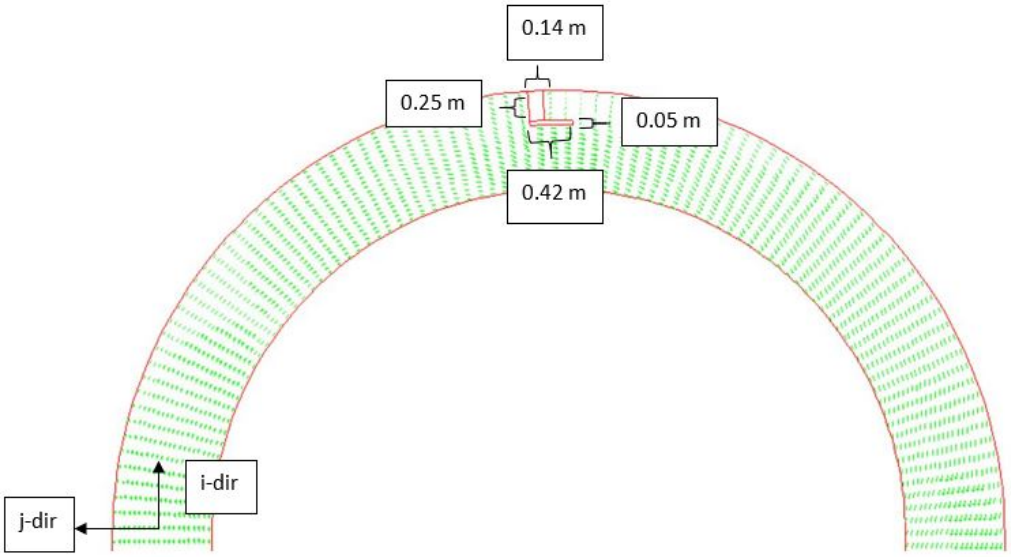

Figure 4.5.1: L shape spur dike (SSIIM view).

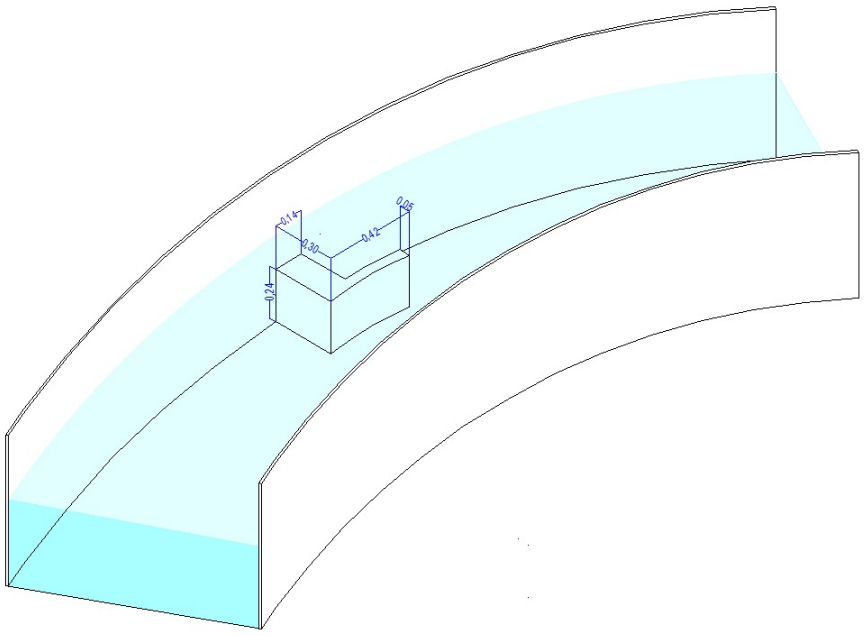

Figure 4.5.2: L shape spur dike (CAD view).

4.6 Singular T-Shape Configuration

T-shape spur dike is the most studied dike-shape (Vaghefi and Radan (2016), Vaghefi et al. (2017), Vaghefi et al. (2018b), Vaghefi et al. (2019), Vaghefi et al. (2018a), Vaghefi et al. (2015), Vaghefi et al. (2012), Nayyer et al. (2019)t). Therefore is interesting to understand the differences in behaviour between a T-shape spur dike and the other shapes and what makes it a competitive alternative. The results are extrapolated in a Paraview file. The dimensions of the spur dike used is reported in the picture 4.6.1, the spur dike height is set to the 60% of the water depth. For a detailed analysis of the *control* file used, see Appendix A Figure IV.

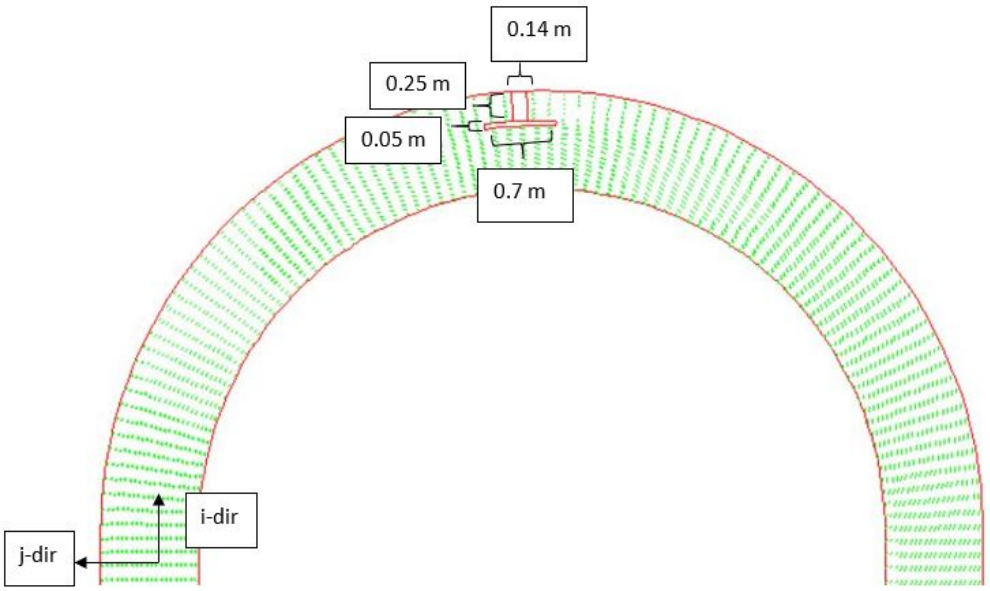

Figure 4.6.1: T shape spur dike (SSIIM view).

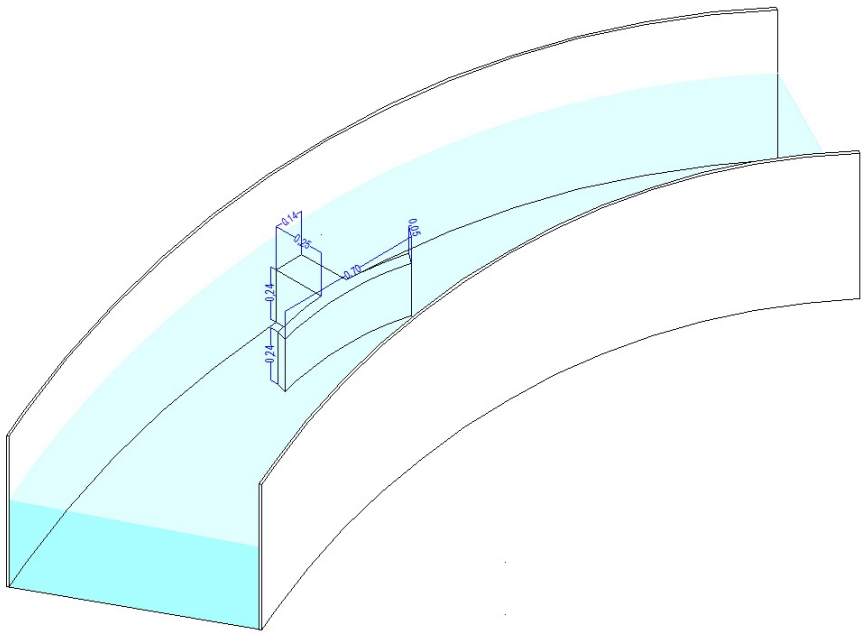

Figure 4.6.2: T shape spur dike (CAD view).

4.7 Singular Broken L-Shape Configuration

This shape was designed by the Author based on the thought that, in order to distribute the bed shear stresses, an alternative flow path will help to decrease flow channelization and consequently the stream velocity and the related shear stress on the boundaries; moreover it will help the continuity of the sediments and decrease the resulting lateral gradient. It consists in an L-shape, similar as the one analyzed before, with an opening in the structure that could be theoretically moved accordingly to the bank-shear protection and bed movement pattern requirements. While the opening is moved towards the outer side of the curve, it will result in a lower bank-shear protection, corresponding in a higher bed shear stress on the outer side, but a higher sediment movement and consequent better sediment continuity. The opening position chosen was conceived to be the options that gave best balance between bank-shear protection, sediment continuity, avoid sediment aggradation and encourage energy dissipation. The results are extrapolated in a Paraview file in order to better understand and visualize the results. The dimension of the spur dike used is reported in the picture 4.7.1. For a detailed analysis of the *control* file used, see Appendix A Figure V.

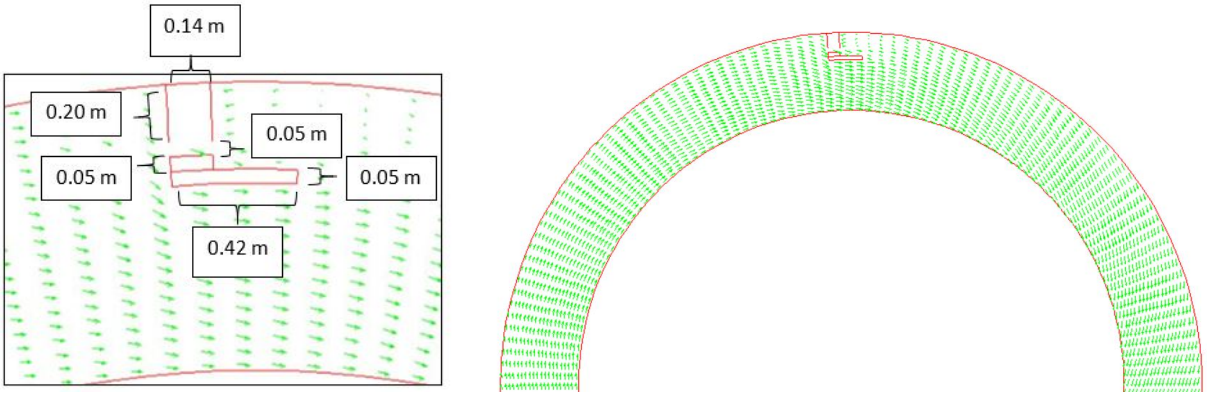

(a) (b)

Figure 4.7.1: BL-shape spur dike (SSIIM view) and details.

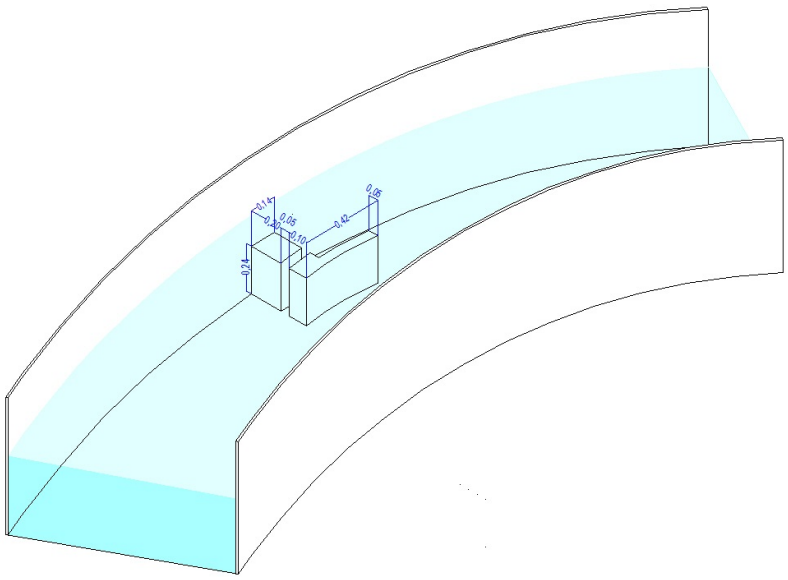

Figure 4.7.2: BL-shape spur dike (CAD view).

4.8 Singular Configuration Shapes Comparison

In order to better understand the differences between the effects of all the analyzed shapes with the flux, is here reported a comparison between all the simulated aspects of the singular spur dike configurations. The result of this comparison shows how all the analysed dikes shapes will help prevent scouring and sediment aggradation also if with different magnitude. Furthermore, a single spur dike seems not to be enough to provide a sufficient scour prevention function along the entirety of the curve due to their not long enough reattachment zone. Successions of spur dikes, then, could be a solution in order to provide sufficient bank protection, avoid sediment aggradation and flow channelization. The number of structure to be used in the successions has been determined from a rough analysis of the reattachment zone length (or angle) of the singular shapes configurations. The reattachment angle is considered as the angle along the curve towards downstream, from the structure position, after that the bed shear stress takes effect again on the outer side of the turn. In particular has been found from the simulation results (see following Sections) that the reattachment angle of singular configuration as T and I is about 35°, wile L and BL have about 30°. Successions of dikes could prevent scouring due to the partial shear-deflection toward the middle of the channel, done by the dike itself, and due to the creation of the "pools" in between the dikes succession. In the pools the velocity is not sufficient to generate high stresses and, in case of BL-shape spur dike, could be dimensioned to help the sediment continuity towards downstream by dimensioning the opening.

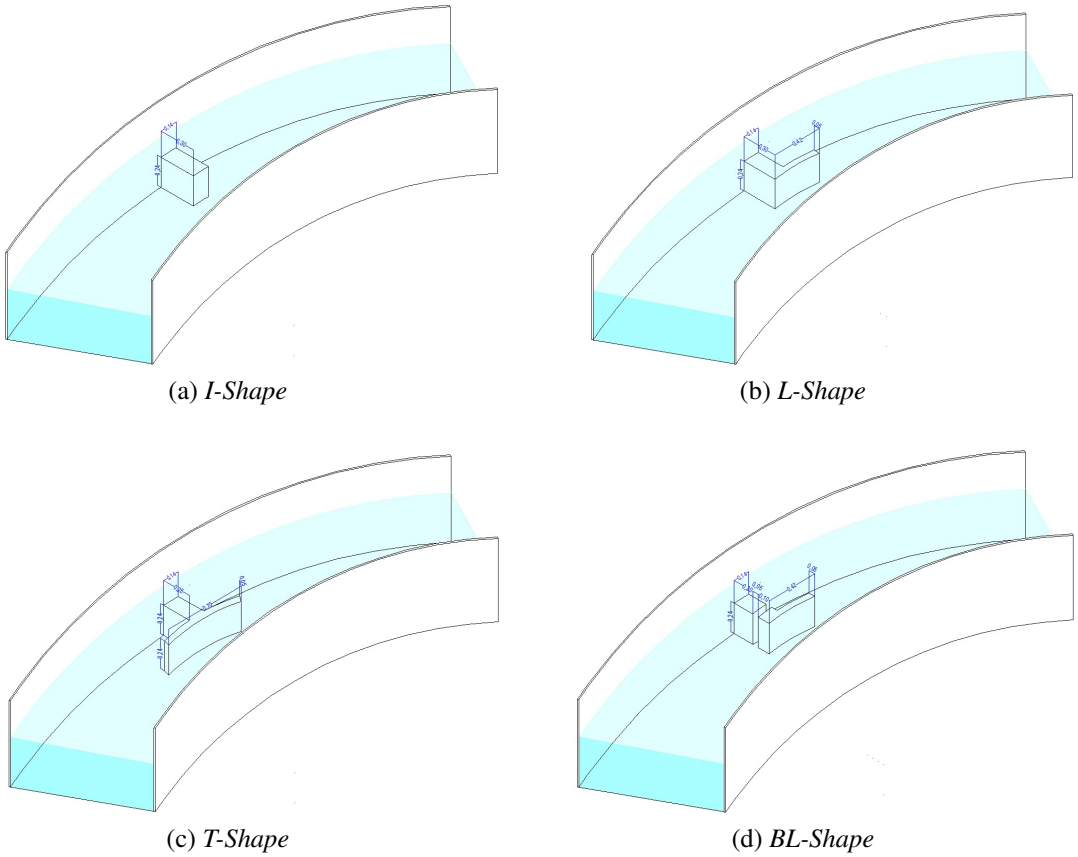

(a) *I-Shape* (b) *L-Shape*

(c) *T-Shape* (d) *BL-Shape*

Figure 4.8.1: Shapes Analyzed.

4.8.1 Bed Level and Bed Movement Comparison

The bed level results (Figure 4.8.2 in the next page) represent the morphological changes in the system due to the action of the flow forces and the interaction of the dike structure/s with the stream. The bed movement results (Figure 4.8.3) represent how much and where the morphological changes happened respect the initial system conditions, due to the action of the flow forces and the interaction of the dike structure/s. The bed movement results are related and very similar to the bed level one, and the causes are the same. The bed level is determined by the interaction of the bed shear stress with the bed layer. This result in scouring and deposition of sediment accordingly to the bed shear stress pattern along the system (see Figure 4.8.5). Bed level, bed movement, bed shear stress, D_{50} and the velocity pattern are all interlinked, as hydraulic and sedimentology relationship. In particular a change in the hydraulic response of the system, due to the presence of a new structure, results in a modification of the velocity parameter due to the change of cross section. The increase/decrease of the velocity parameter generate an accordingly increase/decrease of the bed shear stress pattern, specially around specific areas more under the influence of the new condition. The modification of the bed shear stress pattern turns both in a change in bed level and a consequent modification of the D_{50} distribution over the channel.

The results of the simulations shows similarities among the different shape alternatives. All the shapes present flow channelization corresponding to the dike structure, with a small deeper trench corresponding to the toe of the structure. The flow forces are deflected, due to the dike interaction, from the outer to the mid part of the channel, but a single dike interaction seems to not be able to protect the outer-end-side of the turn, due to the interaction of the second half of the turn with the dike-deflected-flow direction, causing a bed level deepening on the outer side, in all the singular configurations. Towards upstream, all the configurations shows a mitigation of the stream effects on the bed level with milder distribution respect the undisturbed channel. Sediment deposition appears at the inner side of the curve in all configurations, also if with different magnitude. This phenomenon is due to the secondary currents redistribution that promote the movement of the lighter fractions of sediments tangentially respect the main flux, favouring the deposition along the inner side, where the bed shear stresses are lower (see Figure 4.8.5).

Among the different configurations analyzed, T-shape and I-shape are the configurations that have higher sediment deposition at the inner sides, greater depth of the trench corresponding to the dike's toe and greater depth and length of the trench on the outer-end-side. The depth of the trench corresponding to the dike's toe is because of the flow channelization due to the shrinking of the cross section caused by the structure presence. The channelization and shrinking of the cross section increase the flow velocity and the related bed shear stress, resulting in an higher scour of the bed layer due to the flow forces. Milder distribution of the bed level has been achieved with L and BL-shapes. This structures interact with the streamflow resulting in a lower depth of the trenches and lower sediment deposition. L-shape have the best response among the analyzed configurations towards the bed level distribution downstream the structure interference, both as deepness and distribution of the outer-end-side trench and sediment deposition. BL-shape configuration, on the other hand, give the best system response towards the bed level distribution around the dike structure with the milder deepness of the trench related to the structure's toe. Immediately after the dike, on the outer side of the turn, the level is unchanged in all configurations because the shear stress action is approximately zero (see Figure 4.8.5).

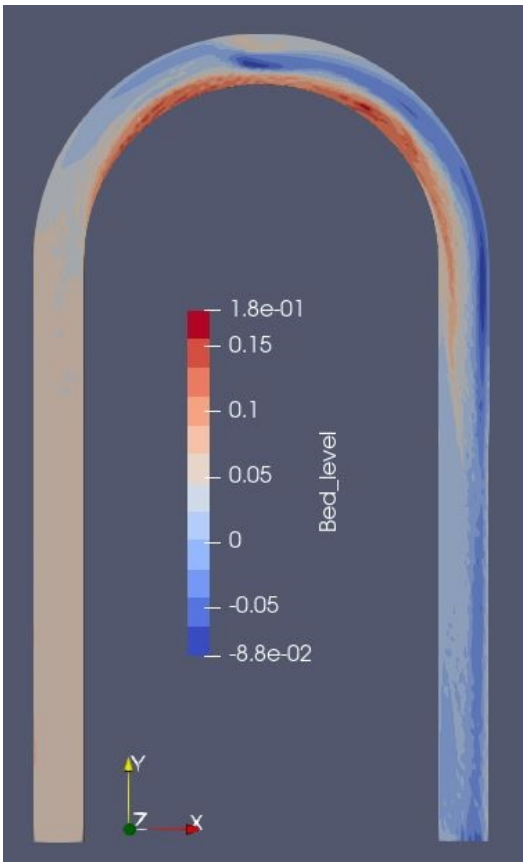

(a) *I-Shape*

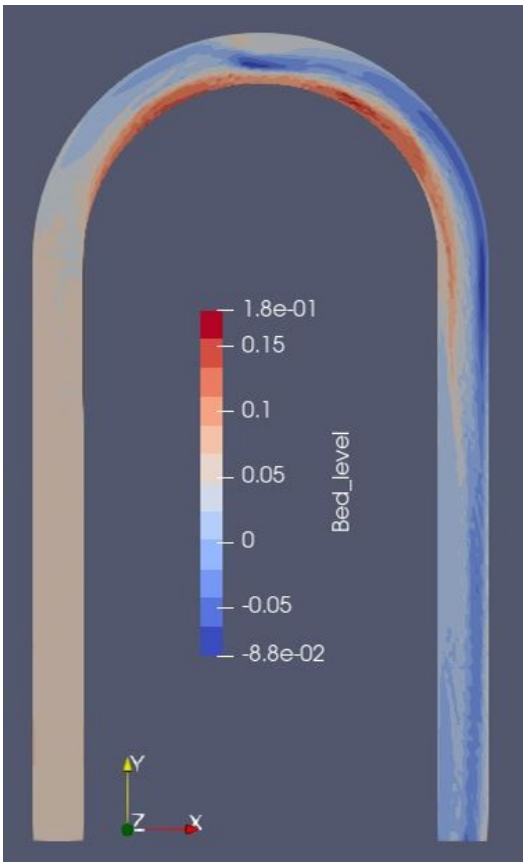

(b) *L-Shape*

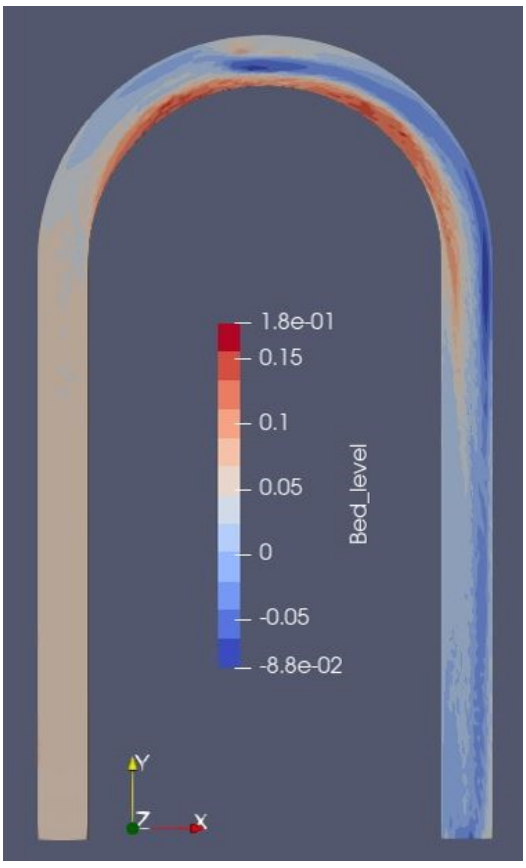

(c) *T-Shape*

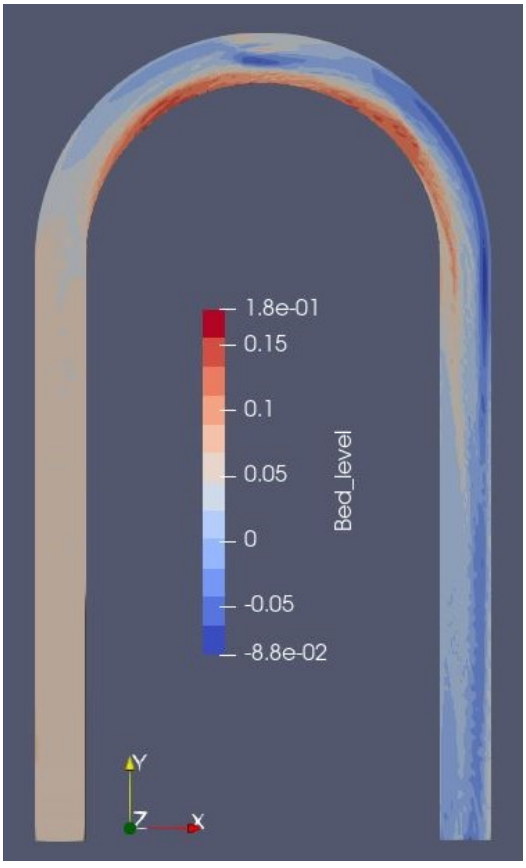

(d) *BL-Shape*

Figure 4.8.2: Bed Level Comparison

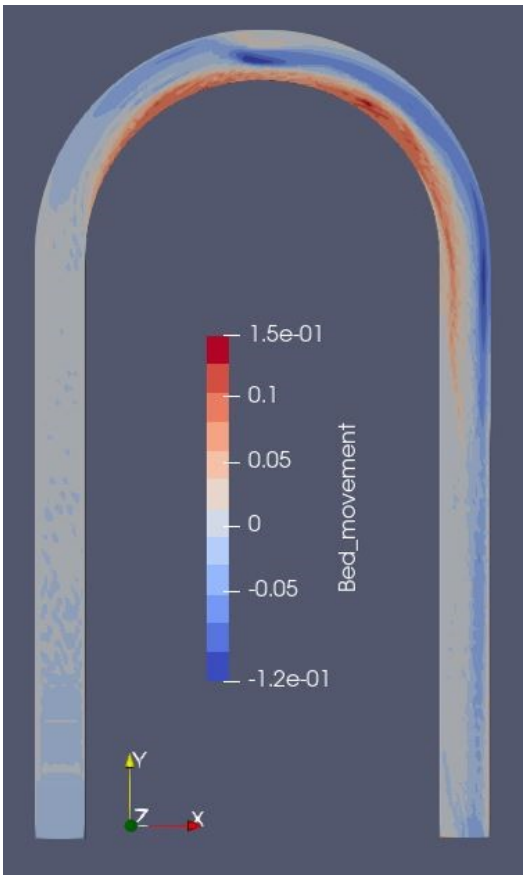

(a) *I-Shape*

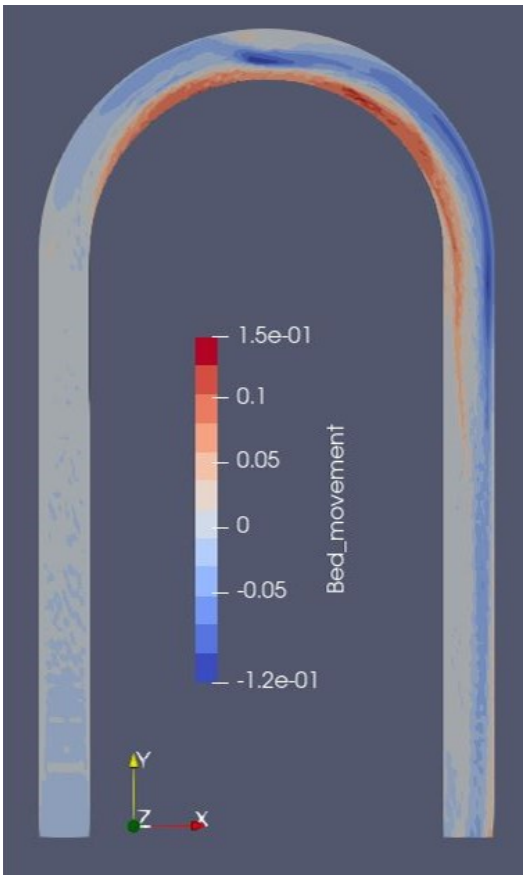

(b) *L-Shape*

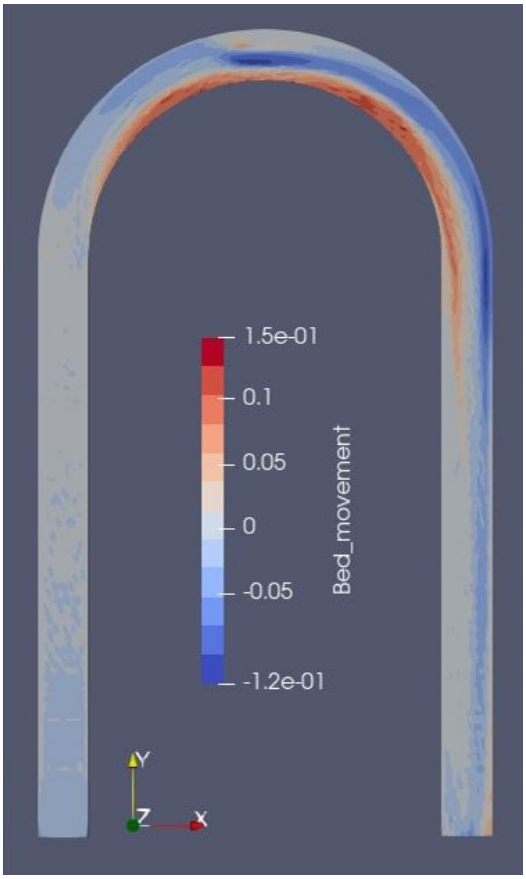

(c) *T-Shape*

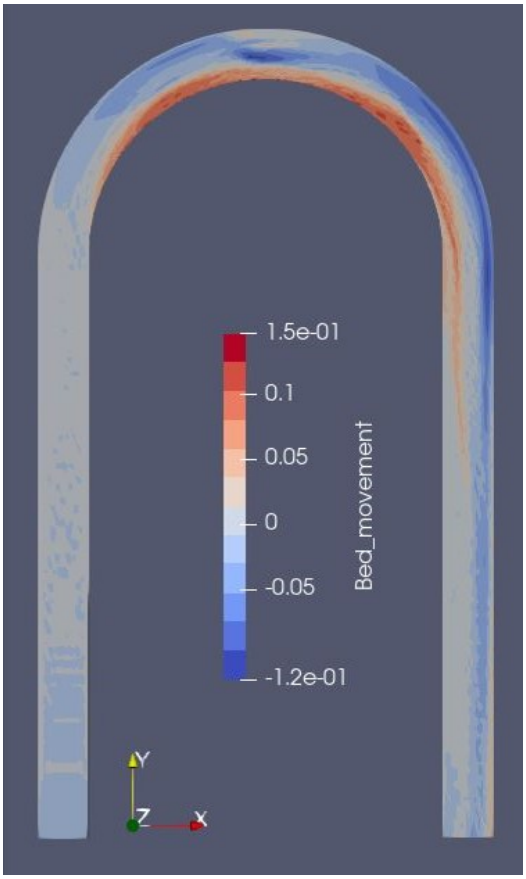

(d) *BL-Shape*

Figure 4.8.3: Bed Movement Comparison

4.8.2 Bed Shear Stress Comparison

The bed shear stress results (Figure 4.8.5 in the next page) represent the shear stress pattern acting on the boundaries of the system due to the action of the flow forces and the interaction of the dike structure/s with the stream. The bed shear stress pattern is the flow force that interact with the bed layer and is the driving parameter that determines morphological changes. Bed shear stress is strictly related to the velocity pattern (see Figure 4.8.7).
The results of the simulations shows similarities among the different shapes alternatives. The flow forces are deflected, due to the dike interaction, from the outer to the mid of the channel, but as stated before, a single dike interaction seems to not be able to protect the outer-end-side of the turn, due to the interaction of the second half of the curve with the dike-deflected-flow direction, resulting in a problematic bed shear stress pattern. Also the upstream reach of the system, respect the dike structure, seems to be affected by bed shear stresses on the outer side of the curve, also if with low magnitude. Low bed shear stresses act along the inner side of the curve for all the singular configurations resulting in a rise of the bed level and sediment deposition. All the configurations have shown an area of particular low bed shear stress at the inner side of the second half of the turn. Immediately after the dike the shear stress action is approximately zero due to the dike shielding, except for BL-shape. BL-shape avoid the calm region behind the dike thanks to the opening in the structure but still maintain the shear protection function.

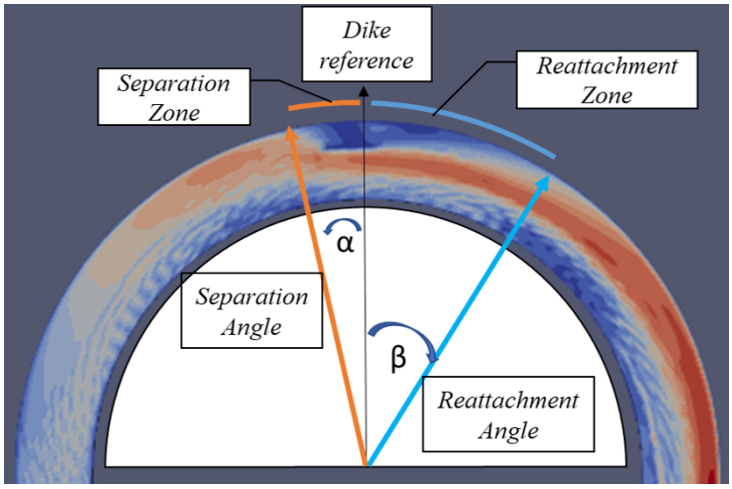

Figure 4.8.4: Separation and Reattachment for T-shape.

Among the different configurations analyzed, the bed shear stress seems to be better handle on the first half of the curve, upstream the structure, by L-shape and T-shape. Nonetheless BL-shape better manage the bed shear stress downstream the structure both at the inner as at the outer side of the curve with milder magnitude and better distribution. The flow channelization caused by the shrinking of the cross section due to the structure presence and the consequent increase of the velocity pattern result in the related increase of the bed shear stress. The downstream area, respect the structure, of bed shear stress pattern close to zero is similar for I, L and T-shapes, while the peculiar dimensions of the BL configuration result in a thinner area, along the outer side of the curve downstream the dike, but almost equal length respect the other shapes. The reattachment angle is the angle corresponding to the reattachment zone after the dike interaction. The reattachment zone is considered as the zone downstream the structure where the bed shear stress is deflected from the boundary, so the area in which the bed shear stress is close to zero. This can therefore be considered as the downstream area, on the outer side of the turn, protected by the dike interaction (see Figure 4.8.4). Separation zone is based on the same concept as reattachment zone, but upstream the dike structure. The reattachment angle for the different configurations are similar. T-shape and I-shape have a reattachment angle about 35°, while L-shape and BL-shape have it at 30°. Therefore, in order to provide sufficient scour prevention function, along the entirety of the turn, a succession of structure is needed.

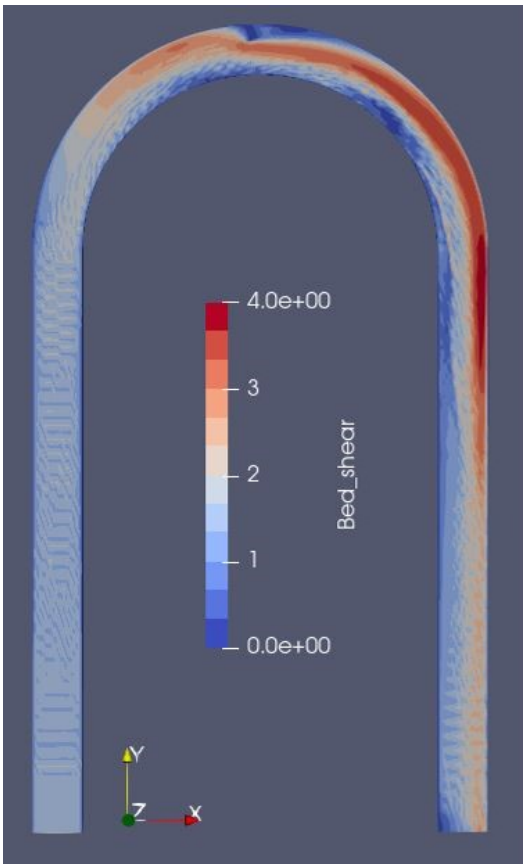

(a) *I-Shape*

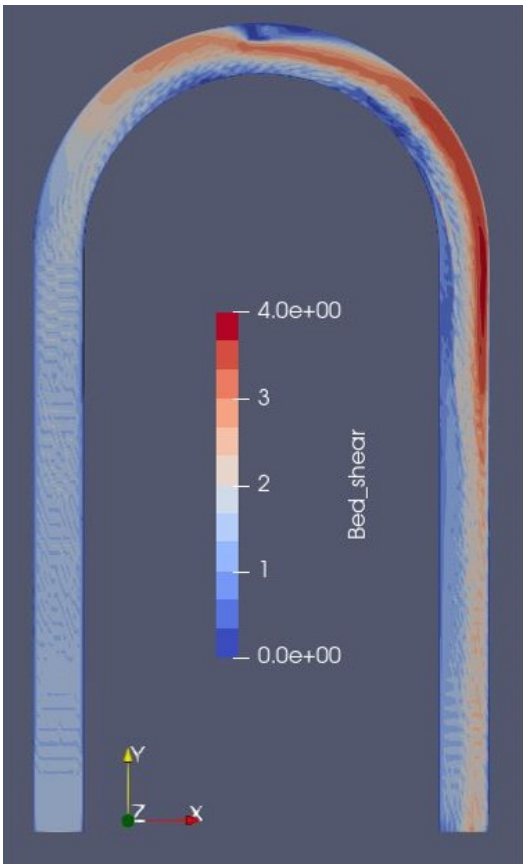

(b) *L-Shape*

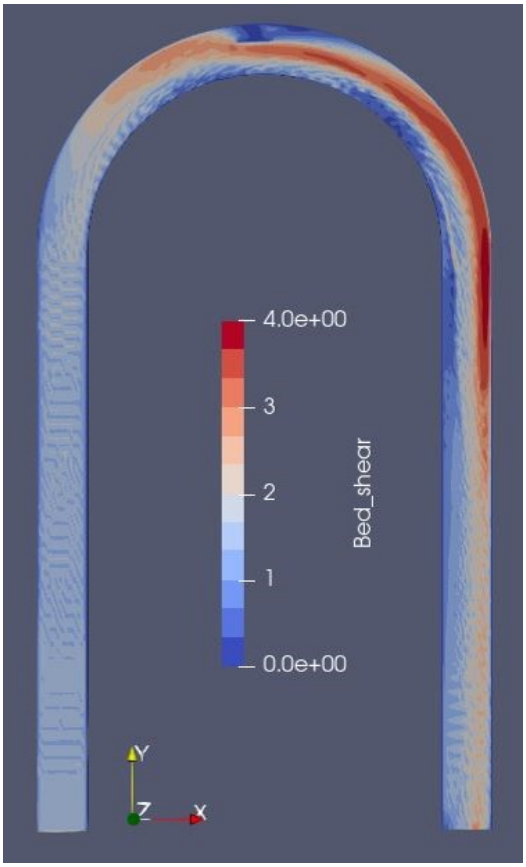

(c) *T-Shape*

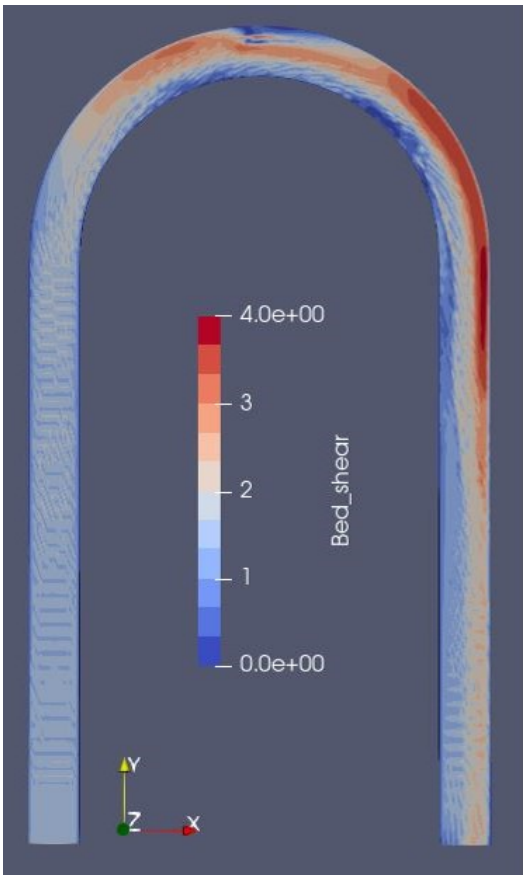

(d) *BL-Shape*

Figure 4.8.5: Bed Shear Stress Comparison

4.8.3 D_{50} Comparison

The D_{50} results (Figure 4.8.6 in the next page) represent the granulometric distribution of the sediments in the system, using a particle size distribution or, more precisely, the median grain size (D_{50}). This parameter is important in order to understand the sediments distribution as function of sediments granulometry and bed shear stress conditions. Therefore, D_{50} distribution is strictly related to the bed shear stress pattern (see Figure 4.8.5).

The results of the simulations show different behaviours from shape to shape. Configurations that resulted in high bed shear stress have shown, as expected, higher values and a wider distribution of D_{50}. The shapes that better manage the upstream bed shear stress pattern have shown a lower D_{50} value on upstream while the spatial distribution is almost the same for all the simulated configurations. Therefore all the shapes, except for BL, have a very similar value of D_{50} on the upstream part. A slightly worse management of the parameter has been detected from BL-shape as a consequence of its worse bed shear stress pattern generated. A calm zone has formed behind the dike due to the structure's shielding. T and I configurations have shown a smaller D_{50} values in the calm zone, while L shape result in a slightly more dynamic behaviour. The main mechanism of deposition in this area is related to secondary currents effects and turbulences that start incipient motion, transport and deposition of just the smallest sediments diameters. Differently, for BL-shape, the area immediately after the dike, due to the opening in the structure, is more dynamic and helps to distribute the energy gradient from the flow in a broader area, avoiding the calm zone and improving the general condition of the overall system downstream the structure. Consequently an overall lower distribution of D_{50} has been shown downstream the BL-shape dike.

On the outer-end-side of the curve, critical areas with high D_{50} have been detected for all the analyzed shapes. Particularly T and I-shape, that have bed shear stress-related problems in that area (see Figure 4.8.5), have shown the higher D_{50} values, among the analyzed alternatives. BL-shape, by this point of view, is presenting the best D_{50} management downstream the dike because of, as stated before, a wider distribution of the flow energy, thanks to the opening interaction. Corresponding to the dike's toe each shape, except BL-shape, have shown high D_{50} values due to flow channelization. BL configuration, thanks to the structure-opening action, is able to widen the flow cross section at the dike structure, decreasing the overall velocity and consequently lowering and distributing the bed shear stresses in a wider area. In the channel corresponding to the BL-dike structure opening, a high D_{50} value, as result from high velocity index and bed shear stress response for that area, has been found. High D_{50} value in that zone is to be considered a good value in order to avoid sedimentation and opening occlusion. Ripples and dunes formations along the channel can be observed from this computations results.

Along the entirety of the inner side of the curve a low D_{50} has been detected for all configurations. Because of that, just the smaller fractions of sediments will be moved and deposited along the inner part of the curve, principally due to secondary currents and turbulence motions. This result confirm the deposition pattern as shown from bed level and bed movement (Figure 4.8.2 and Figure 4.8.3) and bed shear stress results (Figure 4.8.5).

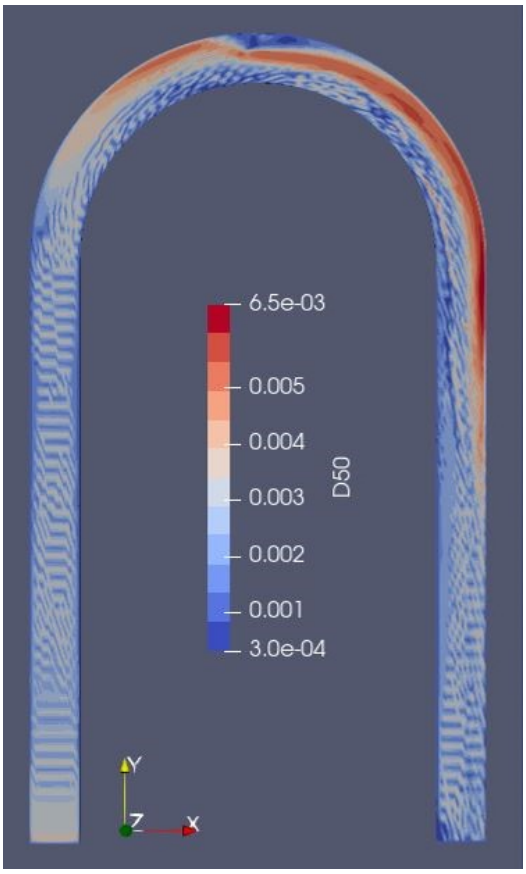

(a) *I-Shape*

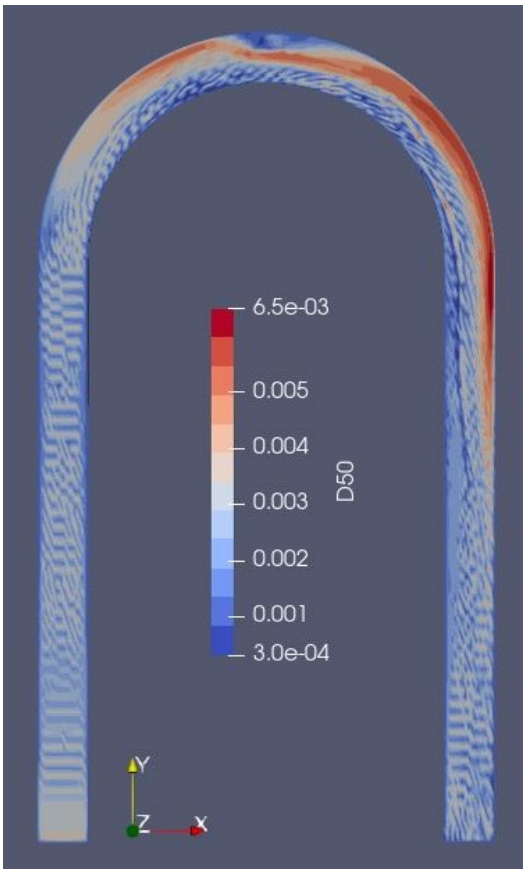

(b) *L-Shape*

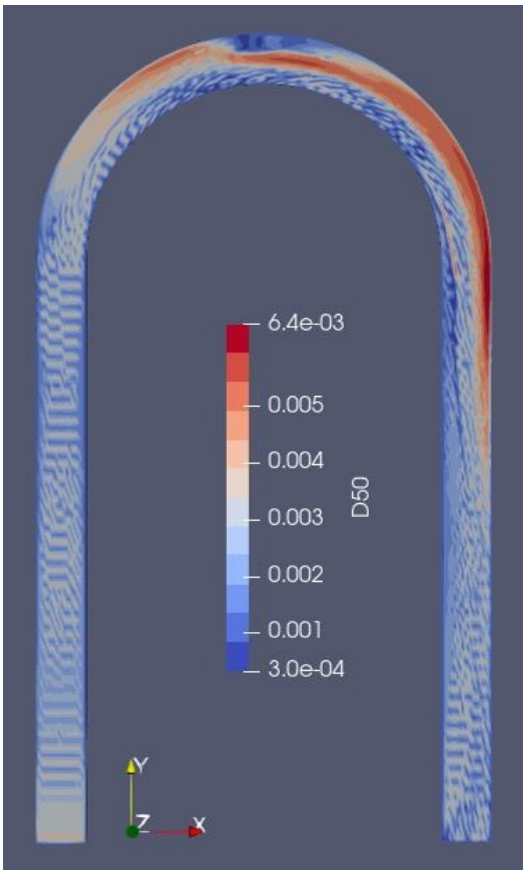

(c) *T-Shape*

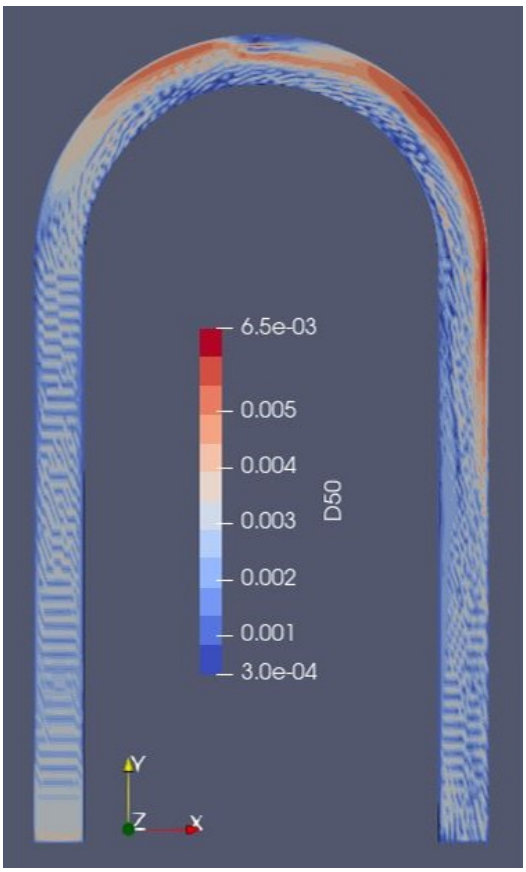

(d) *BL-Shape*

Figure 4.8.6: D_{50} Comparison

4.8.4 Depth-Averaged Velocity and Velocity Magnitude Comparison

The velocity results (Figure 4.8.7 and Figure 4.8.8 in the next pages) represent the hydraulic response of the system after the dike perturbation. In particular the depth-averaged velocity represent the mean velocity averaged over the cross-sectional depth, while the velocity magnitude is the velocity vector calculated as:

$$VelocityMagnitude = \sqrt{U^2 + V^2 + W^2} \tag{4.2}$$

Where U, V and W are the 3 velocity vectors directed towards x-axes, y-axes and z-axes respectively. These parameters are important in order to understand the hydraulic response of the system, the consequent bed shear stress pattern resulting from the velocity conditions along the channel and the sediment distribution.

The results of the simulations shows different magnitude of velocity index between the different simulated shapes, but also similar spatial distributions and same critical areas. The upstream management of the velocity parameters is very similar between I, L and T configurations, while we observe a slightly increase in the upstream velocity index for BL-shape. A zone of relative high velocity indexes on the outer side ha been noticed upstream the dike structure. The worse management of the upstream hydraulics is due, again, to the BL-opening function. Differently from the other shapes, the flux is not completely deflected and diverted from the bottom towards above the structure and the middle part of the channel because of the BL-opening interaction that allows a small fraction of the flow, acting on the outer side, to keep its behaviour, as seen from the undisturbed channel results (Figure 4.3.3). In I, L and T configurations, a calm zone, with low velocity indexes both as depth-averaged and magnitude, has formed behind the dike due to the structure's flow shielding. BL-shape, otherwise, form a calm layer along the outer boundary instead of creating an area throughout the entire length of the dike. As stated before, the opening in the BL configuration is the driving feature that allows the flow to be more dynamic after the dike interaction and allows a broader distribution of the flow forces, improving the general condition of the overall system downstream the structure. The consequent velocity indexes in the BL-opening shows a channelization of the flow and therefore a high velocity index, both as depth-averaged as magnitude.

On the outer-end-side of the curve, critical areas with high flow velocity have been detected for all the analyzed shapes. Particularly I and T-shape, have shown higher velocity values among the analyzed alternatives both as depth-averaged as magnitude. This response is the cause of the bed shear stress-related problems discovered in that area from previous simulations (see Figure4.8.5). L and BL configurations have a better management of the velocity indexes downstream the dike structure. In particular BL-shape, by this point of view, is presenting the best velocity management downstream the dike because of, as stated before, a wider distribution of the flow energy, thanks to the opening interaction. Corresponding to the dike's toe each shape, have shown high velocity values due to flow channelization. BL configuration, thanks to the structure-opening action, is able to widen the flow cross section at the dike cross-section and distribute the flow energy in a wider area, decreasing the overall velocity indexes. Along the entirety of the inner side of the curve a low velocity index has been shown for all the configurations analyzed. A critical low-velocity area has been detected on the inner side of the curve downstream the dike structure. This results confirm this as a critical area where sediment deposition is occurring, as confirmed also from the bed shear stress and bed changes results (Figure 4.8.2).

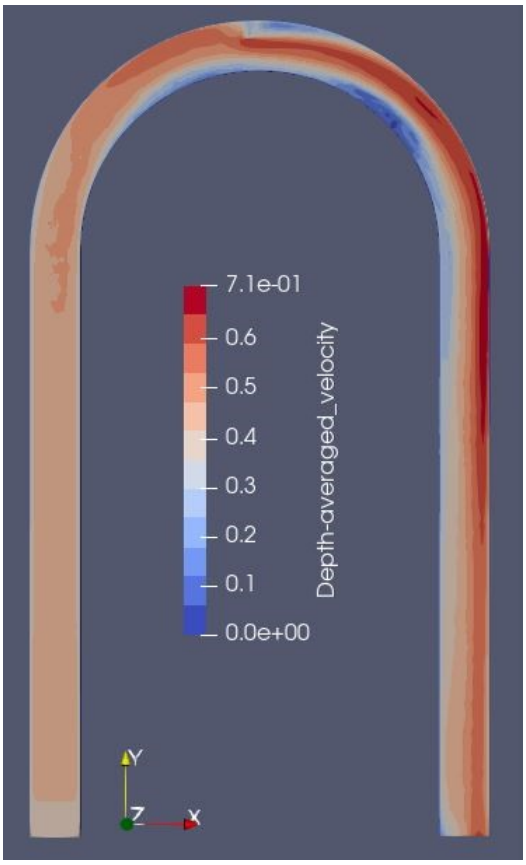

(a) *I-Shape*

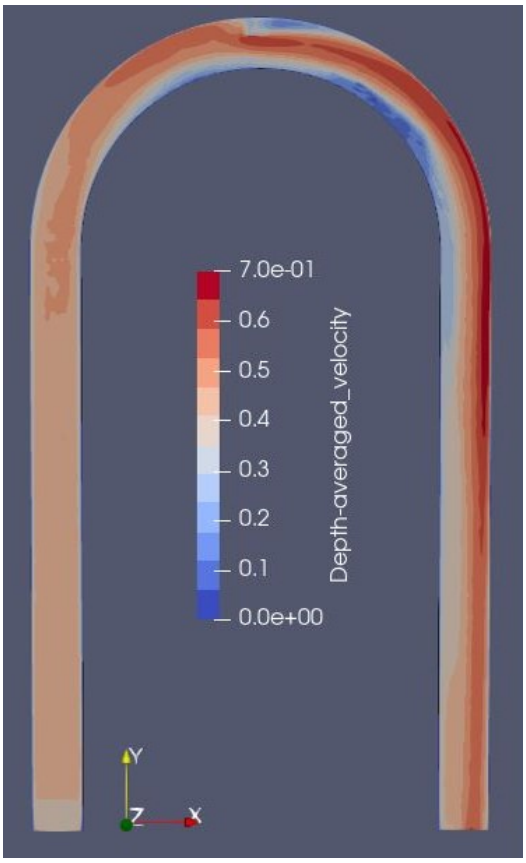

(b) *L-Shape*

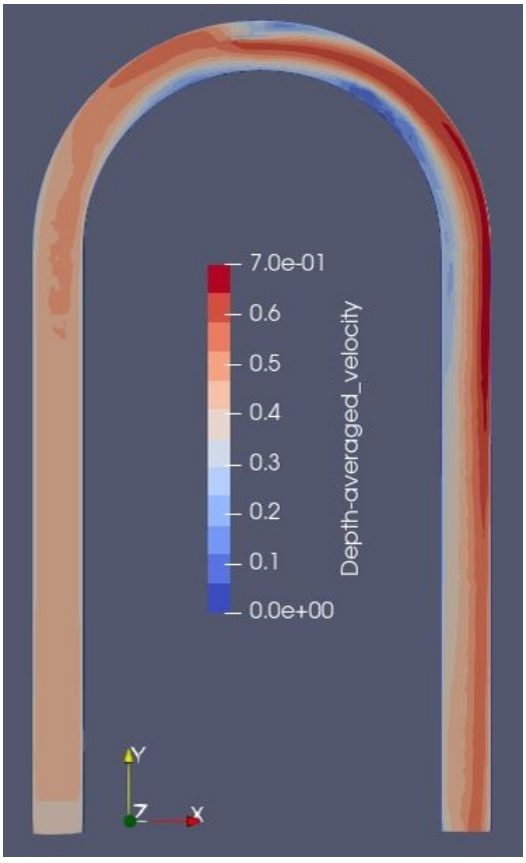

(c) *T-Shape*

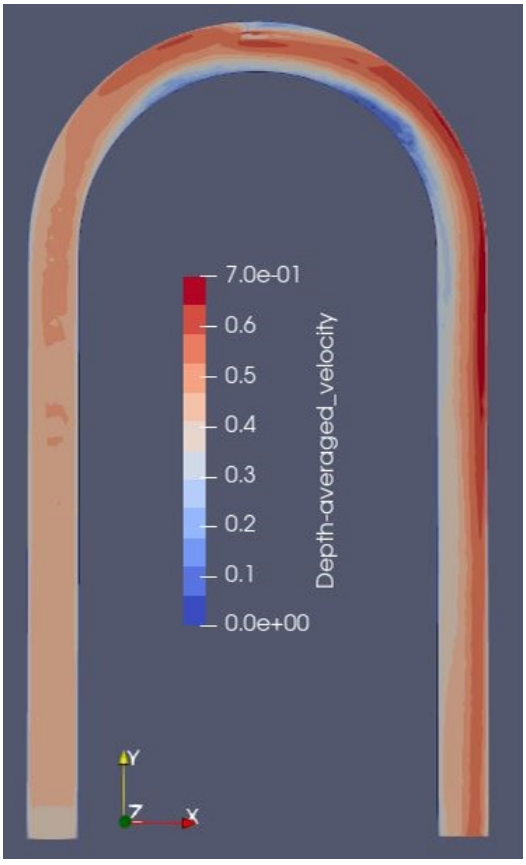

(d) *BL-Shape*

Figure 4.8.7: Depth-Averaged Velocity Comparison

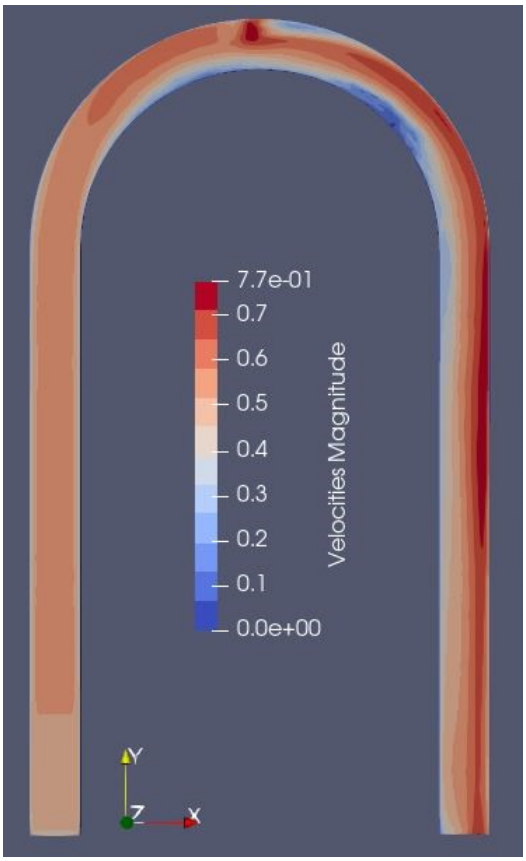

(a) *I-Shape*

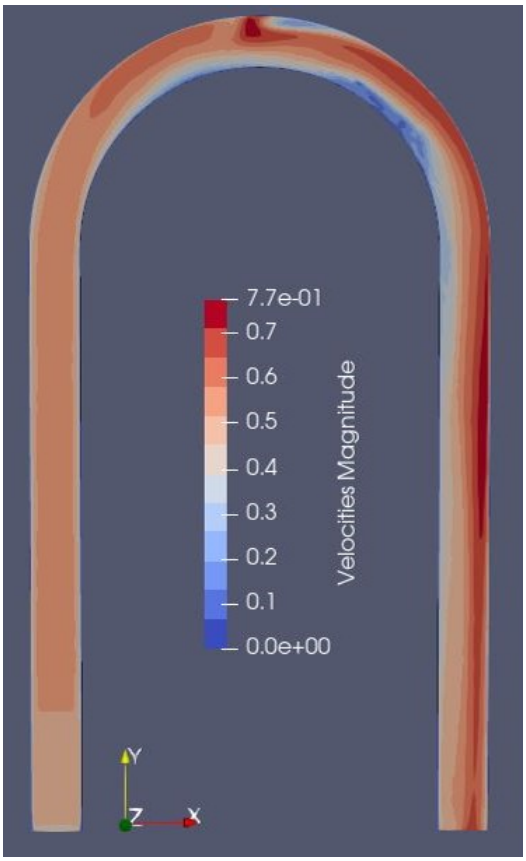

(b) *L-Shape*

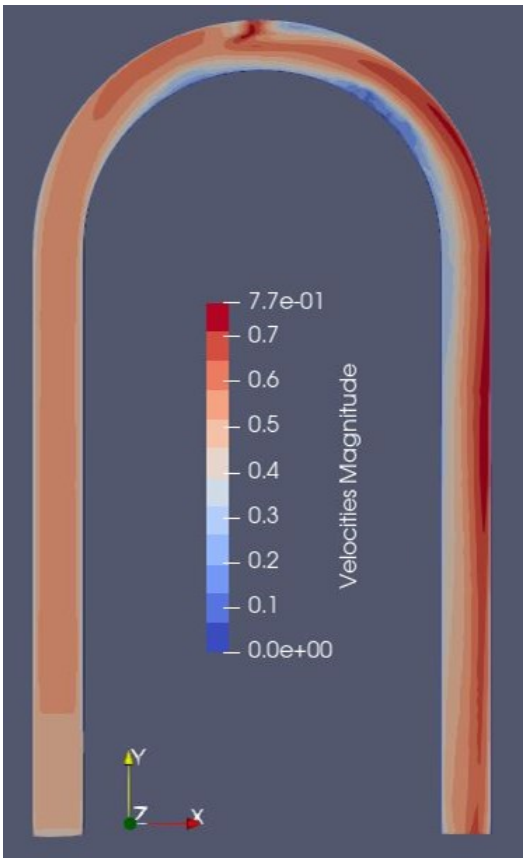

(c) *T-Shape*

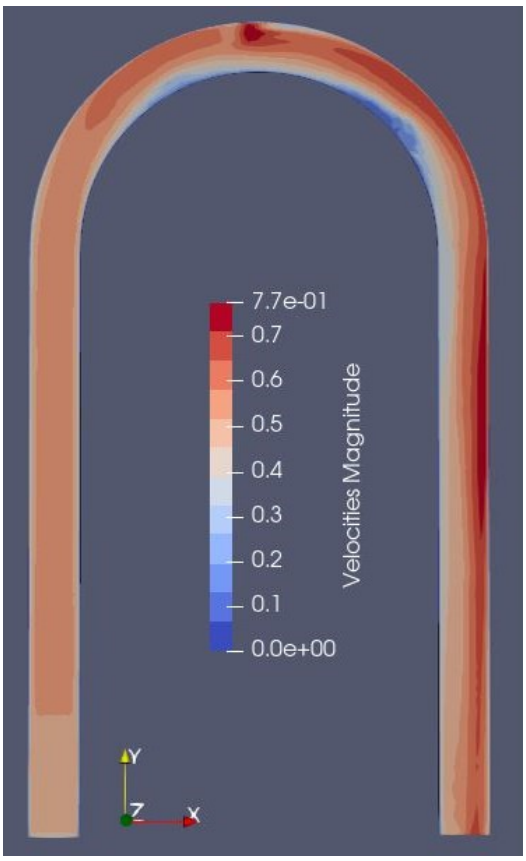

(d) *BL-Shape*

Figure 4.8.8: Velocity Magnitude Comparison

5 Successions Configurations and Comparison

All the singular-dike configurations analyzed have shown a problematic shear stress pattern occurring on the second half outer side of the curve and sediments deposition on the inner side, specially after the structure interaction, with consequent formation of lateral gradient. From an analysis of the reattachment angle for each analyzed shapes (T and I-shape $\cong 35°$; L and BL-shape $\cong 30°$) (see Chapter 4.8.2) a succession of structure is needed in order to have a satisfactorily scour prevention function on the overall curve outer side. Same number of structures for each shape-succession has been chosen in order to have comparable results. Considering the first half of the curve not a critical area, based on single-dike results (see Chapter 4.8.2), a succession of 5 dikes, placed at 60°, 90°, 120°, 150° and 180° along the curve, has been chosen. Then, the different successions of dikes shapes were analyzed to determine whether the succession-solution, instead of the single-dike-solution, could be applied as a preventive measure with respect to the scouring problems aforementioned. Moreover the successions analysis aim also to understand the succession behavioural differences respect the singular shape.

In order to achieve the targeted result, and to have comparable simulations, the same simulation parameters, as for singular shape, were used (see Chapter 4.2). Here follows a short recap of the main parameters used:

- 0.007 Roughness for walls and bed (F16).
- 0.053 m^3/s incoming flow (W1).
- Free surface (F36).
- Transient sediment computation algorithm (F37).
- Bed load calculation from Van Rijn formula (F84).
- Law of walls (K2).
- Block correction (K5).
- Second-order discretization upwind scheme (K6).
- Grid properties (G1, G3, G6):
  - 255 cross sections.
  - 21 grid lines on streamwise direction.
  - 6 grid lines in vertical direction.
  - Vertical grid distribution each 20% of water depth.
  - Free surface option.
- Sediments Properties (G1, S and I and N commands):
  - 7 sediment sizes (see Table 4 in Chapter 4.2).
  - No sediment inflow.
  - Sediments are uniformly distributed in all the cells, at the start.

5.1 I5 Configuration

This configuration consists in a succession of 5 I-shape spur dikes, with same element dimensions as the singular configuration (see Picture 4.4.1 in Chapter 4.4), placed along the curve each 30°, starting from 60°, along the curve as reported in Pictures 5.1.1. For further details see the *control* file in Appendix A Figure VI.

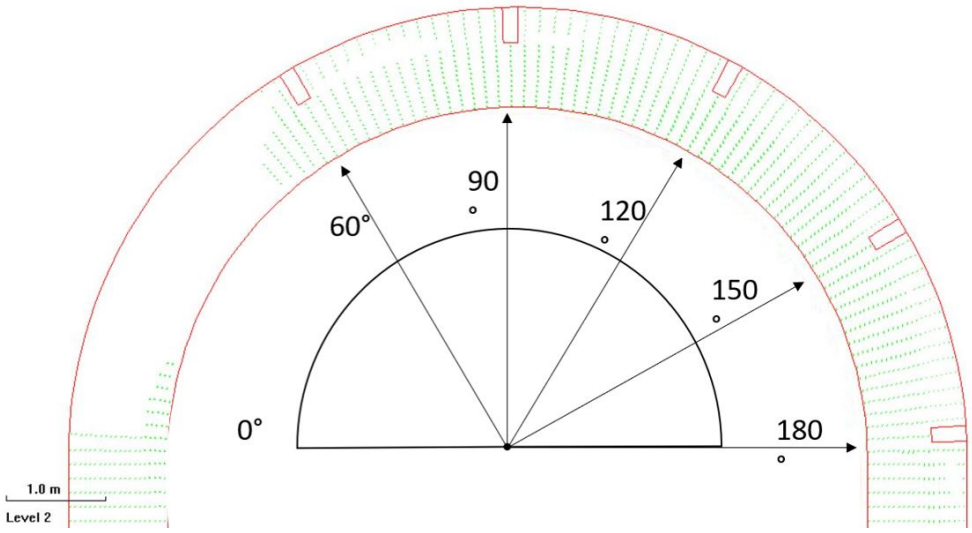

Figure 5.1.1: I5 configuration's layout (SSIIM view).

5.2 L5 Configuration

This configuration consists in a succession of 5 L-shape spur dikes, with same element dimensions as the singular configuration (see Picture 4.5.1 in Chapter 4.5), placed along the curve each 30°, starting from 60°, along the curve as reported in Pictures 5.2.1. For further details see the *control* file in Appendix A Figure VII.

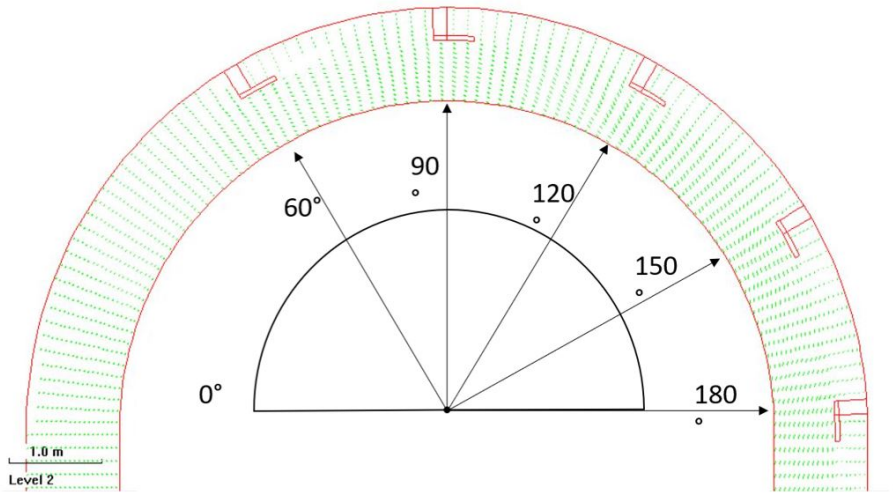

Figure 5.2.1: L5 configuration's layout (SSIIM view).

5.3 T5 Configuration

This configuration consists in a succession of 5 T-shape spur dikes, with same element dimensions as the singular configuration (see Picture 4.6.1 in Chapter 4.6), placed along the curve each 30°, starting from 60°, along the curve as reported in Pictures 5.4.1. For further details see the *control* file in Appendix A Figure VIII.

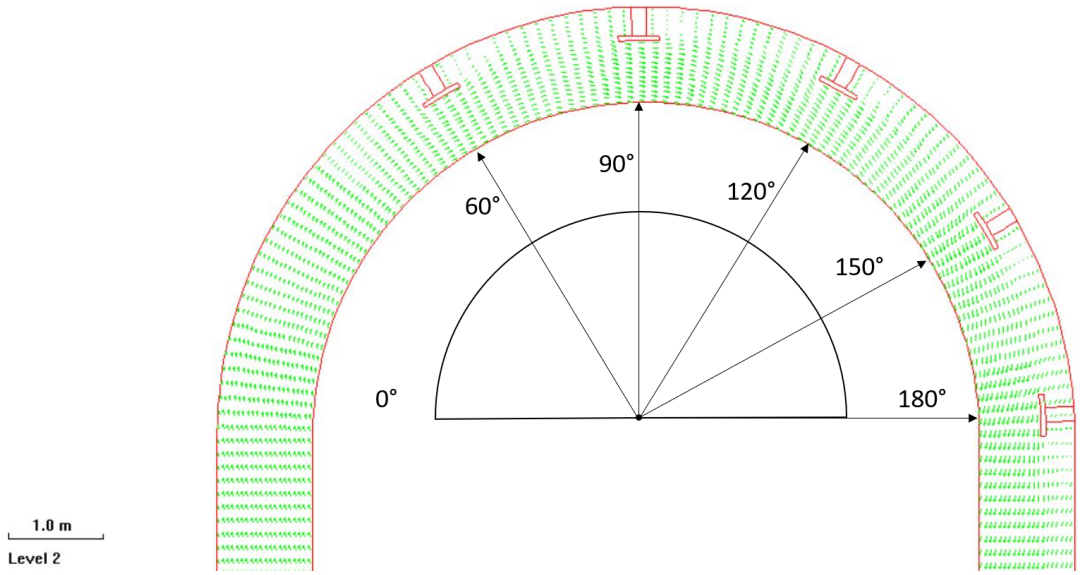

Figure 5.3.1: T5 configuration's layout (SSIIM view).

5.4 BL5 Configuration

This configuration consists in a succession of 5 BL-shape spur dikes, with same element dimensions as the singular configuration (see Picture 4.7.1 in Chapter 4.7), placed along the curve each 30°, starting from 60°, along the curve as reported in Pictures 5.4.1. For further details see the *control* file in Appendix A Figure IX.

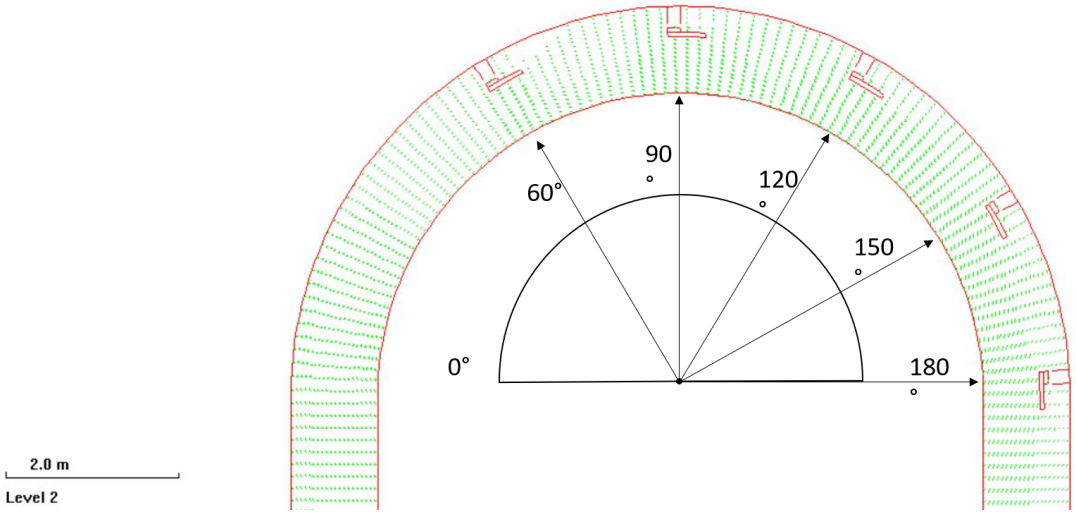

Figure 5.4.1: BL5 configuration's layout (SSIIM view).

5.5 Successions Bed Level and Bed Movement Comparison

The bed level results (Figure 5.5.1 in the next page) represent the morphological changes in the system due to the action of the flow forces and the interaction of the dike structures with the stream. The bed movement results (Figure 5.5.2) represent how much and where the morphological changes happened respect the initial system conditions, due to the action of the flow forces and the interaction of the dike structure/s. The results have shown similarities among all the analyzed succession. In particular the bed level and movement patterns have same spacial distribution, but different magnitude, among the analyzed options. The channelization of the flux has been noticed in all successions. The cause of this phenomena is the flow-diversion towards the middle of the channel caused by the structures interaction. Also sediment deposition specially in the inner second half of the curve has been found. In particular T5 succession has resulted in the formation of the deepest channelization and higher inner-side sedimentation among the analyzed options, while BL5 is managing the bed level distribution better then the other successions, presenting less flow channelization and sediment deposition. The bed level results highlight the formation of small trenches corresponding to the dike's toes. In order to understand the morphological behaviour of each succession, is necessary the comprehension of the different systems responses towards lateral gradient formation. This parameter is not constant throughout the system, so the cross-sectional lateral gradient corresponding to the 5 dikes cross-sections has been calculated, then then set of different lateral gradients, corresponding to each dike cross-section, has been averaged to have a mean succession response towards lateral gradient formation.

Table 6: Successions Averaged Lateral Gradient.

	I5 Succession	***L5 Succession***	***T5 Succession***	***BL5 Succession***
Reference Angle [°]	*Lateral Gradient [°]*	*Lateral Gradient [°]*	*Lateral Gradient [°]*	*Lateral Gradient [°]*
60	*12.9*	*13.4*	*17*	*12.3*
90	*24.8*	*21.5*	*22.2*	*17.9*
120	*18.4*	*21.6*	*21.5*	*17.5*
150	*19.8*	*21.2*	*23.1*	*21.3*
180	*23.1*	*17.5*	*24.3*	*18.6*
Average Lateral Gradient	**19.8°**	**19°**	**21.6°**	**17.5°**

The lateral gradient behaviour results from Table 6 have confirmed what has been deducted from the the results presented in Figure 5.5.1 and Figure 5.5.2. The morphological response of BL5 succession has been proved to be better, from a river training point of view, respect the other shapes by providing the lower lateral gradient, while T5 succession has proven to be the option that handles worse the morphological distribution of the system. From this analysis has been found a peculiar behaviour at the reference angle of 90°. The lateral gradient has been calculated as the angle between the lowest point in the cross section and the highest point on the inner bank. The deepest point corresponded to the lowest point in the trench at the dike's toe. Looking at the bed level and bed movement results, the depth of the trenches deepen as it increase the reference angle. Therefore the expected behaviour from the lateral gradient is to grow as the reference angle increases. At 90° is interesting to notice that, for each succession,

the lateral gradient is higher respect the one corresponding to the next reference angle. This behaviour has been justified by a detailed analysis of the results in Figure 5.5.1 and Figure 5.5.2, showing a local significant increase of the sediment deposition at the inner side of the curve corresponding to 90° reference angle. This local rise of the inner side is the cause of the unexpected behaviour of the lateral gradient at 90° reference angle.

The succession configuration create, in between each dike structure, a calm area generally called "pool". The bed level and bed movement in these areas has been found to be almost unchanged from the starting condition. For BL5 succession, the pools are more dynamic areas respect then the other shapes, due to the opening in the structure that allows a fraction of the flow to pass through. Nonetheless the bed movement in these areas, also for BL5 succession, is anyway almost unchanged from the starting condition. The inner side of the turn is affected, in all simulations, by sedimentation. This phenomenon is caused by secondary current effects and turbulences. Successions like BL5 and L5 better manage the sediment deposition magnitude, as already happened with single-shape configurations. The deflection of the streamflow done by the succession's structures has resulted in a creation of a narrower main channel at the dike's toes. The channelization of the flow has converged the stream forces in a smaller area, resulting in a deeper bed scouring progressively as the flow is deflected, reaching the peak at the end of the turn. Upstream the first succession's structure the system response is similar for all the analyzed configurations. Downstream the last dike structure has been noticed that the effects of the flow deflection are prolonged into the straight part of the channel. Moreover, successions that present higher flow channelization, like T5, have longer effects in the downstream straight channel respect other successions, like BL5.

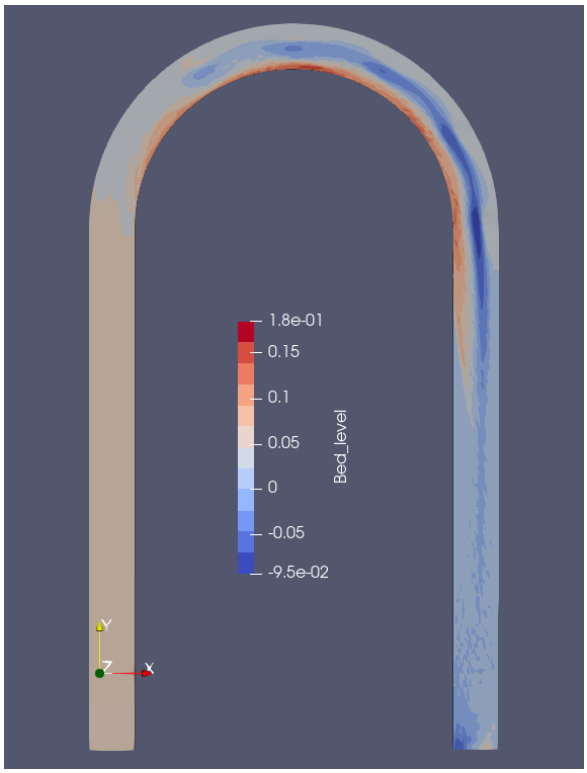

(a) *I5 Succession*

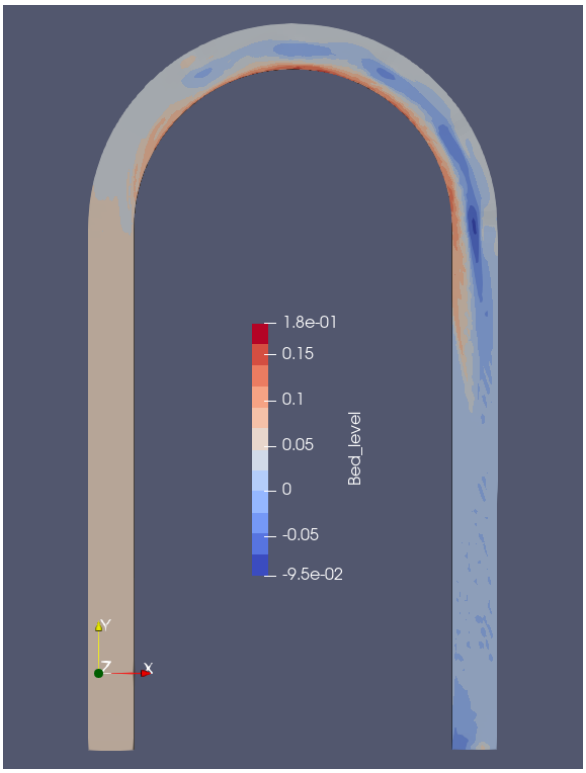

(b) *L5 Succession*

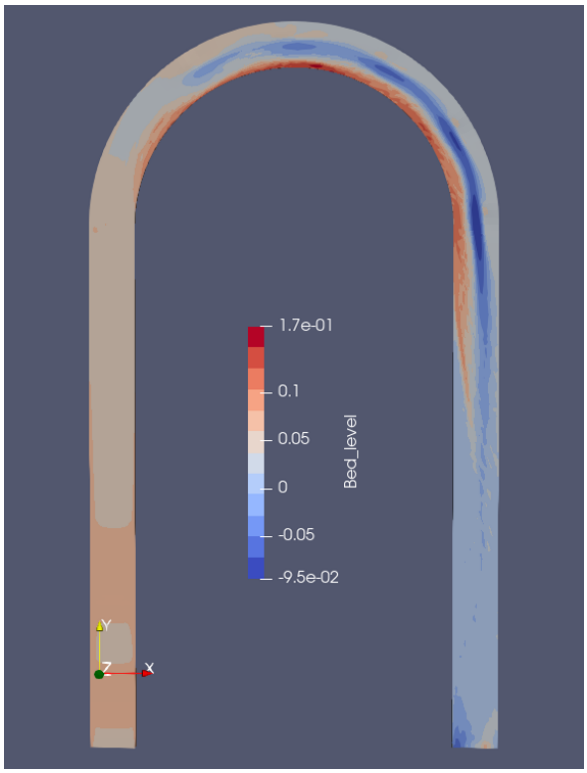

(c) *T5 Succession*

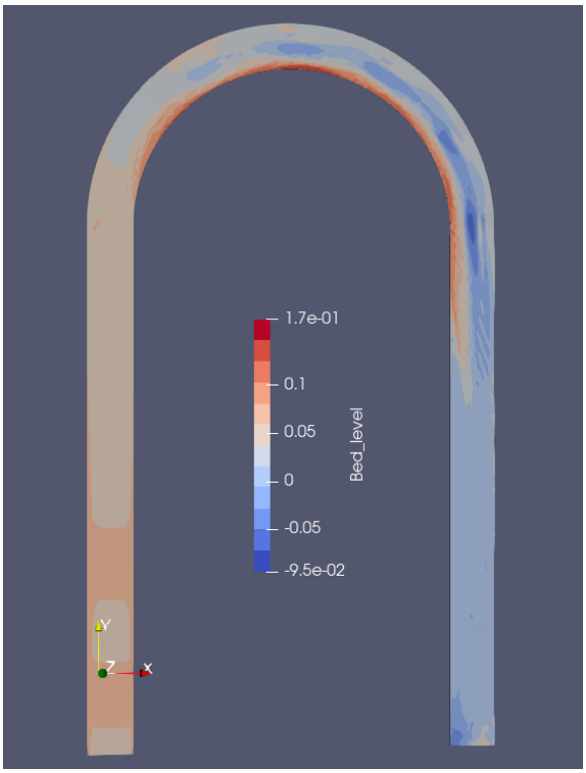

(d) *BL5 Succession*

Figure 5.5.1: Successions Bed Level Comparison.

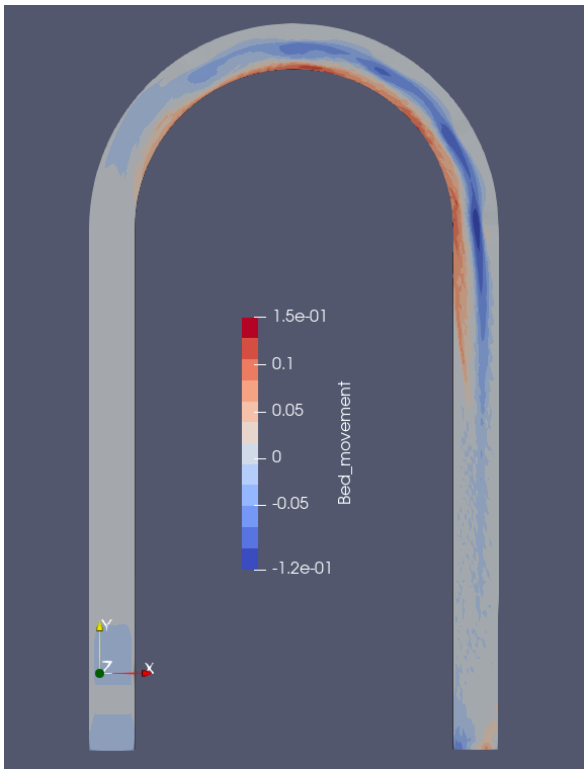

(a) *I5 Succession*

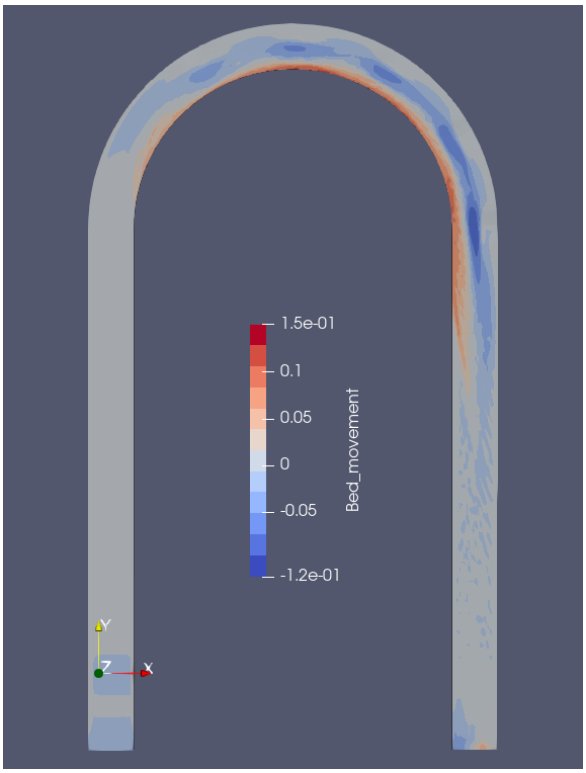

(b) *L5 Succession*

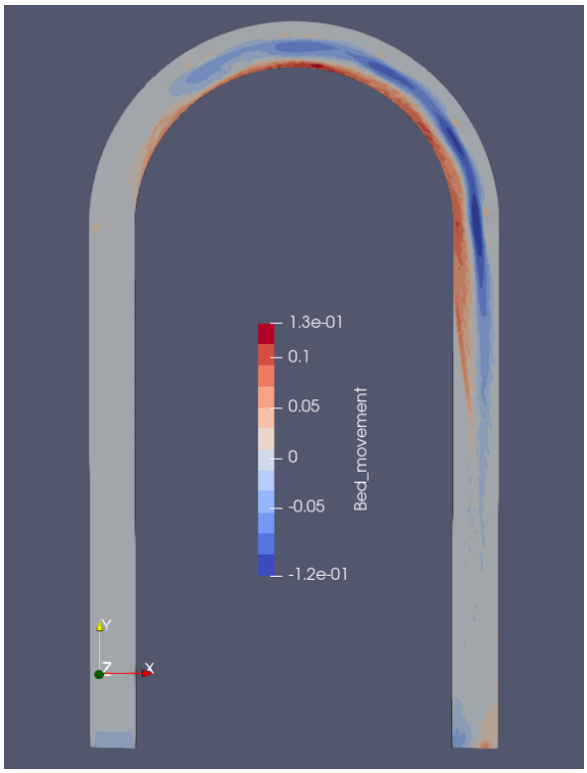

(c) *T5 Succession*

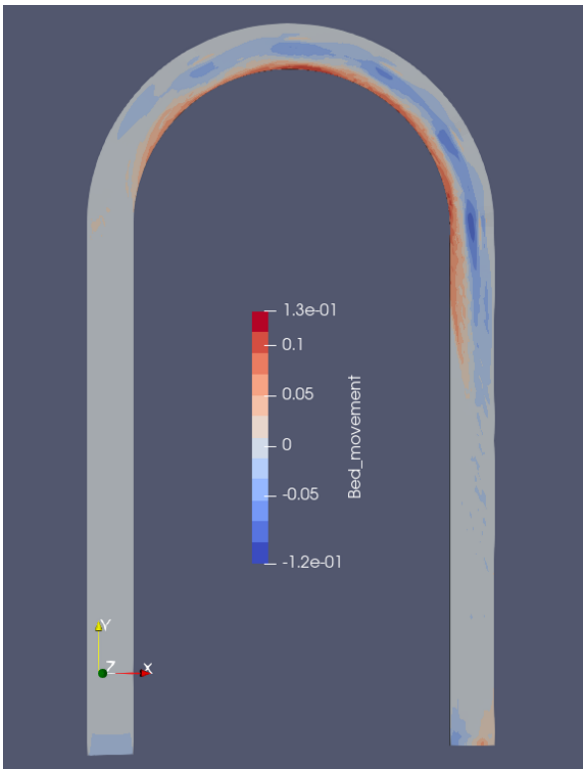

(d) *BL5 Succession*

Figure 5.5.2: Successions Bed Movement Comparison.

5.6 Successions Bed Shear Stress Comparison

The bed shear stress results (Figure 5.6.1 in the next page) represent the shear stress pattern acting on the boundaries of the system due to the action of the flow forces and the interaction of the dike structures with the stream. The bed shear stress pattern is the flow force that interact with the bed layer and is the driving parameter that determines morphological changes. Therefore this comparison is the most relevant in order to understand the behavioural differences between the spur dikes successions. The bed shear stress pattern is clearly different between the different configurations. T5 and BL5 configurations have different extreme outputs. Considering these options as extremes, L5 and I5 results are in between the two previous mentioned successions results. The results of the simulations show that T5 configuration provides the greatest bank scour prevention function and, at the same time, manages in a worse way aspects as flow channelling, lateral gradient creation and sediment deposition and aggradation. BL5 although providing less, but satisfactorily, protection of the outer embankments, obtains a better system response regarding all other aspects, especially from river-training point of view, mitigating the effects of flow channelling, creation of lateral gradient and sediment deposition and aggradation.

From a first analysis of the results, T5 succession seems to manage very well the shear stress, both in pools area and outer bank, where the bed shear stress index is approximately 0. On the other hand, T5 succession is also concentrating the bed shear stress at the dike's toes with higher magnitude respect the other configurations, favouring flow channelization and deepening of the channel. Consequent lateral gradient formation grows, same as the bed shear stresses, as moving towards downstream, reaching the peak corresponding the downstream-last spur dike structure. Increase of lateral gradient result in a relative increase of the sediment aggradation. The smaller cross-section where the flow is conveyed, due to the structure presence, increase the flow velocity resulting in incipient motion of bigger particles and their transport towards downstream, leading also to a high scouring of the bed level and higher forces acting on the structure itself, as possible cause of erosion. The low stress acting on the inner side is favouring the sediment deposition of the fraction that is moved by the secondary currents. The secondary current has lower strength then the main current, resulting in a incipient motion of just the smallest fractions of sediments towards the inner side.

BL5 succession is managing well the overall bed shear stress pattern. The protection function on the outer bank is lower then T5 configuration but however close to 0, therefore satisfactorily. The related shear stress in the pools is slightly higher due to the BL-structure opening interaction that disrupt the pools flow and allows part of the stream energy to reach the pools. The overall BL5 better managing of the bed shear stresses pattern results in a lower flow channelization and bed level deepening, and consequent lower bed level arise in the inner part of the curve. The results shows also the capability of the configurations to deflect the stresses from the bank towards the center of the channel.

In the upstream part of the channel, no remarkable differences between the analyzed options have been found. The critical area upstream the dike structure as shown in the single-configuration result (Figure 4.8.5 in Chapter 4.8.2) is no longer present.
In order to quantify the bank scour protection given by each successions, the histogram of the bed shear stresses values has been extracted for each option (see Appendix B for the histograms). A maximum bed shear stress value, set to 1 N/m^2, has been chosen as threshold. In order to consider an area, affected by bed shear stress, satisfactorily protected from scouring,

the local stress value must be inferior then the chosen threshold. Then, from the histogram, the number of points simulated that presents lower value of bed shear stress then the threshold has been extracted. The threshold has been chosen as the minimum bed shear stress value acting in the middle of the straight upstream undisturbed channel, based on the thought that avoid totally the bed shear stress is impossible in a real application, and the ideal stream that a river-training measure should try to aim is the straight undisturbed channel. The results follows in Table 7. The succession that have highest number of points having inferior value respect the threshold, is the option that works better towards bank scour protection.

Table 7: Bank scour protection ranked behaviours.

	Bank Scour Protection	
Configuration	*Rank*	*Value [n° of points < Threshold]*
Undisturbed Channel		*8764*
I5 Configuration	*2*	*10192*
L5 Configuration	*3*	*9954*
T5 Configuration	*1*	*10983*
BL5 Configuration	*4*	*9282*

From the previous ranking, is clear that exist a correlation between banks scour prevention function and the overall managing of the shear stress by the selected succession. In particular, a better managing of the bed shear stress on the outer side correspond to a higher bank scour protection due to the bed shear stress deflection because of the interaction of the structures with the flow. BL5 succession is not deflecting the same amount of stresses towards the inner side of the channel as T5, this result in a more distributed bed shear stress pattern, but a lower bank scour protection. I5 and L5 response are in between the two extremes given by BL5 and T5 successions.

The flow forces are deflected, due to the dikes interactions, from the outer to the mid of the channel. All the selected successions provide a satisfactorily protection of the outer bank, both upstream and downstream the succession structures, solving the issues which had occurred with single shapes configurations. Low bed shear stresses act along the inner side of the curve for all the analyzed configurations resulting in a rise of the bed level and sediment deposition. In the pools created between each dike structure the bed shear stress action is approximately zero due to the dike shielding, except for BL-shape. BL-shape avoid the calm region behind the dikes thanks to the opening in the structure. This feature creates a more dynamic environment into the pools but still maintain the shear protection function on the outer boundary. Also BL-opening helps to distribute the flow forces avoiding higher magnitude of bed shear stresses and mitigate the impact of the successions structures interactions. Mitigating therefore the related flow channelization caused by the shrinking of the cross section, the consequent increase of the velocity pattern and the related increase of bed shear stress at the dike's toe.

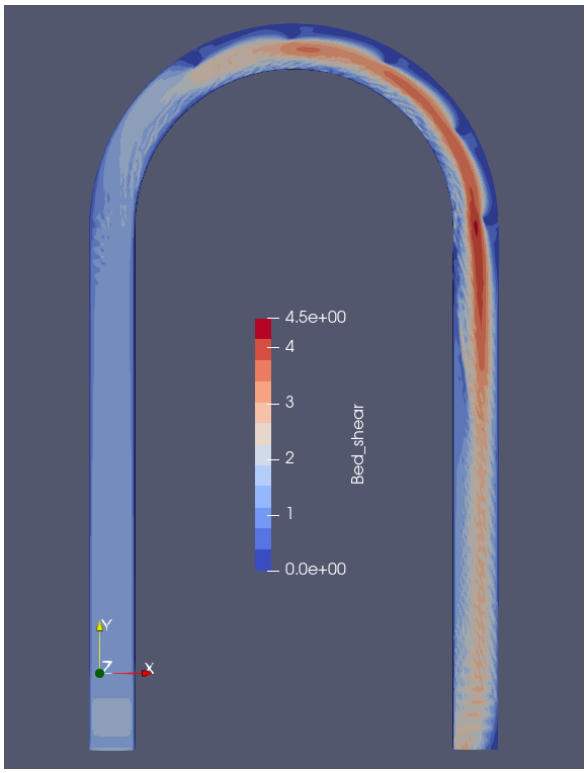

(a) *I5 Succession*

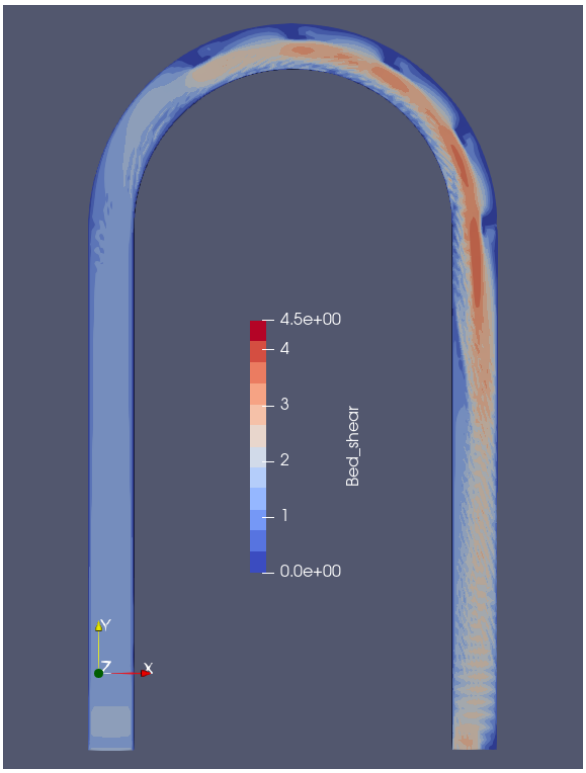

(b) *L5 Succession*

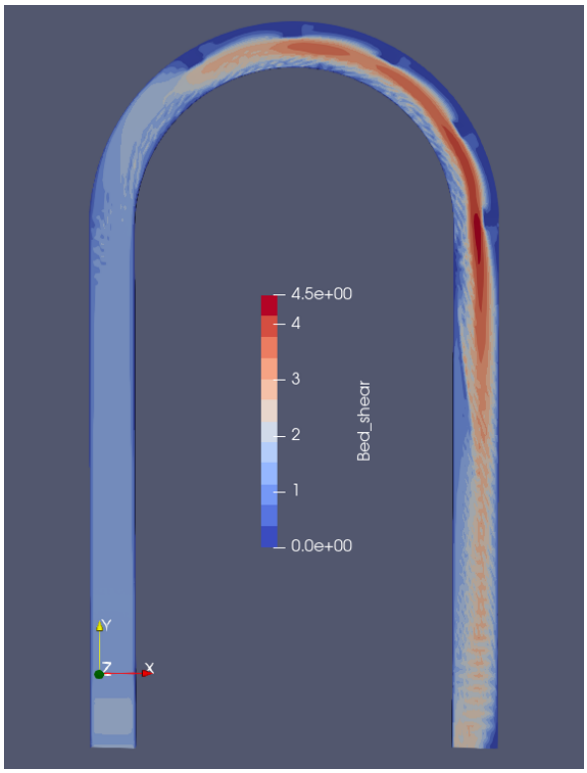

(c) *T5 Succession*

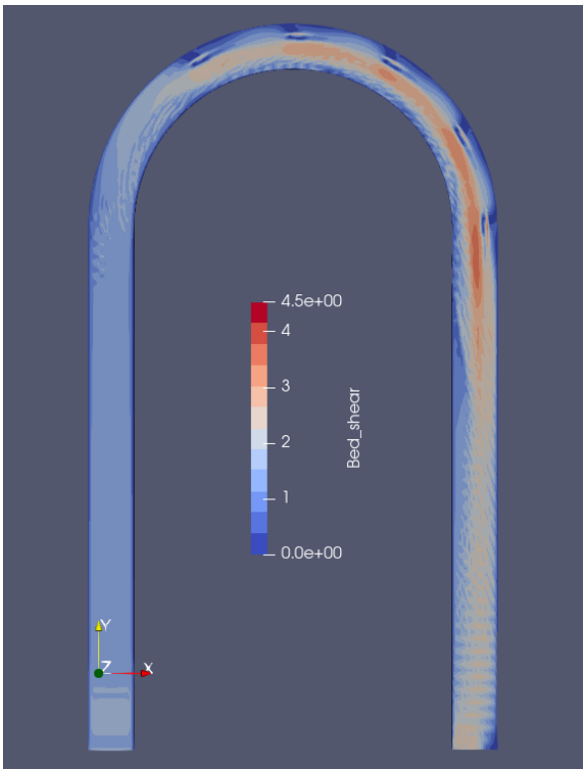

(d) *BL5 Succession*

Figure 5.6.1: Successions Bed Shear Stress Comparison.

5.7 Successions D_{50} Comparison

D_{50} results (Figure 4.8.6 in the next page) represent the granulometric distribution of the sediments in the system, using a particle size distribution or, more precisely, the median grain size (D_{50}). This parameter is important in order to understand the sediments distribution as function of sediments granulometry and bed shear stress conditions. Therefore, D_{50} distribution is strictly related to the bed shear stress pattern (see Figure 5.6.1).

The results of the simulations show different behaviours from shape to shape. Configurations that resulted in high bed shear stress have shown, as expected, higher values and of D_{50}. While no remarkable differences, between the analyzed options, has been found in the upstream part of the channel, a dissimilar system response was noted in the calm zones. T5 and I5 configurations have shown a wider area between the dikes structures with D_{50} value close to 0 respect L5 and BL5 configurations. In these two last aforementioned successions, the index value close to 0 is present in a layer along the outer boundary while the rest of the calm zone is characterized by a slightly higher D_{50} value, meaning a more dynamic environment from an hydraulic point of view. The main mechanism of deposition in this area is related to secondary currents effects and turbulences that start incipient motion, transport and deposition of just the smallest sediments diameters. The characteristic BL5 opening in the structure result, in the area immediately after the dike, in a more dynamic behaviour by helping to distribute the energy gradient from the flow in a broader area, avoiding the calm zone and improving the general management of the overall stress pattern and sediment deposition in the system. In the channel corresponding to the BL-dike structure opening, a high D_{50} value, as result from high velocity index and bed shear stress response for that area, has been found. High D_{50} value in that zone is to be considered a good value in order to avoid sedimentation and opening occlusion.

After the dikes succession, no issues have been detected along the banks. The flow channelization enforced by the succession interaction deflect effectively the flow forces from the outer bank towards the center of the channel. Corresponding to the dike's toe, T5 and I5 successions have shown high D_{50} values in the trenches, due to flow channelization. A milder system response has been obtained from L5 and BL5 successions. In particular BL5 configuration thanks to the structure-opening action, is able to widen the flow cross section at the dike structure, decreasing the overall velocity and consequently lowering and distributing the bed shear stresses in a wider area, resulting in a milder D_{50} values distribution. For all the analyzed successions, the highest value of the median sediment size in the system has been found in the trench corresponding to the downstream-last dike's toe.

Along the entirety of the inner side of the curve a low D_{50} has been detected for all configurations. The main mechanism of deposition in this areas with lower bed shear stress is principally due to secondary currents and turbulence motions. The strength of these currents is enough to start the incipient motion of just the smaller fractions of sediments, as confirmed by D_{50} resulting distribution at the inner side of the curve. The D_{50} deposition pattern is in accordance to what previously shown from bed level and bed movement (Figure 5.5.1 and Figure 5.5.2) and bed shear stress results (Figure 5.6.1).

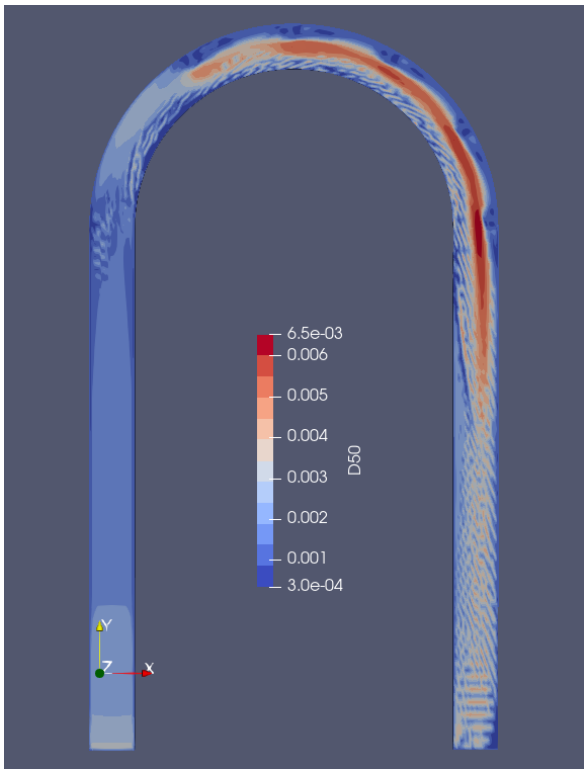

(a) *I5 Succession*

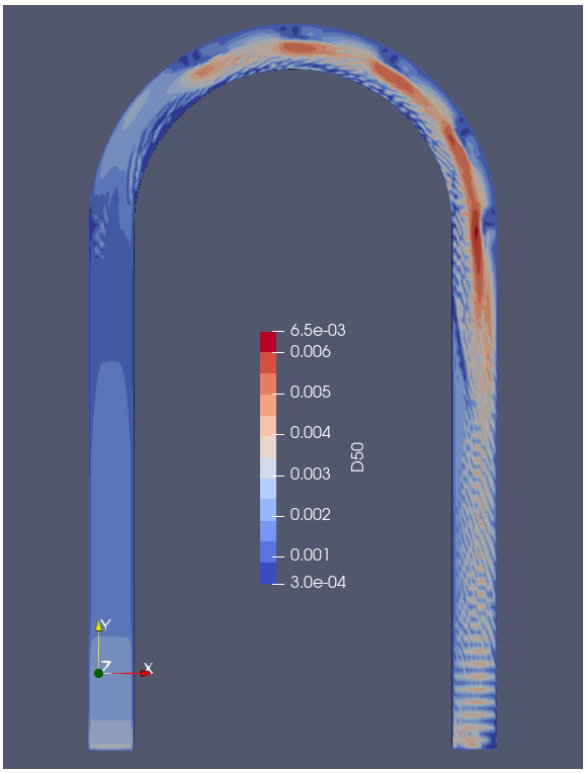

(b) *L5 Succession*

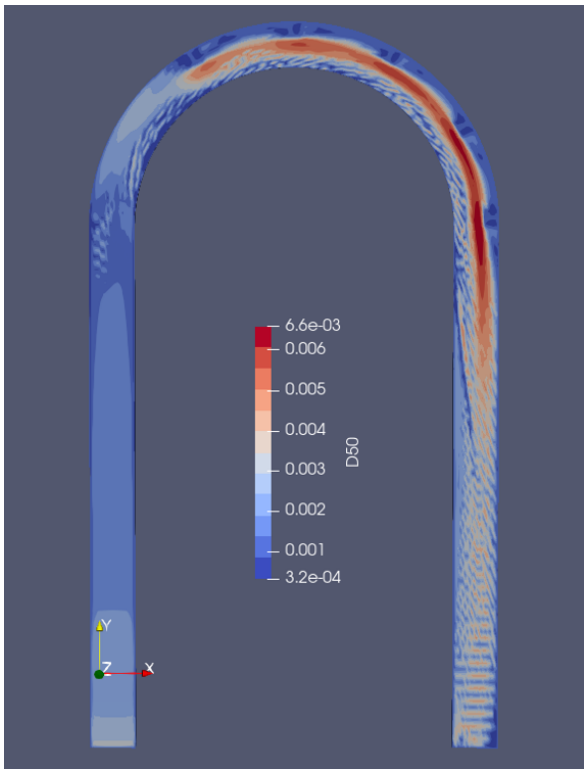

(c) *T5 Succession*

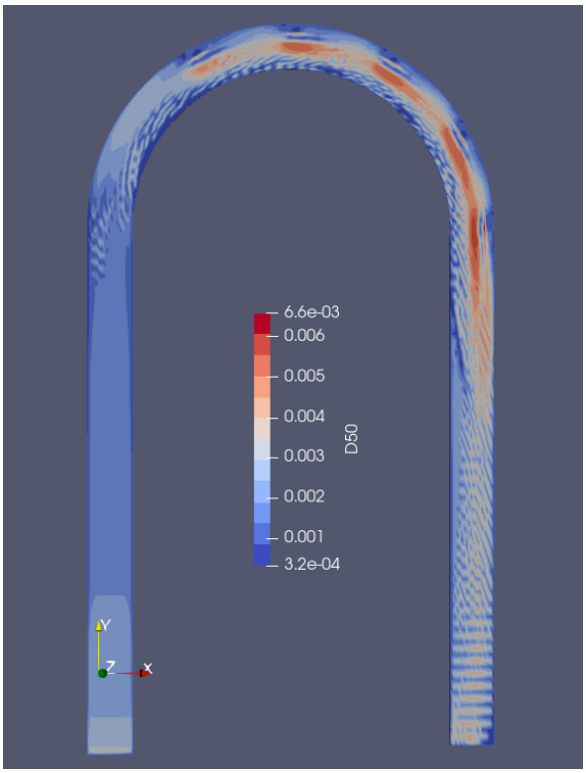

(d) *BL5 Succession*

Figure 5.7.1: Successions D_{50} Comparison.

5.8 Successions Depth-Averaged Velocity and Velocity Magnitude Comparison

The velocity results (Figure 5.8.1 and Figure 5.8.2 in the next pages) represent the hydraulic response of the system after the succession perturbation. In particular the depth-averaged velocity represent the mean velocity averaged over the cross-sectional depth, while the velocity magnitude is the velocity vector resulting from the three dimensional vectors of velocity (See Formula 4.2 in Chapter 4.8.4). These parameters are important in order to understand the hydraulic response of the system, the consequent bed shear stress pattern resulting from the velocity conditions along the channel and the sediment distribution.

From a first analysis of the results, the differences of velocity management between T5, I5 and L5, BL5 succession is clear. In particular the first two configurations results in a strong flow channelization and consequent abrupt change between different velocity layers. L5 and BL5 successions, differently, present a milder response on the overall system and related milder change in the velocity gradient.

In the upstream part of the channel, no remarkable differences between the analyzed options have been found. The critical area upstream the dike structure, as shown in the single-configuration result (Figure 4.8.7 in Chapter 4.8.4), is no longer present. In I5 and T5 configurations, a calm zone, with low velocity indexes both as depth-averaged and magnitude, has formed behind the dike due to the structure's flow shielding. L5 and BL5 successions, otherwise, form a calm layer just along the outer boundary and have a more dynamic behaviour in the rest of the "calm" areas. As stated before, the opening in the BL configuration is the driving feature that allows the flow to be more dynamic after the dike interaction and allows a broader distribution of the flow forces, improving the general condition of the overall system downstream the structure. The velocity indexes in the BL-opening shows a channelization of the flow and therefore a high velocity index, both as depth-averaged as magnitude.

The outer side of the turn is protected against the flow forces. This is represented by low velocity indexes, both as depth-averaged and as magnitude along the outer side of the curve. Downstream the last succession's structure the high velocity indexes are channelled in the middle of the stream and no issues have been detected. Corresponding to the dike's toes each configurations, have shown high velocity values due to flow channelization. In particular, high velocity indexes has been detected at the trenches corresponding at the dike's toes, reaching the peak in the downstream-last trench. Regarding BL5, thanks to the structure-opening action, this configuration is able to widen the flow cross section at the dike cross-section and distribute the flow energy in a wider area, decreasing the overall velocity indexes. Along the entirety of the inner side of the curve a low velocity indexes has been shown for all the configurations analyzed. A critical low-velocity area has been detected on the inner side of the curve corresponding to the 90° dike structure. This critical area has resulted in sediment deposition that caused the aforementioned issue regarding the unexpected value of lateral gradient corresponding to the 90° cross-section. This results are in accordance to the sediment deposition seen form the bed level results (Figure 5.5.1) and to the sediment distribution seen from D_{50} results (Figure 5.7.1).

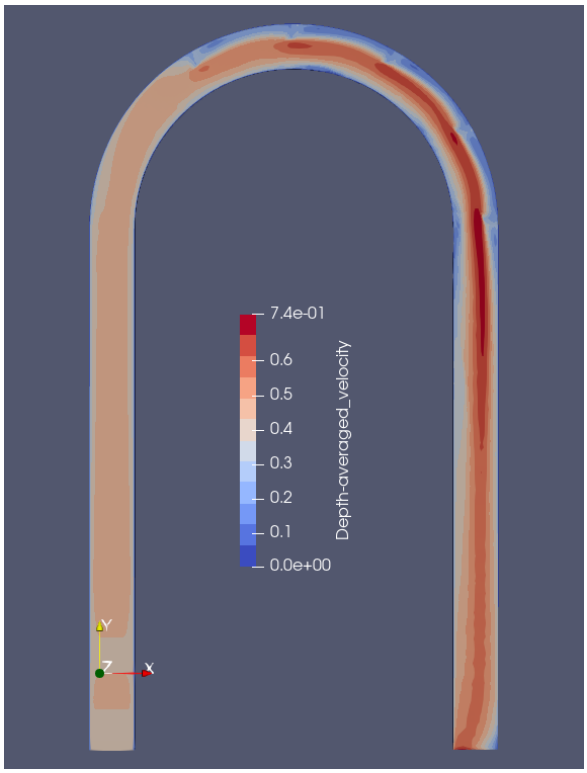

(a) *I5 Succession*

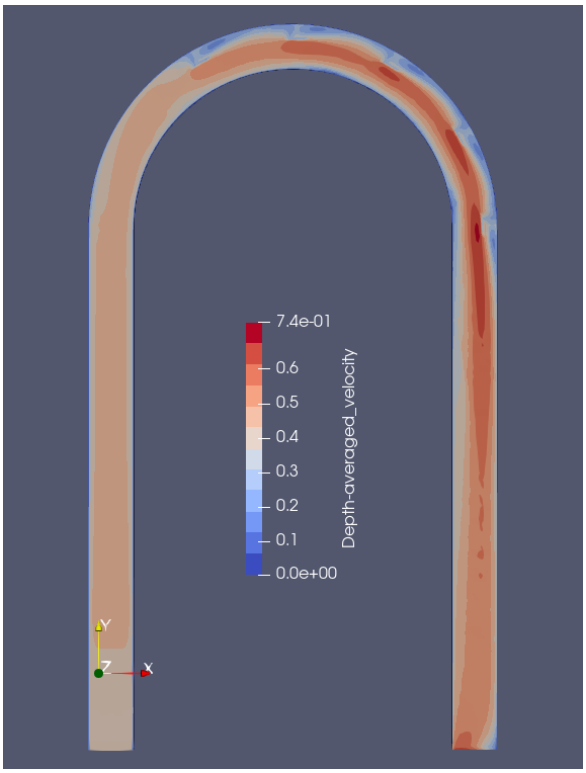

(b) *L5 Succession*

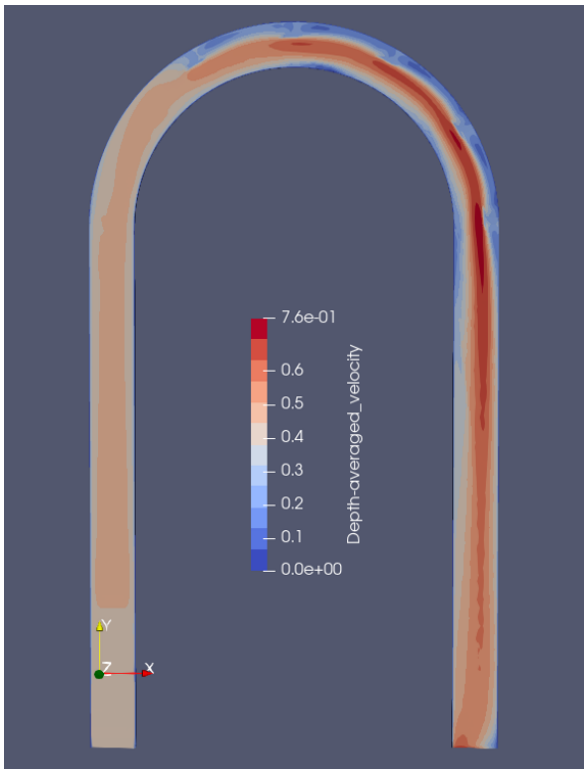

(c) *T5 Succession*

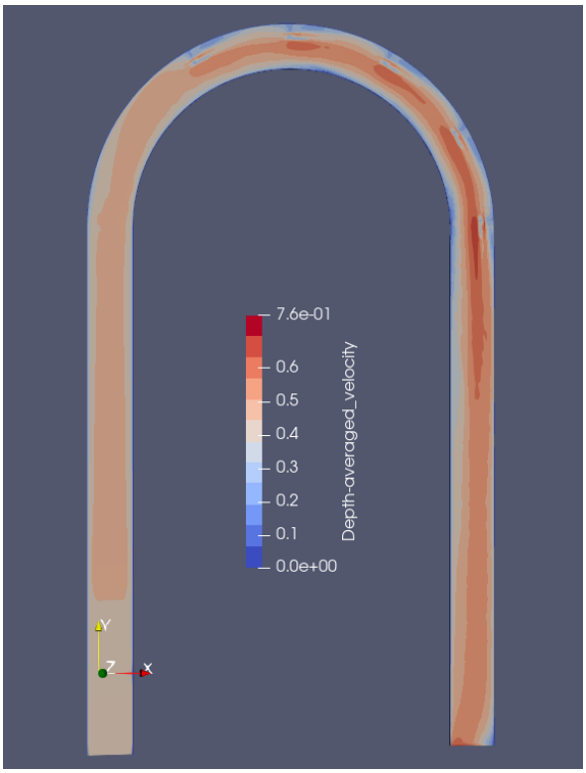

(d) *BL5 Succession*

Figure 5.8.1: Successions Depth-Averaged Velocity Comparison.

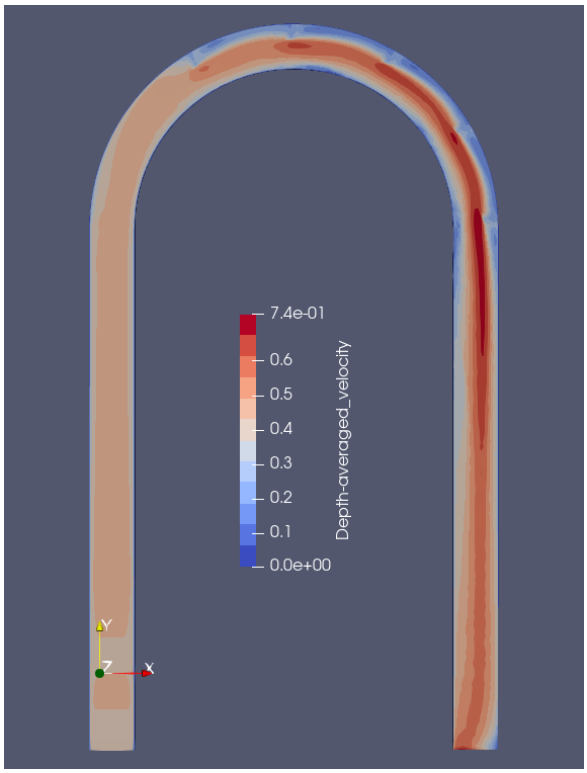

(a) *I5 Succession*

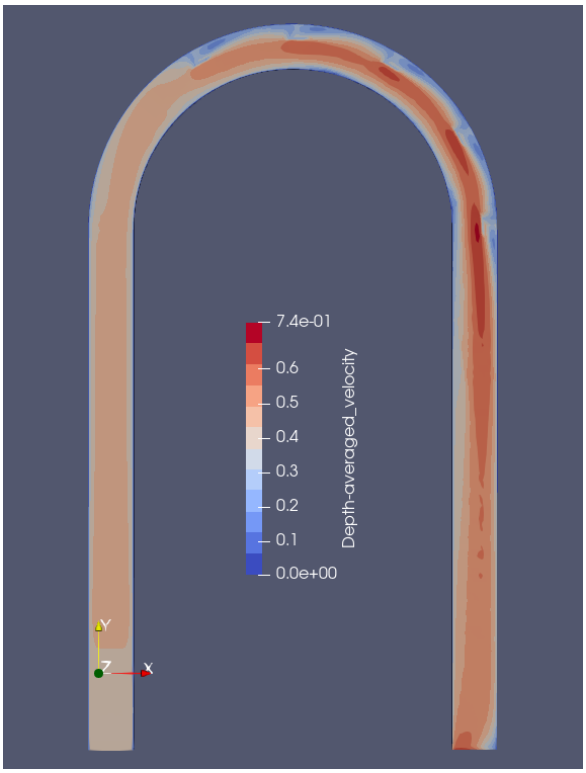

(b) *L5 Succession*

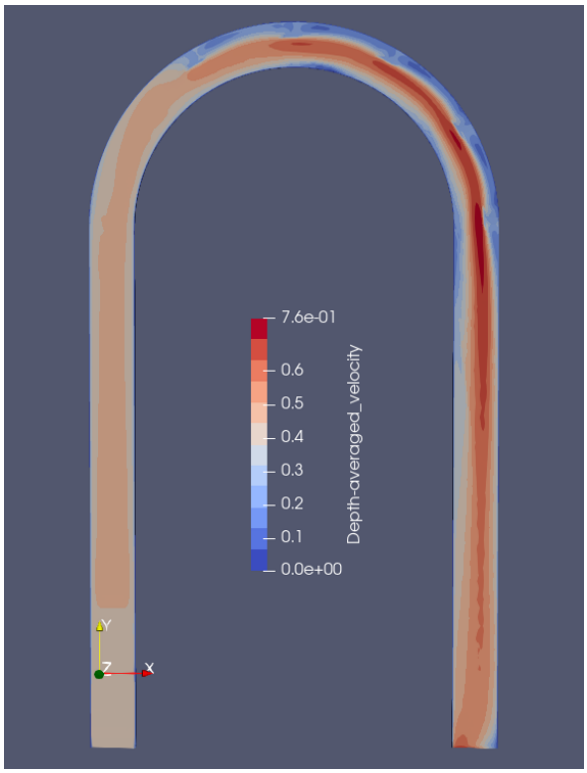

(c) *T5 Succession*

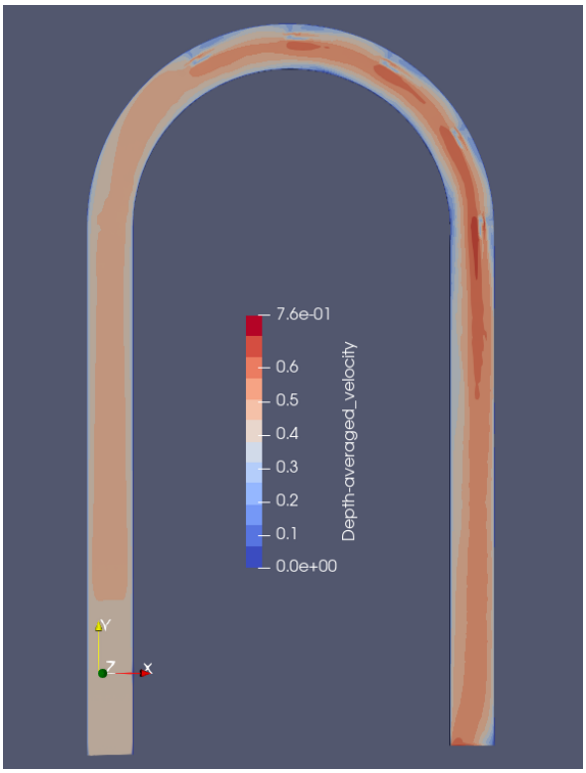

(d) *BL5 Succession*

Figure 5.8.2: Successions Velocity Magnitude Comparison.

6 Sediment Transport Analysis

Appear reasonable to consider the best outcome, from a sediment continuum point of view, the balance between sediments incoming and sediment exiting the system. This consideration is because of the shortness of the system consider, indeed in a real river system the change in deposition ratio appears over long distances or due to particular conditions (like headworks or lakes) that in this study are not considered. The simulation model is not considering any sediment inflow in the system, but provide, at the start of the simulation, 7 different sediments particle-size classes uniformly distributed in all bed cells. The parameter chosen to understand the sediment transport behaviour is the Sediments Transport value, in m^3, for the system. A negative value of Sediments Transport means that the configuration of spur dike under analysis will produce scouring, while a positive value of sediments transport represent deposition. A situation of deposition cannot happen in this case due to the absence of incoming sediment inflow. The optimum sediment transport that should be consider in order to represent the system who better manage the sediment continuity towards downstream is therefore 0. The configuration that will transport less sediments downstream should therefore be considered the one who manage better the sediment continuity of the system.

Table 8: Sediment Transport and relative rank for each configuration.

Configuration	**Rank**	**Sediments Transport [1000*m^3]**
Undisturbed Channel	*9*	-0.095
Singular I-shape	*7*	-0.088
Singular L-shape	*5*	-0.077
Singular T-shape	*8*	-0.090
Singular BL-shape	*6*	-0.087
BL5 Configuration	*2*	-0.034
T5 Configuration	*3*	-0.042
I5 Configuration	*4*	-0.044
L5 Configuration	*1*	-0.030

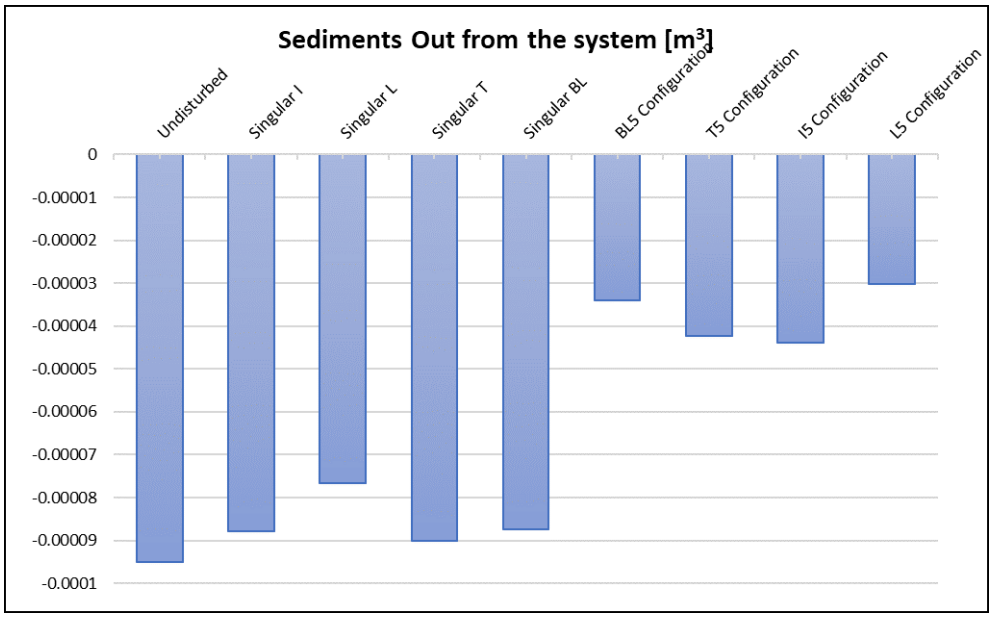

Figure 6.0.1: Sediments out from the system [m^3] histogram.

The simulation results shows the goodness of the hypothesis that successions should work better then a singular structure in order to provide sediment continuity in the system, as also showed in the previous chapters results. The ranks shows L5 configuration as the one who works better towards the sediment continuum point of view. The successions results shows that successions, respect the singular configurations, are able to halve or more the sediment transport in the system. The configurations (specially I5 and T5) that present higher flow channelization works worse, regarding sediment continuity, then succession with lower channelization, due to the higher flow velocity and related bed shear stresses occurring in the channelization areas corresponding to the middle of the channel, which are able to start incipient motion and transport of a wider variety of sediments fractions, favouring scouring of the bed specially along the curve. This is partially confirmed by the behaviour of singular configurations. Particular behaviour has been observed in L5 configuration, where despite the slightly higher flow channelling compared to the BL5 configuration, a lower sediment transport was obtained, both for singular then succession configurations. Change in bed level parameter has been taken from *boogie* file as result of SSIIM simulations for each configuration.

7 Dissipated Energy Analysis

In order to understand the behaviour of each shape and/or succession regarding scouring prevention, the dissipated energy parameter was used. This parameter represent the energy dissipated by the interaction of the flow with the system as function of roughness of the surfaces, sediments, turbulence and structures interactions. Its interesting to see the difference between each shape's dissipated energy result and the undisturbed channel energy dissipation in order to better understand the effect of the specific structure-shape on the total energy dissipation. More energy is dissipated, means less energy available by the streamflow in order to produce scour on the banks; higher value of dissipated energy is considered better in order to achieve scouring protection function. Its important to notice that scour is a local phenomena and cannot be generalized on the overall stream. Energy dissipation is not a local parameter, but gives an overall view of the behaviour of the structure interaction with the flow from an energetic point of view. A local analysis of the scour protection function along the focused areas has been carried (see Table 7 in Chap. 5.6) and compared with the Dissipated Energy Analysis. The dissipated energy, for each configuration, was found as difference between the total energy in the starting section (upstream) and the total energy left in the closing section (downstream).

$$DissipatedEnergy = TotalEnergy_{\text{start}} - TotalEnergy_{\text{end}} \tag{7.1}$$

The Total Energy was found by using the classic Bernoulli equation for open channel and frictionless flow.

$$TotalEnergy = z + h + \frac{v^2}{2g} \tag{7.2}$$

Where z is the base level, h is the water depth and v is the flow velocity in the section. The base level z is constant for each shape and is 0.712 m for the upstream starting section and 0 m for the downstream ending section. The the water depth parameter h and the flow velocity v vary for each cross section and each shape. From SSIIM simulations, each cross section has been defined by a number of points. The value of h and v was found by averaging the values over the

same cross section. Regarding v, due to the system geometry, just the vector in j-direction (V) was considered. For further details see Appendix C, Figure I.

Table 9: Energy Dissipation and relative rank for each configuration.

Configuration	**Rank**	**Dissipated Energy [m]**
Undisturbed Channel	*9*	0.7775
Singular I-shape	*5*	0.7834
Singular L-shape	*7*	0.7796
Singular T-shape	*8*	0.7795
Singular BL-shape	*6*	0.7801
T5 Configuration	*2*	0.7864
BL5 Configuration	*4*	0.7842
I5 Configuration	*1*	0.7865
L5 Configuration	*3*	0.7849

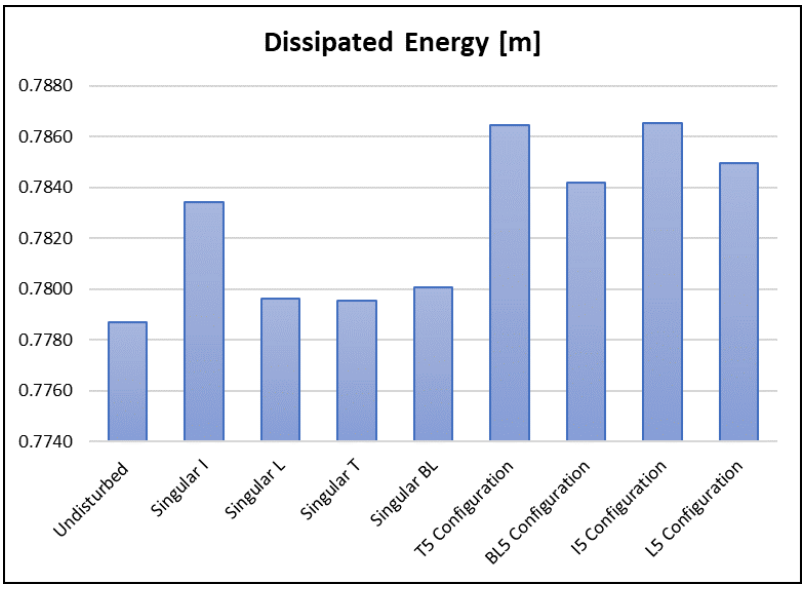

Figure 7.0.1: Dissipated Energy [m] histogram.

Considering the undisturbed channel dissipated energy as base level in order to evaluate the other configurations, the simulation results shows that I5 succession is the one that dissipate more energy, and T5 with a similar result. Particular behaviour has been seen from I single-shape configuration. Its dissipated energy value is much higher then all the other single-shapes. This is partially confirmed by successions results, also if successions behaviour seems to not be generally related to single-shape results. Successions that have higher flow channelization and higher scour bank protection function (see Table 7 in Chapt. 5.6) result in higher dissipated energy level. This due to high velocity generated in the mean channel, higher channel erosion, flow disruption from structures interaction and related turbulences due to abrupt changes in spur dikes structure geometry. Moreover a succession of dikes increases the contact area between the flow and the structures, increasing the frictional losses and related structure-interaction turbulences. BL5 configuration dissipates the least amount of energy, showing that BL5 succession's behaviour aims more to a even distribution of the bed shear stresses then to a dissipation of the flow energy related to it.

8 Conclusions and Recommendation

Referring to the hypothesis stated in Chapter 1.1, the results of the simulations show how spur dikes sequences are more effective then single-shape configuration in order to prevent banks scouring (as already verified in the study from Nayyer et al. (2019)) and deflect the bed shear stresses from critical areas towards the middle of the channel. In particular, the results show that a greater banks scour prevention function correspond to a greater flow channelization and related steep lateral gradient with consequent sediment aggradation (see Table 10). High energy dissipation values result in greater sediment transport from the system. To answer to the Hypothesis 1 (Chapter 1.1), all the different shapes successions analyzed and simulated have provided a satisfactory bank scour protection function, while the single structure was found to be inadequate in terms of scour prevention due to their restricted influence which is not able to cover the entirety of the 180°curve (under the stated system conditions).

Regarding Hypothesis 2, the comparison between successions has shown how different shapes, positioned in the same locations, have different effects and bank scour prevention magnitude in their interaction with the flow. As conclusion the Author cannot state that a specific dike-shape is better among the analyzed. In fact, does not appear a succession which induces a better system response regard to all the different aspects, looking from an hydraulic and river-training point of view. The goodness of each dike succession must be related to the specific conditions of the system in which it must be applied, and moreover to the specific function requested to the selected river-training measure. Table 10 recap the different ranks among specific succession aspects. The results show that a better response on a specific aspect is related to a worse response on a different correlated feature. This behaviour makes sense if we think the system in terms of energy, as much as hydraulic, balance.

Table 10: Successions configurations ranked behaviours.

	Averaged Lateral Gradient		***Bank Scour Protection***		***Sediment Transport***		***Energy Dissipation***	
Configuration	*Rank*	*Value [°]*	*Rank*	*Value [n° of points]*	*Rank*	*Value [1000*m3]*	*Rank*	*Value [m]*
Undisturbed Channel		*10.01*		*8764*		*-0.095*		*0.7775*
I5 Configuration	*3*	*19.7*	*2*	*10192*	*4*	*-0.044*	*1*	*0.7865*
L5 Configuration	*2*	*19.03*	*3*	*9954*	*1*	*-0.030*	*3*	*0.7849*
T5 Configuration	*4*	*21.59*	*1*	*10983*	*3*	*-0.042*	*2*	*0.7864*
BL5 Configuration	*1*	*17.54*	*4*	*9282*	*2*	*-0.034*	*4*	*0.7842*

Spur dike shapes like I, T, L, in both single and combined configurations, have already been studied (Nayyer et al. (2019) and Vaghefi et al. (2019)) and are already considered among the actual available shape-options for a river training measure using spur dikes. The successions comparison show, as in Table 10, T5 as best option, among the analyzed, in order to provide banks scour protection on the outer side and bed shear stress deflection towards the middle of the channel. This configuration is not working as good as other shapes regarding sediment transport, also having the highest flow channelization and the related steep lateral gradient. It also cause the highest stream velocity at the dike's toe among the different shapes analyzed, as possible cause of structure's weathering. I5 succession is working good in providing outer bank scour protection and bed shear stress deflection but its interaction with the stream generate a high later gradient and related flow channelization. It also generate the highest sediment

transport and energy dissipation among the configurations analyzed. L5 configuration provides a moderate bank scour protection function and bed shear stress deflection towards the middle of the channel, while having a good response towards sediment aggradation and the best towards sediment transport, with low flow channelization.
BL-shape is a new concept of spur dike with innovative shape. This study is also focused, as stated in Hypothesis 3, on determining whether this shape can be a valid alternative to the already known and used dike-shapes. In river training, the theoretically optimal lateral gradient is null, while the bed shear stress pattern is required as distributed as possible. The results confirm that BL-shape is a valid alternative to the already known and studied shapes in order to provide banks scour protection and bed shear stress deflection. In particular, BL5 configuration provide a lower but satisfactorily outer bank scour protection function and bed shear stress deflection from banks areas. Moreover the bed shear stress pattern as result from the interaction with the flow is best-distributed and the lateral gradient is the smallest among the analyzed configurations. Must be notice that the lower lateral gradient of the undisturbed configuration is reasonable and consequence of a wider undisturbed cross-section. BL5 configuration milder action towards banks scour protection results in higher performance towards sediment aggradation and transport, being able to minimize the flux channelization effect, and related lateral gradient formation, due to the interaction of the structures successions. The key factor that enables this shape to provide such a distributed patterns is the opening in the structure. This structural feature allows the flow to pass through the opening, dampening the flow shrinkage effect due to the presence of the structure, the correlated flow velocity and the consequent shear stress on the boundaries. From a system level analysis, BL5 succession's behaviour aims more to a even distribution of the bed shear stresses then to a dissipation of the flow energy related to it. This can be an advantage, from both an environmental and energetic (e.g. hydropower) point of view. The overall interaction between BL5 configuration and the stream result in a more even distribution of the bed shear stresses and bed levels with smaller lateral gradient respect the other shapes, making it the configuration that provide the best system response from a river-training perspective, but the lower, but however satisfactorily, outer bend scour protection.
In conclusion, to answer to Hypothesis 3, the results have shown the suitability of BL-shape as a new dike shape for spur dikes river-training measure. In particular, under the set up system conditions, it give the best overall system response from a river-training perspective whilst having low but satisfactorily outer bend shear stress protection function.

8.1 Further Studies

This study has limitations and its results could be improved, detailed, and confirmed by other further researches. Here below follow some of the further studies that the Author believes could be helpful in order to achieve a wider comprehension of the spur dike's interactions and system response, despite the consideration that the goodness of the system's response to a succession of spurs dikes is always determined by the specific conditions of the overall system and is therefore difficult to generalize:

- The grid used in this research could be refined and narrowed in order to obtain better and more detailed results, allowing also a finer resolution of the spur dike structure itself.
- The spur dike's structure used has perfectly vertical walls and therefore not hydrodynamic. The use of inclined walls (trapezoidal shape in a cross-section view), in order to have a more fluid-dynamic structure, could lead to improved results. Also highlight-

ing that in this study no considerations were made regarding the wear of the submerged structures used but only their impact on the flow and bed shear stress distribution.

- Different bed slope can change flow behaviour and system response.
- Structure's wear and related issues and maintenance are not considered in this study.
- No ecological aspects were considered in this study.
- Test the hypothesis of an improvement of the water energy level by using BL shape dike measure, in hydropower context.
- Analyze BL-shape spur dike behaviour in different flow conditions of submergence (as was done by Vaghefi et al. (2017)), with different BL-opening spacing and position.
- Simulate and validate the BL-shape effects on real river sections.
- Innumerable possible successions are could be simulated with different shapes spur dikes.
- Simulate successions with different spacing then the one proposed in this research.
- Use different tilting of the structure, as made by Ning et al. (2019) and Yazdi et al. (2010).
- Use permeable spur dike.
- Validate the simulated results with one or more physical models.

8.2 Acknowledgements

My heartfelt thanks to my family, specially to my parents, who have constantly supported me along this path despite the difficulties encountered. Special thanks to my Supervisor Nils Rüther for the kindness and support received despite the unique situation in which we had to face the challenge of writing a masterful thesis. I would like to thank my old and new friends who have delighted my days and with whom I have shared magnificent experiences that will remain in my heart forever. I owe a special thanks to my best friend Matteo and its constant support that has often helped me to overcome the countless obstacles encountered so far.

References

H. Chanson. The hydraulic of open channel flow: an introduction. Elsevier Butterworth-Heinemann, 2004.

G. Dodaro, A. Tafarojnoruz, F. Stefanucci, C. Adduce, F. Calomino, R. Gaudio, and G. Sciortino. An experimental and numerical study on the spatial and temporal evolution of a scour hole downstream of a rigid bed. *In Proceedings of the International Conference on Fluvial Hydraulics, River Flow*, pages 1415–1422, 2014.

H. Einstein and N. Chien. *Effects of Heavy Sediment Concentration Near the Bed on Velocity and Sediment Distribution*. University of California, Berkeley. Institute of Engineering Research and U.S. Army Engineer Division, 1955.

W. Guo, J. Hong, C. Chen, C. Su, and J. Lai. A simplified simulation method for flood-induced bend scour—a case study near the shuideliaw embankment on the cho-shui river. *Water*, 9: 324, 2017. doi: https://doi.org/10.3390/w9050324.

E. Jamieson, C. Rennie, R. Townsend, and B. Minor. Three-dimensional flow in a barb field. In K. K. C.A. Brebbia, editor, *River Basin Management IV*, volume 104, pages 371–380. WIT Press, 2007. doi: 10.2495/RM070351.

E. Jamieson, C. Rennie, and R. Townsend. Design of stream barbs for field scale application at sawmill creek, ottawa. In C. Brebbia, editor, *River Basin Management V*, volume 124, pages 281–292. WIT Press, 2009. doi: 10.2495/RM090261.

P. Julien. Erosion and sedimentation2nd ed. CAMBRIDGE UNIVERSITY PRESS, 2010.

B. Launder and D. Spalding. The numerical computation of turbulent flow. *Computer Methods in Applied Mechanics and Engineering*, 3:269–289, 1974. doi: https://doi.org/10.1016/0045-7825(74)90029-2.

I. Maddock. The importance of physical habitat assessment for evaluating river health. *Freshwater Biology*, 41:373–391, 1999. doi: https://doi.org/10.1046/j.1365-2427.1999.00437.x.

M. Melaaen. Calculation of fluid flows with staggered and non staggered curvilinear non orthogonal grids - the theory. *Numerical Heat Transfer*, 21:1–19, 1992. doi: https://doi.org/10.1080/10407799208944919.

B. Melville and S. Coleman. Bridge scour. *Water Resources Publications: Highlands Ranch, CO, USA*, 9:324, 2000. doi: https://doi.org/10.3390/w9050324.

B. Minor, C. Rennie, and R. Townsend. Barbs for river bend bank protection: application of a three-dimensional numerical model. *Canadian Journal of Civil Engineering*, 34:1087–1095, 2007. doi: https://doi.org/10.1139/l07-088.

N. Nagata, T. Hosoda, T. Nakato, and Y. Muramoto. Three-dimensional numerical model for flow and bed deformation around river hydraulic structures. *Journal of Hydraulic Engineering*, 131:1074–1087, 2005. doi: 10.1061/ASCE0733-94292005131:121074.

S. Nayyer, S. Farzin, H. Karami, and M. Rostami. A numerical and experimental investigation of the effects of combination of spur dikes in series on a flow field. *Journal of the Brazilian Society of Mechanical Sciences and Engineering*, 41:256, 2019. doi: https://doi.org/10.1007/s40430-019-1757-0.

J. Ning, G. Li, and S. Li. Numerical simulation of the influence of spur dikes spacing on local scour and flow. *Applied Sciences*, 9:2306, 2019. doi: doi:10.3390/app9112306.

A. J. Odegaard. River management with submerged vanes. In N. Sharma, editor, *River System Analysis and Management*, chapter 13, pages 251–261. Springer Science-Business Media Singapore, 2017. doi: 10.1007/978-981-10-1472-7_13.

A. J. Odegaard and Y. Wang. Sediment management with submerged vanes i: Theory. *Journal of Hydraulic Engineering*, 117:267–283, 1991. doi: https://doi.org/10.1061/(ASCE)0733-9429(1991)117:3(267).

N. Olsen. *A numerical model for simulation of sediments movements in water intakes*. Norwegian University of Science and Technology, 1991.

N. Olsen. *SSIIM User's manual*. Department of Civil and Environmental Engineering of Norwegian University of Science and Technology, 2018.

N. Olsen and S. Stokseth. Three-dimensional numerical modelling of water flow in a river with large bed roughness. *Journal of Hydraulic Research*, 33:571–581, 1995. doi: https://doi.org/10.1080/00221689509498662.

S. Patankar. *Numerical heat transfer and fluid flow*. McGraw-Hill, New York, 1980.

A. Roulund, B. Sumer, J. Fredsoe, and J. Michelsen. Numerical and experimental investigation of flow and scour around a circular pile. *Journal of Fluid Mechanics*, 534:351–401, 2005. doi: https://doi.org/10.1017/S0022112005004507.

N. Rüther, T. Fischer-Antze, N. Olsen, and D. Gutknecht. Three-dimensional (3d) modeling of non-uniform sediment transport in a channel bend with unsteady flow. *Journal of Hydraulic Research*, 47:670–675, 2009. doi: 10.3826/jhr.2009.3252.

H. Schlichting. *Boundary layer theory*. McGraw-Hill, 1979.

A. Shields. Awendung der aehnlichkeitsmechanik und der turbulenzforschung auf die geschiebebewegung. Mitt. Preuss. Versuchsanst.Wasserbau Schiffbau, 1936.

M. Vaghefi and P. Radan. Flow and scour pattern around submerged and non-submerged t-shaped spur dike in a 90° bend using the ssiim model. *Intl. J. River Basin Management*, 14:219–232, 2016. doi: 10.1080/15715124.2016.1159570.

M. Vaghefi, M. Ghodsian, and S. Neyashabouri. Experimental study on scour around a t-shaped spur dike in a channel bend. *Hournal of Hydraulic Engineering*, 138:471–474, 2012. doi: 10.1080/15715124.2015.1049181.

M. Vaghefi, Y. Safarpoor, and S. Hashemi. Effect of relative curvature on the scour pattern in a 90° bend with t-shaped spur dike using a numerical method. *International Journal of River Basin Management*, 13:4:501–514, 2015. doi: 10.1080/15715124.2015.1049181.

M. Vaghefi, Y. Safarpoor, and S. Hashemi. Effect of t-shaped spur dike on flow separation in a 90° bend using the ssiim model. *Journal of the National Science Foundation of Sri Lanka*, 45: 159–168, 2017. doi: 10.4038/jnsfsr.v45i2.8181.

M. Vaghefi, M. Ahkbari, B. Faraji, and A. Eghbalzadeh. Numerical investigation of flow pattern around a t-shaped spur dike in the vicinity of attractive and repelling protective structures. *Journal of Brazilian Society of Mechanical Science and Engineering*, 40, 2018a. doi: https://doi.org/10.1007/s40430-017-0954-y.

M. Vaghefi, A. Ahmadi, and B. Faraji. Variation of hydraulic parameters with different wing of a t-shape spur dike in bend channel. *Journal of Central South University*, 25:671–680, 2018b. doi: https://doi.org/10.1007/s11771-018-3770-3.

M. Vaghefi, M. Ahkbari, and P. Radan. Flow pattern around attractive, vertical, and repelling t-shaped spur dike in a mild bend using cfd modeling. *Journal of Civil Engineering*, 17:607–617, 2019. doi: https://doi.org/10.1007/s40999-018-0340-x.

L. C. Van Rijn. Principles of sediments transport in rivers, estuaries and coastal seas. Aqua Publications, 1993.

P. L. Wiberg and J. Smith. Calculations of the critical shear stress for motion of uniform and heterogeneous sediments. *Water Resour. Res.*, 23:1471–1480, 1987. doi: 10.1029/WR023i008p01471.

M. S. Yalin and E. Karahan. Inception of sediment transport. volume 105(11), page 1433– 1443. 1987.

J. Yazdi, H. Sarkardeh, H. M. Azamathulla, and A. A. Ghani. 3d simulation of flow around a single spur dike with free-surface flow. *Intl. J. River Basin Management*, 8:55–62, 2010. doi: 10.1080/15715121003715107.

C. Yen, J. Lai, and W. Chang. Modeling of 3d flow and scouring around circular piers. *Proc. Natl. Sci. Counc. ROC(A)*, 25:17–26, 2001.

H. Zang, H. Nakagawa, T. Ishigaki, and Y. Muto. Prediction of 3d flow field and local scouring around spur dikes. *Journal of Hydraulic Engineering*, 49:1003–1008, 2005. doi: https://doi.org/10.2208/prohe.49.1003.

H. Zang, H. Nakagawa, Y. Kawaike, and Y. Baba. Experimental and simulation of turbulent flow in local scour around a spur dyke. *International Journal of Sediment Research*, 24:33–45, 2009. doi: https://doi.org/10.1016/S1001-6279(09)60014-7.

A

Appendix 1: Detailed *control* file used

```
T vanes_steady53_000
F 2 IS        run options
F 10 R
F 4 0.8 25 0.00001 relax si converge
F 16 0.007 roughness
F 33 10.0 100 ts ii
F 36 2   free surface
F 37 1 tsc algorithm
F 48 10 tecplot print out option
F 84 1 bed load calc
F 90 2 bed roughness option

F 206 2 number of cpu

G 1 255 21 6 7     grid and array sizes
G 3 0.000000 20 40 60 80 100.000000      vertical grid distribution
G 6 255 10 7 0.5 0.001    free surface option
G 24 6 v 0 0 D 0 0 z 0 0 s 0 0 m 0 0 a 0 0 tecplot variable out

S 1 0.0066 0.36  sediment size and fall velocity
S 2 0.0041 0.28  sediment size and fall velocity
S 3 0.0028 0.23  sediment size and fall velocity
S 4 0.0017 0.18  sediment size and fall velocity
S 5 0.0010 0.13  sediment size and fall velocity
S 6 0.0006 0.09  sediment size and fall velocity
S 7 0.0003 0.05  sediment size and fall velocity
I 1 0.0 kg/s index inflow
I 2 0.0 kg/s index inflow
I 3 0.0 kg/s index inflow
I 4 0.0 kg/s index inflow
I 5 0.0 kg/s index inflow
I 6 0.0 kg/s index inflow
I 7 0.0 kg/s index inflow
N 0 1 0.05 fraction
N 0 2 0.05 fraction
N 0 3 0.10 fraction
N 0 4 0.20 fraction
N 0 5 0.20 fraction
N 0 6 0.20 fraction
N 0 7 0.20 fraction
B 0 0 0 0 0               where n is placed

W 1 60.000000 0.0530000 0.10400
W 2 64 1        5       9       13      17      21      25      29      33      37      41      45      49      53
57      61      65      69      73      77      81      85      89      93      97      101     105     109     113
117     121     125     129     133     137     141     145     149     153     157     161     165     169     173
177     181     185     189     193     197     201     205     209     213     217     221     225     229     233
237     241     245     249     255


K 1 1500 5
K 2 0 1
K 3 0.8 0.8 0.8 0.1 0.5 0.5 relax factors
K 5 1 1 1 1 1 1   block correction
K 6 1 1 1 0 0 0   second order
P 10 5  tecplot out interval
```

Figure I: Control file used for undisturbed channel (chapter 4.3) .

```
F 2 IS        run options
F 10 R
F 4 0.8 25 0.00001 relax si converge
F 16 0.007 roughness
F 33 10.0 100 ts ii
F 36 2   free surface
F 37 1 tsc algorithm
F 48 10 tecplot print out option
F 84 1 bed load calc
F 90 2 bed roughness option

F 206 2 number of cpu

G 1 255 21 6 7     grid and array sizes
G 3 0.000000 20 40 60 80 100.000000      vertical grid distribution
G 6 255 10 7 0.5 0.001    free surface option
G 13 2 127 127 15 21 2 4 outblock
G 24 6 v 0 0 D 0 0 z 0 0 s 0 0 m 0 0 a 0 0 tecplot variable out

S 1 0.0066 0.36  sediment size and fall velocity
S 2 0.0041 0.28  sediment size and fall velocity
S 3 0.0028 0.23  sediment size and fall velocity
S 4 0.0017 0.18  sediment size and fall velocity
S 5 0.0010 0.13  sediment size and fall velocity
S 6 0.0006 0.09  sediment size and fall velocity
S 7 0.0003 0.05  sediment size and fall velocity
I 1 0.0 kg/s index inflow
I 2 0.0 kg/s index inflow
I 3 0.0 kg/s index inflow
I 4 0.0 kg/s index inflow
I 5 0.0 kg/s index inflow
I 6 0.0 kg/s index inflow
I 7 0.0 kg/s index inflow
N 0 1 0.05 fraction
N 0 2 0.05 fraction
N 0 3 0.10 fraction
N 0 4 0.20 fraction
N 0 5 0.20 fraction
N 0 6 0.20 fraction
N 0 7 0.20 fraction
B 0 0 0 0 0               where n is placed

W 1 60.000000 0.0530000 0.10400
W 2 64 1        5       9       13      17      21      25      29      33      37      41      45      49      53
57      61      65      69      73      77      81      85      89      93      97      101     105     109     113
117     121     125     129     133     137     141     145     149     153     157     161     165     169     173
177     181     185     189     193     197     201     205     209     213     217     221     225     229     233
237     241     245     249     255


K 1 1500 5
K 2 0 1
K 3 0.8 0.8 0.8 0.1 0.5 0.5 relax factors
K 5 1 1 1 1 1 1   block correction
K 6 1 1 1 0 0 0   second order
P 10 5  tecplot out interval
```

Figure II: Control file used for channel with I-shape spur dike (chapter 4.4) .

```
T vanes_steady53_C1
F 2 IS        run options
F 10 R
F 4 0.8 25 0.00001 relax si converge
F 16 0.007 roughness
F 33 10.0 100 ts ii
F 36 2   free surface
F 37 1 tsc algorithm
F 48 10 tecplot print out option
F 84 1 bed load calc
F 90 2 bed roughness option

F 206 2 number of cpu

G 1 255 21 6 7     grid and array sizes
G 3 0.000000 20 40 60 80 100.000000      vertical grid distribution
G 6 255 10 7 0.5 0.001    free surface option
G 13 2 127 127 16 21 2 4 outblock
G 13 2 127 129 15 15 2 4
G 24 6 v 0 0 D 0 0 z 0 0 s 0 0 m 0 0 a 0 0 tecplot variable out

S 1 0.0066 0.36  sediment size and fall velocity
S 2 0.0041 0.28  sediment size and fall velocity
S 3 0.0028 0.23  sediment size and fall velocity
S 4 0.0017 0.18  sediment size and fall velocity
S 5 0.0010 0.13  sediment size and fall velocity
S 6 0.0006 0.09  sediment size and fall velocity
S 7 0.0003 0.05  sediment size and fall velocity
I 1 0.0 kg/s index inflow
I 2 0.0 kg/s index inflow
I 3 0.0 kg/s index inflow
I 4 0.0 kg/s index inflow
I 5 0.0 kg/s index inflow
I 6 0.0 kg/s index inflow
I 7 0.0 kg/s index inflow
N 0 1 0.05 fraction
N 0 2 0.05 fraction
N 0 3 0.10 fraction
N 0 4 0.20 fraction
N 0 5 0.20 fraction
N 0 6 0.20 fraction
N 0 7 0.20 fraction
B 0 0 0 0 0              where n is placed

W 1 60.000000 0.0530000 0.10400
W 2 64 1       5       9       13      17      21      25      29      33      37      41      45      49      53      57      61
65      69      73      77      81      85      89      93      97      101     105     109     113     117     121     125     129
133     137     141     145     149     153     157     161     165     169     173     177     181     185     189     193     197
201     205     209     213     217     221     225     229     233     237     241     245     249     255


K 1 1500 5
K 2 0 1
K 3 0.8 0.8 0.8 0.1 0.5 0.5 relax factors
K 5 1 1 1 1 1 1   block correction
K 6 1 1 1 0 0 0   second order
P 10 5  tecplot out interval
```

Figure III: Control file used for channel with L-shape spur dike (chapter 4.5) .

```
T vanes_steady53_000
F 2 IS        run options
F 10 R
F 4 0.8 25 0.00001 relax si converge
F 16 0.007 roughness
F 33 10.0 100 ts ii
F 36 2   free surface
F 37 1 tsc algorithm
F 48 10 tecplot print out option
F 84 1 bed load calc
F 90 2 bed roughness option

F 206 2 number of cpu

G 1 255 21 6 7     grid and array sizes
G 3 0.000000 20 40 60 80 100.000000      vertical grid distribution
G 6 255 10 7 0.5 0.001    free surface option
G 13 2 127 127 16 21 2 4 outblock
G 13 2 125 129 15 15 2 4
G 24 6 v 0 0 D 0 0 z 0 0 s 0 0 m 0 0 a 0 0 tecplot variable out

S 1 0.0066 0.36  sediment size and fall velocity
S 2 0.0041 0.28  sediment size and fall velocity
S 3 0.0028 0.23  sediment size and fall velocity
S 4 0.0017 0.18  sediment size and fall velocity
S 5 0.0010 0.13  sediment size and fall velocity
S 6 0.0006 0.09  sediment size and fall velocity
S 7 0.0003 0.05  sediment size and fall velocity
I 1 0.0 kg/s index inflow
I 2 0.0 kg/s index inflow
I 3 0.0 kg/s index inflow
I 4 0.0 kg/s index inflow
I 5 0.0 kg/s index inflow
I 6 0.0 kg/s index inflow
I 7 0.0 kg/s index inflow
N 0 1 0.05 fraction
N 0 2 0.05 fraction
N 0 3 0.10 fraction
N 0 4 0.20 fraction
N 0 5 0.20 fraction
N 0 6 0.20 fraction
N 0 7 0.20 fraction
B 0 0 0 0 0               where n is placed

W 1 60.000000 0.0530000 0.10400
W 2 64 1        5       9       13      17      21      25      29      33      37      41      45      49      53      57      61
65      69      73      77      81      85      89      93      97      101     105     109     113     117     121     125     129
133     137     141     145     149     153     157     161     165     169     173     177     181     185     189     193     197
201     205     209     213     217     221     225     229     233     237     241     245     249     255


K 1 1500 5
K 2 0 1
K 3 0.8 0.8 0.8 0.1 0.5 0.5 relax factors
K 5 1 1 1 1 1 1   block correction
K 6 1 1 1 0 0 0   second order
P 10 5  tecplot out interval
```

Figure IV: Control file used for channel with T-shape spur dike (chapter 4.6) .

```
T vanes_steady53_C1
F 2 IS        run options
F 10 R
F 4 0.8 25 0.00001 relax si converge
F 16 0.007 roughness
F 33 10.0 100 ts ii
F 36 2   free surface
F 37 1 tsc algorithm
F 48 10 tecplot print out option
F 84 1 bed load calc
F 90 2 bed roughness option

F 206 2 number of cpu

G 1 255 21 6 7     grid and array sizes
G 3 0.000000 20 40 60 80 100.000000      vertical grid distribution
G 6 255 10 7 0.5 0.001    free surface option
G 13 2 127 127 18 21 2 4 outblock
G 13 2 127 127 16 16 2 4
G 13 2 127 129 15 15 2 4
G 24 6 v 0 0 D 0 0 z 0 0 s 0 0 m 0 0 a 0 0 tecplot variable out

S 1 0.0066 0.36  sediment size and fall velocity
S 2 0.0041 0.28  sediment size and fall velocity
S 3 0.0028 0.23  sediment size and fall velocity
S 4 0.0017 0.18  sediment size and fall velocity
S 5 0.0010 0.13  sediment size and fall velocity
S 6 0.0006 0.09  sediment size and fall velocity
S 7 0.0003 0.05  sediment size and fall velocity
I 1 0.0 kg/s index inflow
I 2 0.0 kg/s index inflow
I 3 0.0 kg/s index inflow
I 4 0.0 kg/s index inflow
I 5 0.0 kg/s index inflow
I 6 0.0 kg/s index inflow
I 7 0.0 kg/s index inflow
N 0 1 0.05 fraction
N 0 2 0.05 fraction
N 0 3 0.10 fraction
N 0 4 0.20 fraction
N 0 5 0.20 fraction
N 0 6 0.20 fraction
N 0 7 0.20 fraction
B 0 0 0 0 0               where n is placed

W 1 60.000000 0.0530000 0.10400
W 2 64 1       5       9       13      17      21      25      29      33      37      41      45      49      53      57      61
65      69      73      77      81      85      89      93      97      101     105     109     113     117     121     125     129
133     137     141     145     149     153     157     161     165     169     173     177     181     185     189     193     197
201     205     209     213     217     221     225     229     233     237     241     245     249     255


K 1 1500 5
K 2 0 1
K 3 0.8 0.8 0.8 0.1 0.5 0.5 relax factors
K 5 1 1 1 1 1 1   block correction
K 6 1 1 1 0 0 0   second order
P 10 5  tecplot out interval
```

Figure V: Control file used for channel with BL-shape spur dike (chapter 4.7) .

```
T vanes_steady53_000
F 2 IS        run options
F 10 R
F 4 0.8 25 0.00001 relax si converge
F 16 0.007 roughness
F 33 5.0 100 ts ii
F 36 2   free surface
F 37 1 tsc algorithm
F 48 10 tecplot print out option
F 84 1 bed load calc
F 90 2 bed roughness option

F 206 2 number of cpu

G 1 255 21 6 7     grid and array sizes
G 3 0.000000 20 40 60 80 100.000000      vertical grid distribution
G 6 255 10 7 0.5 0.001    free surface option
G 13 2 113 113 15 21 2 4 outblock 1
G 13 2 128 128 15 21 2 4 outblock 2
G 13 2 143 143 15 21 2 4 outblock 3
G 13 2 158 158 15 21 2 4 outblock 4
G 13 2 172 172 15 21 2 4 outblock 5
G 24 6 v 0 0 D 0 0 z 0 0 s 0 0 m 0 0 a 0 0 tecplot variable out

S 1 0.0066 0.36  sediment size and fall velocity
S 2 0.0041 0.28  sediment size and fall velocity
S 3 0.0028 0.23  sediment size and fall velocity
S 4 0.0017 0.18  sediment size and fall velocity
S 5 0.0010 0.13  sediment size and fall velocity
S 6 0.0006 0.09  sediment size and fall velocity
S 7 0.0003 0.05  sediment size and fall velocity
I 1 0.0 kg/s index inflow
I 2 0.0 kg/s index inflow
I 3 0.0 kg/s index inflow
I 4 0.0 kg/s index inflow
I 5 0.0 kg/s index inflow
I 6 0.0 kg/s index inflow
I 7 0.0 kg/s index inflow
N 0 1 0.05 fraction
N 0 2 0.05 fraction
N 0 3 0.10 fraction
N 0 4 0.20 fraction
N 0 5 0.20 fraction
N 0 6 0.20 fraction
N 0 7 0.20 fraction
B 0 0 0 0 0 0               where n is placed

W 1 60.000000 0.0530000 0.10400
W 2 64 1        5       9       13      17      21      25      29      33      37      41      45      49      53      57      61
65      69      73      77      81      85      89      93      97      101     105     109     113     117     121     125     129
133     137     141     145     149     153     157     161     165     169     173     177     181     185     189     193     197
201     205     209     213     217     221     225     229     233     237     241     245     249     255


K 1 1500 5
K 2 0 1
K 3 0.5 0.5 0.5 0.1 0.3 0.3 relax factors
K 5 1 1 1 1 1 1   block correction
K 6 1 1 1 0 0 0   second order
P 10 5  tecplot out interval
```

Figure VI: Control file used for I5 configuration (chapter 5.1) .

```
T vanes_steady53_000
F 2 IS        run options
F 10 R
F 4 0.8 25 0.00001 relax si converge
F 16 0.007 roughness
F 33 4.0 100 ts ii
F 36 2   free surface
F 37 1 tsc algorithm
F 48 10 tecplot print out option
F 84 1 bed load calc
F 90 2 bed roughness option

F 206 2 number of cpu

G 1 255 21 6 7     grid and array sizes
G 3 0.000000 20 40 60 80 100.000000      vertical grid distribution
G 6 255 10 7 0.5 0.001    free surface option
G 13 2 113 113 16 21 2 4 outblock 1
G 13 2 113 115 15 15 2 4
G 13 2 128 128 15 21 2 4 outblock 2
G 13 2 128 130 15 15 2 4
G 13 2 143 143 15 21 2 4 outblock 3
G 13 2 143 145 15 15 2 4
G 13 2 158 158 15 21 2 4 outblock 4
G 13 2 158 160 15 15 2 4
G 13 2 172 172 15 21 2 4 outblock 5
G 13 2 172 174 15 15 2 4
G 24 6 v 0 0 D 0 0 z 0 0 s 0 0 m 0 0 a 0 0 tecplot variable out

S 1 0.0066 0.36  sediment size and fall velocity
S 2 0.0041 0.28  sediment size and fall velocity
S 3 0.0028 0.23  sediment size and fall velocity
S 4 0.0017 0.18  sediment size and fall velocity
S 5 0.0010 0.13  sediment size and fall velocity
S 6 0.0006 0.09  sediment size and fall velocity
S 7 0.0003 0.05  sediment size and fall velocity
I 1 0.0 kg/s index inflow
I 2 0.0 kg/s index inflow
I 3 0.0 kg/s index inflow
I 4 0.0 kg/s index inflow
I 5 0.0 kg/s index inflow
I 6 0.0 kg/s index inflow
I 7 0.0 kg/s index inflow
N 0 1 0.05 fraction
N 0 2 0.05 fraction
N 0 3 0.10 fraction
N 0 4 0.20 fraction
N 0 5 0.20 fraction
N 0 6 0.20 fraction
N 0 7 0.20 fraction
B 0 0 0 0 0              where n is placed

W 1 60.000000 0.0530000 0.10400
W 2 64 1       5       9       13      17      21      25      29      33      37      41      45      49      53      57      61      65      69      73
77      81      85      89      93      97      101     105     109     113     117     121     125     129     133     137     141     145     149     153
157     161     165     169     173     177     181     185     189     193     197     201     205     209     213     217     221     225     229     233
237     241     245     249     255


K 1 1500 5
K 2 0 1
K 3 0.5 0.5 0.5 0.1 0.3 0.3 relax factors
K 5 1 1 1 1 1 1   block correction
K 6 1 1 1 0 0 0   second order
P 10 5  tecplot out interval
```

Figure VII: Control file used for L5 configuration (chapter 5.2) .

```
T vanes_steady53_000
F 2 IS        run options
F 10 R
F 4 0.8 25 0.00001 relax si converge
F 16 0.007 roughness
F 33 5.0 100 ts ii
F 36 2   free surface
F 37 1 tsc algorithm
F 48 10 tecplot print out option
F 84 1 bed load calc
F 90 2 bed roughness option

F 206 2 number of cpu

G 1 255 21 6 7     grid and array sizes
G 3 0.000000 20 40 60 80 100.000000      vertical grid distribution
G 6 255 10 7 0.5 0.001    free surface option
G 13 2 113 113 16 21 2 4 outblock 1
G 13 2 112 114 15 15 2 4
G 13 2 128 128 16 21 2 4 outblock 2
G 13 2 127 129 15 15 2 4
G 13 2 143 143 16 21 2 4 outblock 3
G 13 2 142 144 15 15 2 4
G 13 2 158 158 16 21 2 4 outblock 4
G 13 2 157 159 15 15 2 4
G 13 2 172 172 16 21 2 4 outblock 5
G 13 2 171 173 15 15 2 4
G 24 6 v 0 0 D 0 0 z 0 0 s 0 0 m 0 0 a 0 0 tecplot variable out

S 1 0.0066 0.36  sediment size and fall velocity
S 2 0.0041 0.28  sediment size and fall velocity
S 3 0.0028 0.23  sediment size and fall velocity
S 4 0.0017 0.18  sediment size and fall velocity
S 5 0.0010 0.13  sediment size and fall velocity
S 6 0.0006 0.09  sediment size and fall velocity
S 7 0.0003 0.05  sediment size and fall velocity
I 1 0.0 kg/s index inflow
I 2 0.0 kg/s index inflow
I 3 0.0 kg/s index inflow
I 4 0.0 kg/s index inflow
I 5 0.0 kg/s index inflow
I 6 0.0 kg/s index inflow
I 7 0.0 kg/s index inflow
N 0 1 0.05 fraction
N 0 2 0.05 fraction
N 0 3 0.10 fraction
N 0 4 0.20 fraction
N 0 5 0.20 fraction
N 0 6 0.20 fraction
N 0 7 0.20 fraction
B 0 0 0 0 0               where n is placed

W 1 60.000000 0.0530000 0.10400
W 2 64 1       5       9       13      17      21      25      29      33      37      41      45      49      53      57      61      65      69      73
77      81      85      89      93      97      101     105     109     113     117     121     125     129     133     137     141     145     149     153
157     161     165     169     173     177     181     185     189     193     197     201     205     209     213     217     221     225     229     233
237     241     245     249     255


K 1 1500 5
K 2 0 1
K 3 0.5 0.5 0.5 0.1 0.3 0.3 relax factors
K 5 1 1 1 1 1 1   block correction
K 6 1 1 1 0 0 0   second order
P 10 5  tecplot out interval
```

Figure VIII: Control file used for T5 configuration (chapter 5.3) .

```
T vanes_steady53_000
F 2 IS        run options
F 10 R
F 4 0.8 25 0.00001 relax si converge
F 16 0.007 roughness
F 33 5.0 100 ts ii
F 36 2   free surface
F 37 1 tsc algorithm
F 48 10 tecplot print out option
F 84 1 bed load calc
F 90 2 bed roughness option

F 206 2 number of cpu

G 1 255 21 6 7     grid and array sizes
G 3 0.000000 20 40 60 80 100.000000      vertical grid distribution
G 6 255 10 7 0.5 0.001    free surface option
G 13 2 113 113 18 21 2 4 outblock 1
G 13 2 113 113 16 16 2 4
G 13 2 113 115 15 15 2 4
G 13 2 128 128 18 21 2 4 outblock 2
G 13 2 128 128 16 16 2 4
G 13 2 128 130 15 15 2 4
G 13 2 143 143 18 21 2 4 outblock 3
G 13 2 143 143 16 16 2 4
G 13 2 143 145 15 15 2 4
G 13 2 158 158 18 21 2 4 outblock 4
G 13 2 158 158 16 16 2 4
G 13 2 158 160 15 15 2 4
G 13 2 172 172 18 21 2 4 outblock 5
G 13 2 172 172 16 16 2 4
G 13 2 172 174 15 15 2 4
G 24 6 v 0 0 D 0 0 z 0 0 s 0 0 m 0 0 a 0 0 tecplot variable out

S 1 0.0066 0.36  sediment size and fall velocity
S 2 0.0041 0.28  sediment size and fall velocity
S 3 0.0028 0.23  sediment size and fall velocity
S 4 0.0017 0.18  sediment size and fall velocity
S 5 0.0010 0.13  sediment size and fall velocity
S 6 0.0006 0.09  sediment size and fall velocity
S 7 0.0003 0.05  sediment size and fall velocity
I 1 0.0 kg/s index inflow
I 2 0.0 kg/s index inflow
I 3 0.0 kg/s index inflow
I 4 0.0 kg/s index inflow
I 5 0.0 kg/s index inflow
I 6 0.0 kg/s index inflow
I 7 0.0 kg/s index inflow
N 0 1 0.05 fraction
N 0 2 0.05 fraction
N 0 3 0.10 fraction
N 0 4 0.20 fraction
N 0 5 0.20 fraction
N 0 6 0.20 fraction
N 0 7 0.20 fraction
B 0 0 0 0 0 0               where n is placed

W 1 60.000000 0.0530000 0.10400
W 2 64 1       5       9       13      17      21      25      29      33      37      41      45      49      53      57      61      65      69      73
77      81      85      89      93      97      101     105     109     113     117     121     125     129     133     137     141     145     149     153
157     161     165     169     173     177     181     185     189     193     197     201     205     209     213     217     221     225     229     233
237     241     245     249     255


K 1 1500 5
K 2 0 1
K 3 0.5 0.5 0.5 0.1 0.3 0.3 relax factors
K 5 1 1 1 1 1 1   block correction
K 6 1 1 1 0 0 0   second order
P 10 5  tecplot out interval
```

Figure IX: Control file used for BL5 configuration (chapter 5.4) .

B

Appendix 2: Successions Bed Shear Stress Histograms

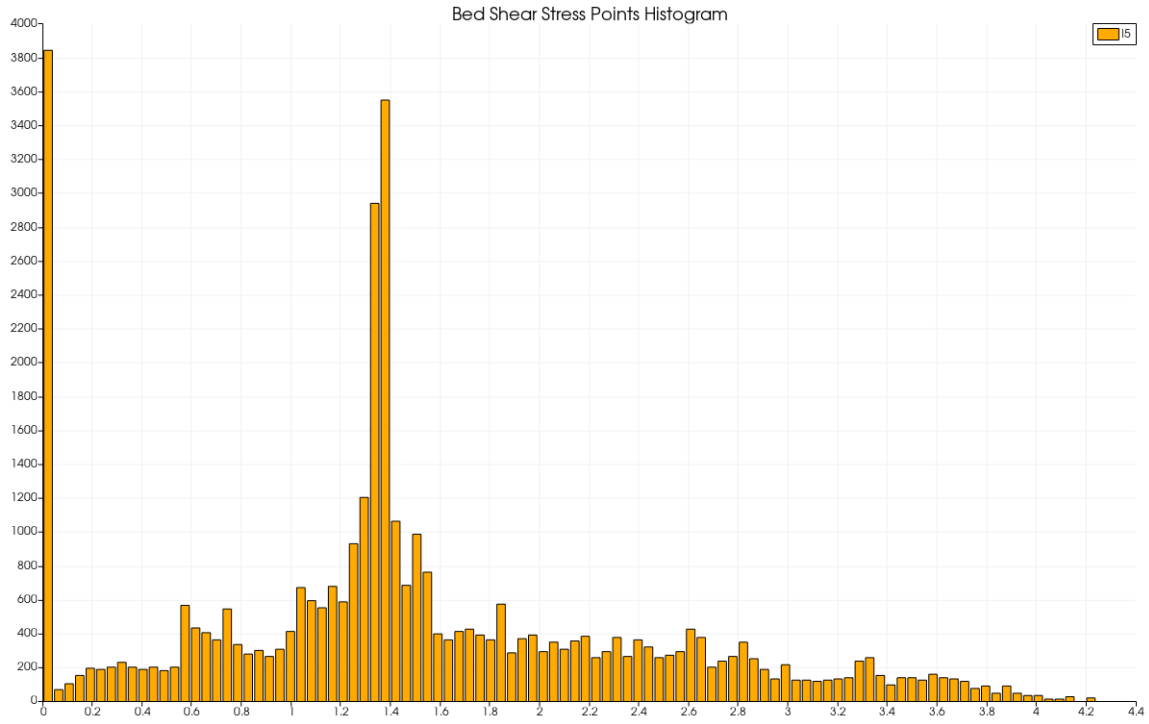

Figure I: I5 succession Bed Shear Stress Histogram.

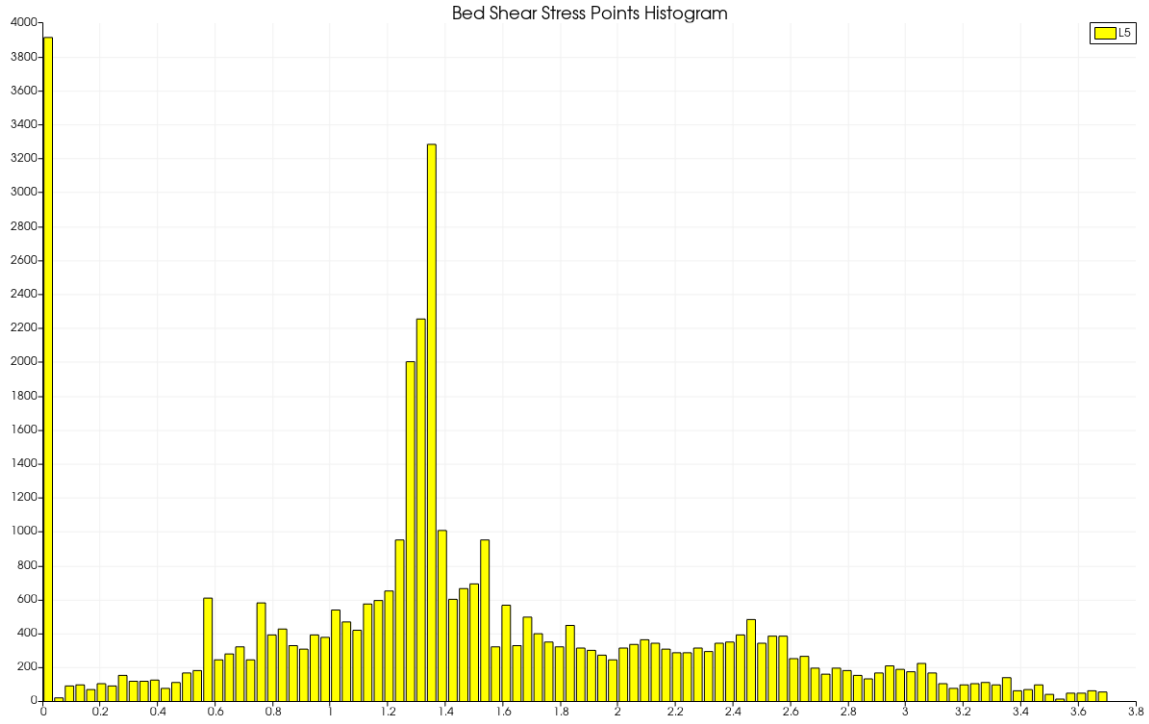

Figure II: L5 succession Bed Shear Stress Histogram.

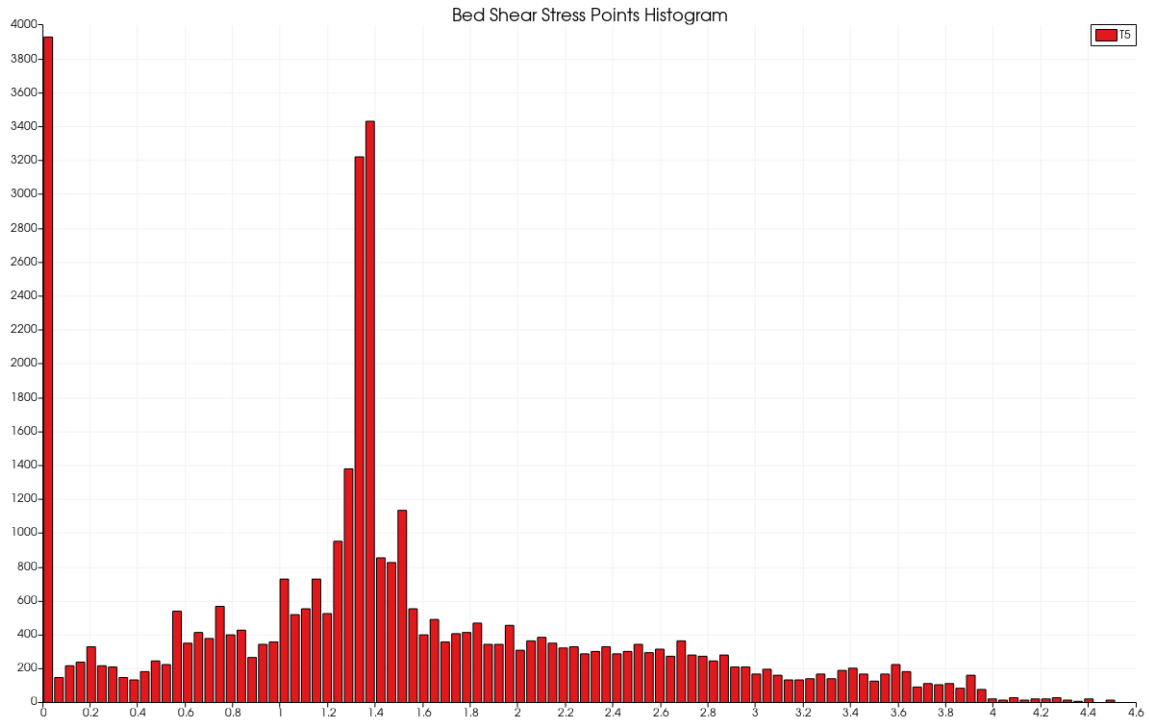

Figure III: T5 succession Bed Shear Stress Histogram.

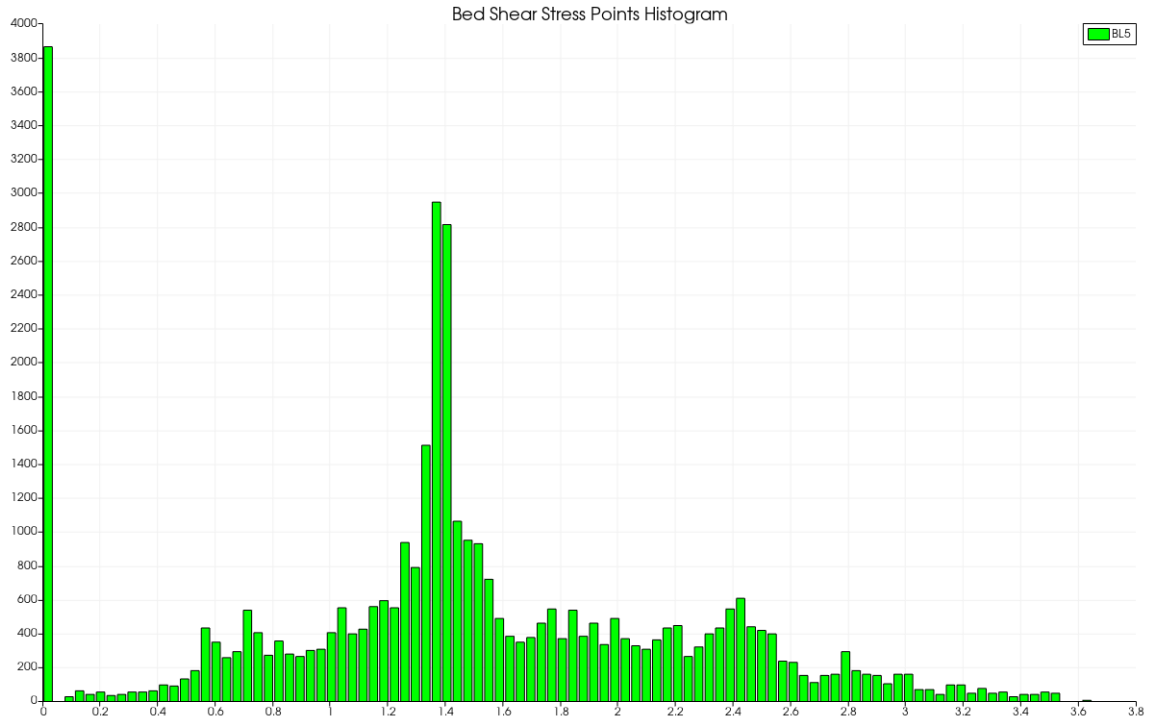

Figure IV: BL5 succession Bed Shear Stress Histogram.

C

Appendix 3: Detailed Energy Dissipated results

Undisturbed Channel					
START					
z base level	0.712	**Energy**	**0.83304**		
Level avg	U avg	**V avg**	W avg	k avg	eps avg
0.114907722	-1.1E-06	0.346863	0.000894	0.002676	0.003261
END					
z base level	0	**Energy**	**0.055471**		
Level avg	U avg	**V avg**	W avg	k avg	eps avg
0.046419684	-0.01132	-0.4214	-0.00127	0.002595	0.00396
Energy dissipation			**0.777569**	[m]	

Singular I-Shape					
START					
z base level	0.712	**Energy**	**0.834426**		
Level avg	U avg	**V avg**	W avg	k avg	eps avg
0.116416759	-3.8E-06	0.343368	0.001165	0.002651	0.003189
END					
z base level	0	**Energy**	**0.051008**		
Level avg	U avg	**V avg**	W avg	k avg	eps avg
0.043392684	0.037155	-0.38653	-0.00971	0.002417	0.003218
Energy dissipation		**I**	**0.783418**	[m]	

Singular L-Shape					
START					
z base level	0.712	**Energy**	**0.834555**		
Level avg	U avg	**V avg**	W avg	k avg	eps avg
0.116560624	6.77E-07	0.342944	0.001183	0.002647	0.00318
END					
z base level	0	**Energy**	**0.054941**		
Level avg	U avg	**V avg**	W avg	k avg	eps avg
0.046566744	-0.01127	-0.40533	-0.00619	0.002455	0.00351
Energy dissipation		L	**0.779615**	[m]	

Singular T-Shape					
START					
z base level	0.712	**Energy**	**0.834539**		
Level avg	U avg	**V avg**	W avg	k avg	eps avg
0.116540361	-2E-06	0.343068	0.001186	0.002648	0.003183
END					
z base level	0	**Energy**	**0.055006**		
Level avg	U avg	**V avg**	W avg	k avg	eps avg
0.046217925	0.002851	-0.41524	-0.0011	0.002543	0.003844
Energy dissipation		**T**	**0.779533**	[m]	

Singular BL-Shape					
START					
z base level	0.712	**Energy**	**0.834**		
Level avg	U avg	**V avg**	W avg	k avg	eps avg
0.115949068	-4.2E-07	0.344553	0.001092	0.002659	0.003214
END					
z base level	0	**Energy**	**0.053939**		
Level avg	U avg	**V avg**	W avg	k avg	eps avg
0.045047609	-0.02413	-0.41768	0.00325	0.002639	0.003848
Energy dissipation		BL	**0.780061**	[m]	

BL5 Configuration					
START					
z base level	0.712	**Energy**	**0.838764**		
Level avg	U avg	**V avg**	W avg	k avg	eps avg
0.120798165	2.85E-06	0.342125	0.002072	0.002636	0.003171
END					
z base level	0	**Energy**	**0.05457**		
Level avg	U avg	**V avg**	W avg	k avg	eps avg
0.046546722	-0.09824	-0.39676	-0.0018	0.002992	0.004701
Energy dissipation		**BL5**	**0.784194**	[m]	

T5 Configuration					
START					
z base level	0.712	**Energy**	**0.839786**		
Level avg	U avg	**V avg**	W avg	k avg	eps avg
0.121811722	3.29E-06	0.342379	0.002303	0.002635	0.003174
END					
z base level	0	**Energy**	**0.053359**		
Level avg	U avg	**V avg**	W avg	k avg	eps avg
0.045669677	-0.10983	-0.38841	-0.00583	0.003035	0.004638
Energy dissipation		T5	**0.786428**	[m]	

I5 Configuration					
START					
z base level	0.712	**Energy**	**0.839487**		
Level avg	U avg	**V avg**	W avg	k avg	eps avg
0.121516707	3.12E-06	0.342243	0.002233	0.002635	0.003172
END					
z base level	0	**Energy**	**0.05295**		
Level avg	U avg	**V avg**	W avg	k avg	eps avg
0.045256226	-0.11048	-0.38854	-0.00649	0.003038	0.004587
Energy dissipation		**I5**	**0.786536**	[m]	

L5 Configuration					
START					
z base level	0.712	**Energy**	**0.840368**		
Level avg	U avg	**V avg**	W avg	k avg	eps avg
0.122429083	3.48E-06	0.341363	0.002371	0.002626	0.003149
END					
z base level	0	**Energy**	**0.055427**		
Level avg	U avg	**V avg**	W avg	k avg	eps avg
0.047287045	-0.09355	-0.39962	0.00022	0.002992	0.004697
Energy dissipation		L5	**0.784942**	[m]	

Figure I: Detailed Energy Dissipated values obtained by *interpol-interres* SSIIM simulation (chapter 7) .

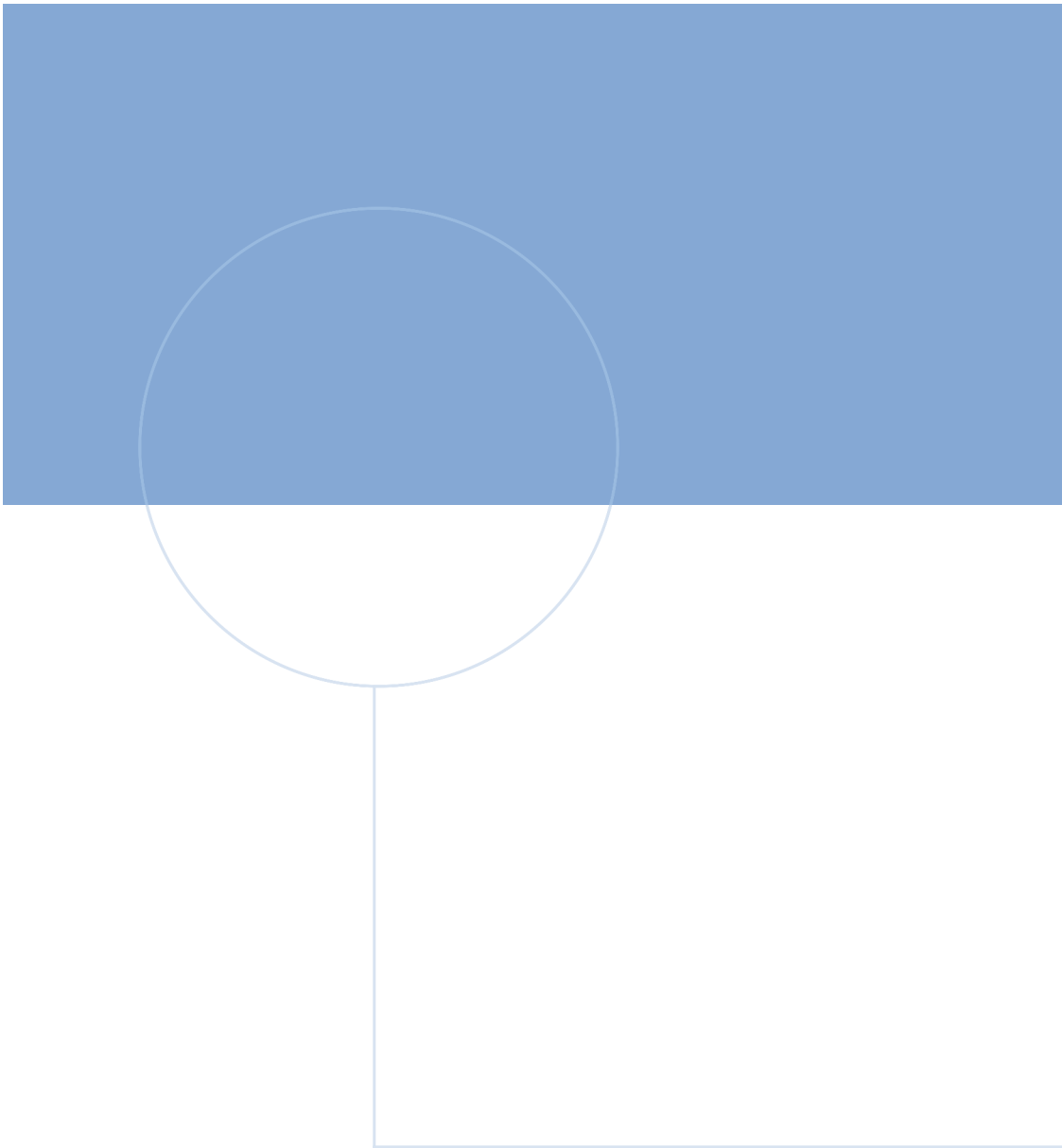

NTNU

Norwegian University of
Science and Technology